COHERENT SHOCK WAVE AMPLIFICATION IN PHOTOCHEMICAL INITIATION OF GASEOUS DETONATIONS

by

© N. Yoshikawa

A thesis submitted to the Faculty of Graduate Studies and Research in partial fulfillment of the requirements for the degree of Doctor of Philosophy

Department of Mechanical Engineering

McGill University

Montreal, Quebec
Canada

March 1980

TABLE OF CONTENTS

APPENDICES

ABSTRACT

The present thesis reports the results of a study on the basic features and mechanisms of shock wave amplification in explosive gases. The results of an investigation of photochemical detonation initiation have shown that a rapid shock wave amplification occurring in a non-uniformly photo-dissociating gas plays a significant role in the early stage of the detonation initiation. An important concept on the shock wave amplification has emerged through the investigation. It is found that the coherent energy release from the non-uniformly reacting gas to the shock wave, provides one of the most effective means of shock wave amplification. It is shown that the coherent energy release can be established either by the induction time gradient field of the non-uniformly reacting gas, or in the later stages by the gasdynamic compression effect of the amplified wave itself.

Further insight into the fundamental mechanisms of shock wave amplification has been obtained by considering a relatively simple theoretical model. This model illustrates the important role of the induction time gradient field in the shock wave amplification. Finally, the concept of shock wave amplification has been further extended to include the problem of transition to detonation in a non-uniformly preheated mixture.

SOMMAIRE

Cet ouvrage présente les resultats d'une étude sur les caractéristiques fondamentales et les mécanismes d'amplification d'une onde de choc dans les mélanges de gaz explosifs. Les résultats d'une recherche sur l'initiation photochimique des ondes de détonation ont démontré qu'une amplification rapide de l'onde de choc résultant de la photo-dissociation non-uniforme du mélange gazeux joue un rôle significatif dans les premiers stages de l'initiation de détonations. Un important concept au sujet de l'amplification d'une onde de choc a transpiré de cetter étude. Il a été constaté que la libération cohérente d'énergie, émanant du mélange gazeux en réaction non-uniforme vers l'onde de choc, procure un moyen des plus efficace pour amplifier cette même onde de choc. Il a été démontré que la libération cohérente d'énergie peut être obtenue par le gradient spacial de temps d'induction du gaz en réaction non-uniforme, ou, dans les stages plus avancés, par les effets de compression du gaz dû à l'onde amplifiée.

Afin de mieux comprendre les mécanismes fondamentaux régissant le phénomène d'amplification de l'onde de choc, une nouvelle analyse fût entreprise. Cette dernière consiste en un modèle théorique relativement simple illustrant le rôle important du gradient spacial de temps d'induction dans le processus d'amplification. Enfin, le concept d'amplification de l'onde de choc dans un champs de gradient spacial de temps d'induction fût modifié afin d'inclure le problème de transition à une détonation dans un mélange non-uniformément préchauffé.

ACKNOWLEDGEMENTS

The author sincerely expresses his gratitude to his research supervisor, Professor J.H.S. Lee, without whose constant support and encouragement during the course of the present research this thesis would never have been completed. The author also acknowledges Professor R. Knystautas who has made available to the author his schlieren photographs of photochemical detonation initiation.

Special thanks are due to Dr. P.A. Thibault who has provided stimulating discussions and valuable suggestions during the present work, and offered helpful suggestions for the improvement of this manuscript. The cooperation of Mr. M.A. Bergeron in the early phase of the experimental work is also appreciated. The author also wishes to thank Professors G.G. Bach, C.M. Guirao (McGill University), S. Taki (Fukui University, Japan) and T. Fujiwara (Nagoya University, Japan), for providing valuable suggestions and discussions on the numerical analysis techniques. Finally, the typing of the thesis by Miss J. Armour is sincerely appreciated.

The present research has been supported by US-AFOSR Contract 72-2387, Canada -- NRC Grants A3347 and A7091.

LIST OF SYMBOLS

Å	Angstrom units
A	energy source Mach number $A = V_o/c_o$
C_{pi}	constant pressure specific heat of chemical species i
c	speed of sound
$\frac{d}{dt}$	substantial derivative
e	sum of internal energy and kinetic energy $e = \frac{pv}{\gamma-1} + \frac{1}{2}u^2$
E	energy integral defined in Eqs. (3-12) or (3-13)
E_{act}	activation energy
f	defined in Eq. (IV-2); also defined in Eq. (V-2)
$\underset{\sim}{f}$	defined in Eq. (IV-3); also defined in Eq. (V-3) and (V-4)
$\overline{f}$	defined in Eq. (IV-6); also defined in Eq. (V-5)
g	defined in Eq. (IV-2); also defined in Eq. (V-2)
$\underset{\sim}{g}$	given in Eq. (V-4)
H	Heaviside function
h	Planck's constant; also specific enthalpy
h_i	specific enthalpy of chemical species i
I	radiation intensity
I_o	incident radiation intensity
k	constant; also chemical reaction rate
L	length of preheated gas mixture
ℓ^*	characteristic photon absorption length defined in Eq. (2-2)
M_{CJ}	Chapman-Jouguet detonation Mach number
M_i	molecular weight of chemical species i
p	pressure
$p_{V.N.}$	pressure of the von Neumann spike

$p_{C.V.}$	pressure of the constant volume combustion
p_s	pressure behind the shock wave
$\dot{q}$	heat release rate per unit mass
Q_o	heat release per unit mass
R_o	universal gas constant
R	gas constant
S	defined in Eq. (IV-2); also defined in Eq. (V-2)
$\tilde{S}$	given in Eq. (V-4)
t	time
Δt	time step size of numerical computation
T	temperature
T_{ig}	ignition temperature
T_w	initial temperature of the gas particle at x=0
u	particle velocity
U	specific internal energy
V_o	energy source velocity
v	specific volume
W_i	production rate of chemical species i
x	distance
x_s	position of shock wave
x_r	position of reaction front
Δx	spatial mesh size of numerical computation
Y_i	weight fraction of chemical species i
α	ratio of characteristic gasdynamic time to reaction time $\alpha = \tau_g/\tau_R$
β	ratio of characteristic gasdynamic time to induction time $\beta = \tau_g/\tau_{ind.w.}$

γ	specific heat ratio
$\Lambda_{m+1/2}$	defined in Eq. (IV-7); also defined in Eq. (V-6)
ϵ	photon absorption coefficient of chlorine molecule
$\eta_{m+1/2}$	diffusion-antidiffusion coefficient (Eq. (IV-6)); also Eqs. (V-5) and (V-10)
$\kappa_{m+1/2}$	defined in Eq. (IV-9); also defined in Eq. (V-8)
Ω	Courant number
λ	induction progress parameter
$\lambda^n_{m+1/2}$	defined in Eq. (IV-4)
ν	frequency of light wave
ξ	Lagrangian spatial coordinate (Eq. (4-12))
$\Delta\xi$	mesh size of Lagrangian spatial coordinate for numerical computation
ρ	density
τ	defined in Eqs. (3-11) or (4-5)
τ_R	reaction time
$\tau_{ind.}$	induction time
$\tau_{ind.w}$	induction time for the gas particle at x=0
τ_g	characteristic gasdynamic time $\tau_g = L/c_o$
$\phi_{m+1/2}$	defined in Eq. (IV-8); also defined in Eq. (V-7)
ω	function defined in Eq. (3-10)

Subscripts and Superscripts

$( )^*$	dimensionless quantity
$( )_o$	initial or undisturbed condition
$( )^n_m$	quantity at the lattice point of the n^{th} in time and m^{th} in spatial coordinate
$[i]$	concentration of chemical species i

CHAPTER 1

INTRODUCTION

Detonation Initiation and Shock Wave Amplification

The initiation phenomena of gaseous detonation waves have intrigued many research workers, and a significant number of experiments have been carried out in the past. In general, there are two initiation modes which have been extensively studied over the last few decades. One is the blast initiation mode where detonation is formed almost instantaneously by a strong shock wave generated by a powerful igniter. The other is the transition mode where detonation is generated via an accelerating turbulent flame.

For blast initiation, the ignition source plays an important role. Successful blast initiation depends on whether or not a sufficiently strong shock wave can be generated by the igniter. Thus, in general, the igniter energy governs the initiation. If a sufficient amount of energy is released by the igniter, rapid auto-ignition occurs immediately behind the shock wave. The reaction coupled shock wave propagates at a velocity above the Chapman-Jouguet velocity in the early stages. As the wave propagates away from the igniter, the influence by the igniter energy becomes less significant. The wave eventually starts to propagate at the Chapman-Jouguet velocity; that is, a self-sustained detonation wave is established. Since the detonation is formed directly without a deflagration process, this initiation mode is referred to as the direct initiation. Below a certain threshold value of the igniter energy, the shock wave generated by the igniter progressively decouples from the reaction front,

and the direct initiation does not occur. Bach, Knystautas, and Lee (1,2) have developed a theoretical model of reacting blast wave, and Lee and Ramamurthi (3) have more recently developed a relatively simple theoretical model which can predict the minimum initiation energy for the direct initiation.

In transition process, an auto-igniting shock wave is generated via an accelerating turbulent flame. Strong interactions between the flame and the flow-field ahead of the flame are the principal flame acceleration mechanisms. In particular, Oppenheim's research group (4-6) in Berkeley, California has most successfully elucidated the transition phenomena using the stroboscopic laser schlieren technique. In view of commonly accepted mechanism of transition, the gasdynamic compression effect of flame is significant. The accelerating flame front emits a series of compression waves which coalesce into an auto-igniting shock wave. The onset of detonation occurs in the region of shocked gas between the flame and the shock wave.*

In addition to those initiation processes, there is another initiation process in which detonation initiation is largely facilitated by intense interactions between flame and obstacles. This transition process has recently received an interest in connection with the accidental vapor cloud explosions (11-13).

---

* The basic aspects of gaseous detonation waves, such as the structure or the propagation behaviour of the waves, as well as more detailed descriptions of blast initiation and transition mode, are obtained by the excellent review papers by Oppenheim (7), Strehlow (8), Lee, Soloukhin and Oppenheim (9), and Lee (10).

Dorge, Pangritz, and Wagner (14) have recently conducted experiments of rapid formation of detonation by obstacles. They have observed that the onset of detonation suddenly occurs when a hemispherical flame passes through hemispherically-shaped grid obstacles.

The more recent experiment by Knystautas et al (15) has elucidated the basic features of the above-mentioned transition process. Their schlieren photographs have shown that the intense turbulent flame generated by an obstacle entrains the surrounding fresh gas mixture to form a turbulent mixing flow-field and that a detonation wave suddenly emerges from such a turbulent field. This transition mechanism differs from the transition mechanism previously mentioned. No shock wave has been observed outside the turbulent mixing field prior to the onset of detonation. This indicates that the gasdynamic compression effect of the turbulent flame front does not play a significant role in generating auto-igniting shock waves. The auto-igniting shock wave is generated inside the turbulent flow-field. It has been proposed that a shock wave amplification mechanism inside the turbulent field is responsible for the rapid formation of detonation. Since the obstacle effects are important factors involved in the actual accidental explosions, it appears that the basic research on the shock wave amplification phenomena should provide some valuable information to the practical important problem of the accidential explosions.

The shock wave amplification in combustible gases is basically a phenomenon which involves the interactions between pressure waves and heat release of chemical reactions. Toong's research group (16-19) at MIT has been carrying out an interesting research on the basic aspects of this subject. They have studied the amplification of weak pressure waves (acoustic waves or weak shock waves) in reacting gases. Their analysis

has shown that the waves propagating in reacting media is largely amplified due to the gasdynamic-chemical coupling effects. However, their research has so far been limited to weak pressure waves in homogeneously reacting media. More complicated phenomena, such as strong shock wave amplification in non-uniformly reacting gases, have not been analyzed in their works.

Oppenheim and co-workers (20,21) have theoretically pursued the phenomenon of rapid shock formation in explosive gases. In their analysis (20), a localized reaction center is considered, and the surrounding gas is assumed to be non-reacting. The flow-field generated by the expansion of the reaction center has been numerically solved. The influence of flow geometries (i.e. plane, cylindrical, and spherical cases) on the shock wave formation was studied. The results have shown that shock wave is not formed in the case of spherical reaction center. Obviously, this result does not account for the actual shock formation which occurs in the three dimensional geometry. Thus, the phenomenon can not be explained solely by the expansion of the reaction center. This indicates that the reaction of the surrounding gas mixture should be considered. In other words, the pressure wave originating from the reaction center is amplified in the ambient gas mixture.

Meyer and Oppenheim (21) have emphasized the importance of energy release rate of gas mixture in the shock wave formation, and they have developed a theory. They have considered that explosive gas mixture consists of the reaction centers. Further, they have postulated that the shock formation depends only on the average power pulse (energy release rate) of different reaction centers. This indicates that the simultaneous heat release of the reaction centers provides an ideal condition for the

development of shock wave. However, in reality, such an explosion mode should be nothing less than a homogeneous explosion, in which no shock wave is formed. This contradiction in their theory stems from the lack of precise analysis of the shock wave amplification phenomenon. Although the energy release rate of gas mixture is one of the important factors involved in the development of shock waves, it should not totally govern the shock amplification phenomenon.

For a better understanding of the shock wave amplification phenomena, a more rigorous study on the amplification mechanism should be carried out. Furthermore, in general, the real shock amplification occurs in non-uniformly reacting media. This fact should be fully recognized.

In the present research, the basic features of shock wave amplification in non-uniformly reacting gas mixtures have been pursued. An investigation of photochemical detonation initiation has first been made. Based on the results obtained through the investigation, some theoretical analyses have been carried out. In the following, the basic characteristics of the photochemical ignition technique are described, and a brief review concerning the photochemical detonation initiation is then provided.

Photochemical Initiation of Gaseous Detonations

Rapid photochemical ignition can be obtained using the flash photolysis technique. In flash photolysis, intense ultra-violet light generated by a flash lamp penetrates the gas mixture containing a photon-sensitive gas (e.g. nitrogen dioxide or chlorine). The photo-dissociation of the sensitive gas generates a sufficient amount of free radicals in the irradiated mixture. The free radicals then initiate the chain reactions

leading to the explosion of the gas mixture. Since the photon energy itself creates no hydrodynamic disturbances, detonation initiation starts in the quiescent field of the photo-dissociating mixture. Thus, in comparison with the flow-fields of other detonation initiation modes, the quiescent photo-dissociating field involves less complexities. Indeed, this is the motivation of studying the photochemical detonation initiation phenomena in the present research.

The flash photolysis technique was developed by Norrish, Porter, and Thrush (22-25) at Cambridge in the early fifties. The main purpose of this ignition technique has been to study the chemical kinetics of fast gas phase reactions. In a typical experiment for chemical kinetic studies, a cylindrical explosion tube filled with a test gas mixture is irradiated alongside by a linear flash tube. The diameter of the explosion tube is chosen to be smaller than the characteristic photon absorption length of the mixture. If the photons from the flash tube can be distributed uniformly along the explosion tube, we can expect to produce a homogeneous reacting system. It has been believed for some time that accurate quantitative measurement of chemical kinetics can be made in the flash-induced reacting system under such an experimental condition.

Using the above-mentioned experimental apparatus, Norrish, Porter, and Thrush (26) studied the chemical kinetics of nitrogen dioxide sensitized oxy-acetylene and oxy-hydrogen systems. In thier experiments, the light emission from intermediate chemical species, such as OH or CH, was monitored together with the temperature measurement by the absorption spectrum. Some very sharp spikes were observed in the records of the light emission - time curves as well as in the temperature measurement. The magnitude of either

the light emission or the temperature at the peaks of the spike was much greater than those of the expected uniform constant volume combustion. This experiment showed the existence of some inhomogeneity in the photochemically initiated reactions. It was conjectured that the inhomogeneous reactions are caused by the presence of detonation waves.

Thrush (27) further investigated on the inhomogeneity in the flash induced reaction of C_2H_2-O_2-NO_2 using the same experimental apparatus. He monitored the light emission at several different observation points along the explosion tube. He measured the propagation velocity of the above-mentioned sharp spike along the tube. The velocity was found to be about that of the Chapman-Jouguet detonation wave for the gas mixture. Thus, his experiments confirmed that the inhomogeneous reaction is attributed to the presence of detonation waves. This also indicates that the flash photolysis technique does not provide uniform excitation of gas mixture, for the completely uniform excitation should result in homogeneous constant volume combustion.

Later, Birkby and Hutton (28) carried out some experiments similar to the above experiments by Thrush. Kinbara and Noda (29-31), Takahashi et al. (32,33) also studied flash-induced reactions. Their experimental results also showed that detonation initiation can easily be triggered in the photochemically ignited gas mixtures.

Wadsworth (34) was perhaps the first one to intentionally use the flash photolysis in the detonation research. His experimental set-up consisted of a flash igniter section and a tube extension. In the igniter section, a gas mixture of C_2H_2-O_2-NO_2 (below 100 torr) in an explosion tube (10 cm long, 5 cm I.D.) was irradiated alongside by a flash tube. The

diameter of the explosion tube was at least about five times larger than the characteristic photon-absorption length of NO_2 ($\lesssim$ 1 cm). The concentration of free radicals decreases sharply from the side of flash irradiation to the other side across the tube diameter. The detonation initiation occurred in a highly non-uniformly photo-dissociating gas mixture. The propagation of detonation waves in the tube extension was recorded on a streak camera. Although the initiation phenomenon inside the igniter section was not elucidated, his streak photograph showed that a fully-developed detonation wave emerges directly from the short length of the flash igniter section. His experiments indicate that rapid detonation initiation without a deflagration process, viz., direct initiation, is possible by the flash photolysis.

Although the initiation mechanism itself has not been revealed in the previous works, we may make the following important remarks on the photochemical initiation: Firstly, the flash photolysis technique does not provide completely homogeneous excitation of gas mixture; Secondly, detonation initiation occurs in the non-uniformly photo-dissociating gas mixture; Thirdly, the detonation can be initiated very rapidly within a small volume of gas mixture. Since the radiation source itself does not create any shock waves in photochemical initiation, the rapid detonation initiation observed indicates that a rapid shock wave amplification plays an important role in photochemical detonation initiation.

Aim and Outline of Thesis

The main purpose of the present research has been to elucidate the basic features of the shock wave amplification in combustible gas mixtures. In this research, the investigation of photochemical detonation

initiation has aimed to obtain a better understanding of the shock wave amplification phenomena. An important concept concerning the shock wave amplification mechanism has emerged from the investigation. The research has been further extended to some theoretical analyses of the shock wave amplification phenomena.*

This manuscript aims to describe the basic features of shock wave amplifications in non-uniformly reacting gases as well as the importance of the wave amplification in some of the detonation initiation phenomena.

It is well known that the detonation initiation phenomena involve other important aspects, such as three-dimensional shock wave interactions or chemical-gasdynamic instabilities. These aspects, however, are not within the scope of the present thesis, since the author does not intend to provide an overall discussion on the detonation initiation phenomena.

In Chapter 2, the basic features of photochemical detonation initiation are discussed. The schlieren photographs of the initiation phenomena, which have been obtained by Professor R. Knystautas, are described and discussed. In the present research, the reacting flow-field of a photochemically ignited gas mixture is numerically analyzed. The results show that a rapid shock wave amplification in the non-uniformly photo-dissociating gas mixture plays an important role in the photochemical detonation initiation. The results also indicate that the induction time gradient field generated by the strong irradiation provides an effective

---

* Since the important concept on the shock wave amplification mechanism (as will be shown in this thesis, "Shock Wave Amplification Through Coherent Energy Release") has emerged from the investigation of photochemical detonation initiation, the thesis title "Coherent Shock Wave Amplification in Photochemical Initiation of Gaseous Detonations" has been decided.

means of shock wave amplification. Based on the results of the numerical analysis, the concept of "SWACER" (Shock Wave Amplification through Coherent Energy Release) is proposed.

In Chapter 3, a simple theoretical model of moving energy source is introduced to illustrate the importance of the induction time gradient field in shock wave amplification. The coherence between the pressure waves and the temporal sequence of the energy release is particularly emphasized. The induction time gradient field is expressed in terms of the velocity of the moving energy source, and the non-steady flow-fields for different energy source velocities are numerically solved. The framework of the theoretical model is provided in the second section of the chapter, and the results of the numerical analysis are then discussed.

In Chapter 4, the shock wave amplification in non-uniformly preheated combustible gas mixtures is numerically analyzed in relation to the problem of detonation transition. In the introduction of this chapter, the relevant previous works are described. The following section is devoted to the presentation of a theoretical model. Finally, the results of the numerical analysis for the model are described and discussed.

Chapter 5 summarizes the main concluding remarks of the present research and provides some recommendations for future work.

In addition to the five chapters, five appendices are provided in the present thesis. These appendices also contain some of the important results obtained in the present research. Particularly, in Appendices I and II, the basic aspects of the photochemical explosions are reported. Interested readers should read these appendices.

CHAPTER 2

PHOTOCHEMICAL INITIATION OF GASEOUS DETONATIONS

1. Introduction

In this chapter, the basic features of photochemical detonation initiation are discussed. In Section 3, the initiation phenomena occurring in a photon-sensitive gas mixture of H_2-Cl_2 are described, based on the schlieren photographs obtained by Professor R. Knystautas. In Section 4, the flow-field of the photochemically ignited mixture is numerically solved using a finite difference method.

One of the main reasons for choosing H_2-Cl_2 gas mixture is that the mixture can easily detonate with relatively low radiation intensities. In fact, through a preliminary experiment*, the mixture was found to detonate most easily among all the gas mixtures tested. H_2-Cl_2 mixture has relatively simple and well-established chemical kinetics. Thus, the above-mentioned numerical analysis of the reacting non-steady flow-field was carried out relatively easily.

The following section is provided to illustrate the chemical kinetic aspects of the photochemical explosion in H_2-Cl_2 mixtures. The photon-absorption and photo-dissociation of Cl_2 are first described, and the constant volume combustion of a photochemically ignited H_2-Cl_2 mixture is then presented.

---

*In the preliminary experiment, measurement of the induction times for detonation initiation was made for C_2H_2-O_2, C_2H_2-O_2-NO_2, and H_2-Cl_2 mixtures. Details and results of this experiment are given in Appendix I-A.

2. Some Basic Aspects of Photochemically Initiated H_2-Cl_2 Reaction

A) Photon-Absorption and Photo-Dissociation of Molecular Chlorine

The absorption of a weak monochromatic light beam by molecular chlorine gas is described by the following Beer-Lambert law (see Sketch 1):

$$I = I_o \exp(-\varepsilon[Cl_2]x) \qquad (2\text{-}1)$$

where I represents the radiation intensity (energy per unit area per unit time) at a distance x from the window x=0; I_o is the incident radiation intensity at the window; ε denotes the photon-absorption coefficient of chlorine molecule which is a constant at a given wavelength; and $[Cl_2]$ is the concentration of chlorine molecule.

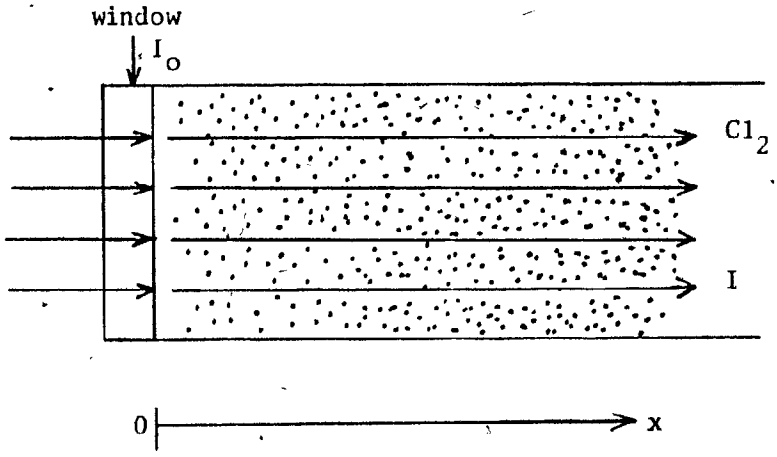

Sketch 1

From the above equation, we can define a characteristic photon-absorption length for a given wavelength and chlorine concentration by the following equation:

$$\ell^* = \frac{1}{\varepsilon[Cl_2]} \qquad (2\text{-}2)$$

The characteristic length ℓ^* is sometimes called the e-folding length.

In the Beer-Lambert equation (2-1), since the weak light beam generates negligibly weak photo-dissociation, the chlorine molecule concentration is assumed to be constant. However, when an intense light beam is used to induce strong and rapid photo-dissociation of chlorine molecules in a hydrogen-chlorine mixture, a significant change in the chlorine molecule concentration should result. This is not only because of the effect of strong photo-dissociation, but also because of the rapid consumption of chlorine molecules in the subsequent chain reactions of the mixture. The Beer-Lambert law will not apply in this case, since the variation of chlorine molecule concentration with time and distance must be considered. The loss of radiation intensity of a monochromatic light beam by the absorption of Cl_2 is given by the following equation:

$$\frac{\partial I}{\partial x} = -I\varepsilon[Cl_2] \qquad (2\text{-}3)$$

Since $[Cl_2]$ is a function of time and distance, integration of the above equation gives the following equation:

$$I = I_o \exp\left(-\varepsilon \int_0^x [Cl_2]\, dx\right) \qquad (2\text{-}4)$$

Fig. 1 shows the photon-absorption spectrum of chlorine molecule at room temperature. Since the bond energy of chlorine molecule is about 57.3 Kcal/mole corresponding to 4900 Å, photo-dissociation occurs only below this wavelength. Noticeable photon-absorption is in the range of 2500-4500Å, and the maximum absorption coefficient is situated at 3300 Å. Below 4990 Å, one chlorine molecule dissociates into two chlorine atoms: one normal ($^2P_{3/2}$) and one excited ($^2P_{1/2}$) chlorine atom:

$$Cl_2(^1\Sigma_g^+) + h\nu \rightarrow Cl(^2P_{3/2}) + Cl(^2P_{1/2}) \qquad (2\text{-}5)$$

where Cl_2 ($^1\Sigma_g^+$) is a normal chlorine molecule; h is the Planck's constant; and $h\nu$ is the energy of a quantum of light of frequency ν. The molecular

physics of chlorine photo-dissociation process are provided in the book by Calvert and Pitts (35). Since only ground-state chemical kinetics are considered in the present research, hereafter the photo-dissociation process (2-5) is expressed as follows:

$$Cl_2 + h\nu \rightarrow 2Cl \qquad (2\text{-}6)$$

The production rate of chlorine atom via photo-dissociation is obtained from Eq. (2-3). Since in Eq. (2-3) $(-\partial I/\partial x)$ is the photon energy absorbed by chlorine molecule per unit time and per unit volume, the change of concentration of the photo-dissociating chlorine molecules can be expressed by $I\varepsilon[Cl_2]/h\nu$. Since one chlorine molecule dissociates into two chlorine atoms, the production rate of chlorine atom via photo-dissociation $\frac{\partial[Cl]}{\partial t})_{photo}$ is given by:

$$\frac{\partial[Cl]}{\partial t})_{photo} = \frac{2I\varepsilon}{h\nu}[Cl_2] = \frac{2I_o\varepsilon \exp(-\varepsilon \int_0^x [Cl_2]dx)}{h\nu}[Cl_2] \qquad (2\text{-}7)$$

where [Cl] is the concentration of chlorine atom, and it is a function of time and distance.

The above equation indicates two points: The maximum production rate of chlorine atom occurs at the window (x=0) in the early stage of irradiation of light beam, thus the chain reaction of H_2-Cl_2 mixture first starts at the window; if the irradiation is provided after the start of the chain reaction at the window, the light beam will penetrate deeper into the H_2-Cl_2 mixture in the later times. This is because rapid decrease in chlorine molecule concentration occurs near the window by the chain reaction.

B) Reaction Mechanism of H_2-Cl_2 System

The H_2-Cl_2 reaction system has been extensively studied by many researchers, and detailed chemical kinetics of this reaction system are now available. Cohen et al. (36) have listed the most reliable rate constants of all the elementary reaction steps including excited chemical species. Kondratiev (35) has also collected some of the reaction rate constants from the recently published papers. The elementary reaction steps of groundstate chemical species are listed below:

$$Cl_2 + h\nu \rightarrow 2Cl \qquad (2\text{-}6)$$

$$H_2 + M \rightleftarrows 2H + M \qquad (2\text{-}7)$$

$$Cl_2 + M \rightleftarrows 2Cl + M \qquad (2\text{-}8)$$

$$H + Cl + M \rightleftarrows HCl + M \qquad (2\text{-}9)$$

$$H_2 + Cl \rightleftarrows HCl + H \qquad (2\text{-}10)$$

$$Cl_2 + H \rightleftarrows HCl + Cl \qquad (2\text{-}11)$$

where M denotes the third body.

The chain reaction of H_2-Cl_2 system starts by the generation of chain carriers (free radicals) H or Cl from H_2 or Cl_2. Reaction (2-6) is the chain-initiation step when an H_2-Cl_2 mixture is photochemically ignited. The forward reactions in (2-7) and (2-8) are the chain initiation steps when the mixture is thermally ignited. The forward reaction in (2-9) is a recombination reaction in which chain carriers H and Cl generate HCl. The forward reactions in (2-10) and (2-11) are called chain-carrying steps, and their net effect is that one Cl_2 molecule and one H_2 molecule are converted into two HCl molecules. A Cl atom or an H atom reappears and may therefore initiate the processes (2-10) and (2-11) again. Thus, the presence of a few free radicals causes the overall reaction to proceed very rapidly, and the exothermic process of H_2-Cl_2 reaction is mainly governed by these chain carrying steps.

A computer program was written to obtain the basic characteristics of the constant volume combustion of photochemically ignited H_2-Cl_2 mixtures. Governing equations of the constant volume combustion, assumptions made in the numerical analysis, and computation techniques are given in Appendix II-A*.

Fig. 2 illustrates the time-evolution of the chemical reaction of a photochemically ignited H_2-Cl_2 mixture. The variations of chemical species and temperature are shown in the figure. An equi-molar H_2-Cl_2 mixture at 100 torr initial pressure and 298°K initial temperature, and a 3300 Å (which corresponds to the peak Cl_2 absorption) 5 KW/cm^2 monochromatic light beam, are considered in this case. The increase of Cl concentration in the early stages (till about 15 μsec) is mainly attributed to the photo-dissociation of Cl_2. During this stage, the photochemically produced Cl atoms are relatively slowly entrained in the chain-carrying steps and, as a result, the concentration of HCl and H and the temperature increase. The reaction changes from the photochemical phase to the thermal phase at about 20 μsec. This may be indicated by the change of chlorine atom concentration. After the temporary decrease, the Cl concentration increases again due to the chain reaction in the thermal phase**. The reaction rates of chain-carrying steps are noticeably increased due to the thermal effect; the production rates of H, Cl and HCl as well as the temperature increase very rapidly. The production rate of Cl atom by Cl_2 photo-dissociation becomes less significant than that by the chain-carrying steps. After this very rapid chain reaction in the thermal phase, the rate of temperature rise begins to drop, and finally the reaction approaches an equilibrium state.

---

* In Appendix II-A, some results concerning the comparison between the photochemical and thermal ignitions of H_2-Cl_2 mixture are also given.

** The recent study on photochemical ignition of H_2-O_2 system by Cerkanowicz and Stevens (38) has also shown a similar behaviour of oxygen atom concentration.

As shown in the figure, in the present study, induction time is determined by taking the intercept of the tangent to the maximum slope of the temperature-time curve with the initial temperature line.

From the above description of the photochemical constant volume combustion and Eq. (2-7), we can see that the induction process prior to the thermally accelerated reaction is primarily governed by the production rate of chlorine atom, thus, the radiation intensity. Thus, the induction time decreases with increasing the radiation intensity. As will be shown in Section 4, the developments of pressure waves in the same H_2-Cl_2 mixture for different incident radiation intensities, are theoretically analyzed. For a better understanding of the results, it was required to estimate the effect of radiation intensity on induction time. The induction times for different radiation intensities are listed in Table 1, and are plotted in Fig. 3.

3. Detonation Initiation Phenomena Observed by Schlieren Photography (Based on the experiments by Professor R. Knystautas)

A) Brief Description of Experiments

Two different experimental apparatus were employed to observe the phenomena of photochemical detonation initiation by schlieren photography.

Fig. 4 shows a photograph of the first experimental apparatus, and Fig. 5 is a schematic diagram of the cross-section of the apparatus. A stainless steel rectangular box chamber (75x75 mm of square cross-sections and 15 cm long) was used. Four ultra-violet transmitting quartz plates (75 mm x 150 mm and 6 mm thick) were placed on the four sides of the chamber, and the other two sides were closed by stainless steel plates. At the center of each stainless steel plate, a piezoelectric pressure

transducer was mounted to monitor the explosion pressure inside the chamber. Two xenon flash tubes were placed about 3 cm from two opposite quartz windows. The flash tubes were connected in series with a high energy condenser. Two stainless steel plate reflectors covered the flash tubes to redirect as much of the flash irradiation as possible back into the chamber. The schlieren photography was taken through the other pair of quartz windows orthogonal to the direction of the flash irradiation. Due to the presence of the frames in which the quartz windows were mounted, the total unobstructed schlieren field was 5 x 12 cm, and about 12 mm of the gas from the quartz windows were not visible for schlieren photographic observation.

The second experimental apparatus was designed to permit schlieren observations of the phenomena occurring in the gas immediately adjacent to the incident flash irradiation. Fig. 6 shows a schematic diagram of the cross-section of the apparatus. A stainless steel cylindrical explosion chamber (10 cm I.D. and 10 cm long) was employed. The ends of the chamber were closed by two quartz windows through which a light beam for schlieren photography passed. A quartz window (85 mm diameter and 6 mm thick) was mounted on a cylinder (35 mm I.D.), and the quartz window was inserted inside the chamber at right angles to the axis of the chamber. The flash tube was the same one used in the first experimental apparatus and was placed 3 cm behind the quartz window. The gas mixture inside the chamber was irradiated through a 35 mm aperture of the window. In this apparatus, an edge-on view of the window of incident irradiation could be obtained, and the initiation phenomena occurring at the window surface were completely within the schlieren field.

The flash tube used in both the experimental apparatus was found to provide 250 μsec long flash irradiation irrespectively of the flash energy

(energy stored in the condenser). Detailed measurements of the flash tube output, such as spectrum analysis or measurement of actual radiation intensity were not pursued.

Detailed descriptions of the radiation source system, diagnostic tolls and techniques etc. are given in Appendix I-B.

B) Experimental Results and Discussions*

An equi-molar H_2-Cl_2 mixture at 100 torr initial pressure was used throughout the experiments.

At the start, although it seemed to be self-evident that the detonation initiation results from the combustion of the mixture itself and not from some shock waves which might be caused by strong photo-dissociation of Cl_2, this was carefully checked using the first experimental apparatus. Chlorine gas alone (100 torr) was loaded in the rectangular box chamber and irradiated by the flash tubes. Fig. 7 shows typical records of schlieren photograph and pressure transducers. The black arrow-like marker in the schlieren photograph indicates the center of the explosion chamber. The first hump in the pressure record corresponds to the electromagnetic noise generated by the rapid energy discharge inside the flash tubes. The small interruption following the first hump corresponds to the noise which is generated when the schlieren light spark is fired. Neither the schlieren record nor the pressure records show any recognizable pressure

---

* The author was involved in the early stage of these experimental studies. Using the rectangular box chamber and some pressure transducers, the author observed the pressure spikes of detonation waves. However, the author could not obtain schlieren photographs of the detonation initiation phenomena. This is because the author pursued the initiation phenomena for very high radiation intensity in which the detonation discontinuity was later found to disappear. Professor R. Knystautas refined the experimental system and kindly carried out these difficult experiments with a great patience. The author sincerely appreciates his kindness for his making the schlieren photographs and the pressure records available to the author.

waves, confirming that the photo-dissociation process of Cl_2 itself does not generate any shock waves.

The detonation initiation phenomena in an equi-molar H_2-Cl_2 mixture at 100 torr initial pressure were observed by the above experimental technique. A series of schlieren photographs and pressure records in Fig. 8 show the effect of flash energy on detonation initiation. As shown in Fig. 8-a, when the radiation intensity is above a certain critical value, two fully-developed detonation waves emerge from the top and bottom irradiated quartz windows into the schlieren field. The reason for the wavy contours of the detonation fronts may be due to some non-uniformity of flash irradiation. The reason why the top wave is initiated earlier than the bottom one may be that the radiation intensity of the top flash tube is larger than that of the bottom one. The abrupt jumps following the schlieren spark signals in the pressure records correspond to the reflected pressures of the two colliding detonation waves near the center of the chamber*. The time lag between the start of flash irradiation and the collision of detonation waves is about 50 μsec. Fig. 8-b corresponds to the case when the flash intensity is increased further. As far as the pressure records are concerned, in comparison with the previous case, no salient change is observed. However, the schlieren photograph shows some fading or "washing out" of the detonation fronts in this case. Fig. 8-c corresponds to the case when the flash intensity is increased furthermore. Since the schlieren photograph is taken in the early stage of the explosion, in this case, only one detonation wave emerges from the top window into

---

* The reflected pressure behind symmetrically colliding Chapman-Jouguet detonation waves is theoretically calculated in Appendix III. The result shows that the pressure is 6.46 atm (94.9 psi).

the schlieren field, and the other detonation wave generated near the bottom window can not be seen. The pressure records show that the time lag between the start of flash irradiance and the collision of waves becomes shorter ($\sim$ 40 μsec), and that the pressure jumps are noticeably reduced in comparison with the previous two cases. These changes of the appearance of detonation wave front indicate that very high radiation intensity does not necessarily result in formation of detonation wave in this explosion chamber. If very high radiation intensity is used, we may expect that gas mixture inside the chamber is uniformly excited, and that the explosion phenomenon rather approaches uniform constant volume combustion.

One of the most important conclusions obtained from the above experiments is that detonation is initiated directly using the flash photolysis technique. It has been shown that fully-developed detonation waves are established within a distance of about a centimeter from the flash irradiated windows.

Since the interesting region immediately adjacent to the flash irradiated window was not available for schlieren observations in the first experimental apparatus, the second experimental apparatus was employed.

In Fig. 9, a series of schlieren photographs show a phenomenon when the flash intensity is not sufficient to initiate detonation. The flash energy was about 580 J in this case. The photographs were accumulated from different experimental runs, and time intervals of the photographs are approximately 5 μsec. In the first frame of the figure, a dark region immediately adjacent to the quartz window shows the start of chemical reactions. A roughly hemispherical reaction front propagates outwardly from this dark region and, as shown in the fifth frame, a hemispherical

shock wave is then formed ahead of the reaction front. However, the shock wave is not strong enough to induce rapid chemical reaction in its wake, and consequently it decouples from the reaction front. Thus, detonation is not formed but rather a deflagration results.

Fig. 10 shows the phenomenon of detonation initiation when the flash intensity exceeds a certain critical value. The flash energy was about 700 J in this case. In contrast with the first frame in the previous figure, where the dark reaction zone is observed, the first frame in this figure shows that two hemispherical reaction-shock waves are already formed at the window. It seems that two strong reaction spots are formed due to some inhomogeneous excitation of the gas mixture, and that the waves originate from the spots. In the later times, the waves expand and collide with each other, as shown in the second to fourth frames, and consequently a fully developed detonation wave is formed (fifth frame) and propagates.

The above detonation initiation phenomenon is divided into two stages. The first stage involves the process of rapid formation of strong reaction shock waves, while the second stage is governed by the three-dimensional shock wave interactions. Since the time and spatial resolution of the schlieren photography was insufficient to permit capturing the detailed process of the phenomenon, it is improper to discuss which process is more significant. Nevertheless, we can conclude that the rapid formation of the reaction shock waves plays a significant role in the photochemical detonation initiation.

4. Numerical Analysis of Flow-Field of Photochemically Ignited H_2-Cl_2 Mixture

The flow-fields of photochemically ignited H_2-Cl_2 mixtures are numerically analyzed in this section. Although the present theoretical analysis does not simulate the above experimental conditions, it nevertheless elucidates the basic features of the rapid shock wave formation observed in the experiments.

The basic chemical kinetic aspects of photochemical H_2-Cl_2 reaction have already been presented in Section 2. In the following analysis, the coupled equations of gasdynamics and chemical kinetics are solved using a finite difference method.

The basic premise of the numerical analysis is that a 3300Å monochromatic light beam continuously penetrates through a window into an equi-molar H_2-Cl_2 mixture at 100 torr initial pressure and 298°K initial temperature. The flow-field is assumed to be one-dimensional. The length of the flow-field analyzed has been limited to about 3.5 cm from the radiation irradiated window, because the cost of numerical computation otherwise would have become formidably expensive due to the complex computation involved in the coupled gasdynamic-chemical equations. The numerical computation primarily analyzes the development of the reacting flow-field for different radiation intensities.

The finite difference method used is a modified leap-frog method. Governing equations for the reacting flow-field, details of the finite difference method, and procedures of the numerical computation are given in Appendix II-B.

In order to estimate the penetration of a 3300 Å light beam into an equi-molar H_2-Cl_2 mixture at 100 torr, a theoretical calculation was

made using the absorption spectrum of chlorine molecule and the Beer-Lambert law. Fig. 11 shows the normalized radiation intensity I/I_o (I_o; incident radiation intensity) with respect to the distance from the radiation transmitting window. The characteristic photon-absorption length (Eq. (2-2)) is about 2.5 cm. Thus, we see that the length of flow-field calculated in the numerical computation (3.5 cm) is sufficient to analyze the early stage of the development of pressure waves.

Figs. 12-14 show the development of pressure waves for incident radiation intensities $I_o = 5\times10^2$, 2.5×10^3, and 7×10^3 w/cm^2, respectively. In each figure, five pressure profiles at different times are provided. In order to indicate the development of the chemical reaction, positions at different HCl mole fractions (5, 10, 20, 30, 40, 50 and 60%) are given on the pressure profiles. Also, positions of the maximum pressure point are indicated on the pressure profiles. Temperature and HCl mole fraction at the maximum pressure point are given in the upper part of the figure.

Fig. 12 shows the development of pressure wave for the case in which the radiation intensity is not high enough to generate strong wave amplification. The first pressure profile shows that a pressure wave with relatively gentle gradient is developed near the window. Although the pressure wave thereafter grows and increases its gradient, its amplification process is slow and weak. In fact, we do not observe any salient increase in temperature and HCl mole fraction at the maximum pressure point* (pressure profiles 1-4 (time = 101.0 - 115.6 μsec)). As a result of this weak amplification, temperature and HCl mole fraction at the maximum pressure

---

* The slight non-smooth behaviour in temperature and HCl mole fraction at the maximum pressure point (profiles 1-4) may be attributed to some numerical instability.

point start to decrease noticeably (pressure profile 5 (time = 118.3 μsec)), indicating that the wave front may decouple from the reaction zone. Thus, in this case, detonation can not be formed, and a deflagration results.

Fig. 13 shows a rapid development of pressure wave for a higher incident radiation intensity. As shown in the first pressure profile, the gas mixture ahead of the maximum pressure point is already in process of strong reactions (20% HCl mole fraction in front of the maximum pressure point). As the pressure wave propagates forward into the reacting gas, the wave rapidly increases its amplitude and pressure gradient. Also, temperature and HCl mole fraction at the maximum pressure point increase.

Two major factors should be noticed for the above rapid wave amplification process. One is that the wave can be amplified by the combustion energy release from the already reacting gas mixture. The wave propagating into the reacting mixture is effectively amplified through such a mode of energy release. In other words, the amplification is due to the energy release in phase with the wave propagation. The other is that the amplified wave itself is capable of providing rapid chemical reaction by the compression effect; the rate of combustion energy release is further increased to enhance the wave amplification. Thus, as a whole, these two effects result in a rapid wave amplification, which may eventually lead to initiation of detonation.

Fig. 14 shows a development of pressure wave when radiation intensity is further increased. Due to the very high radiation intensity, very rapid chemical reaction starts near the window. Since chlorine molecule concentration rapidly decreases near the window, the irradiance penetrates much deeper into the gas mixture as the time goes on. Although the chemical reaction proceeds faster and the amplitude of the wave itself is

higher in this case than in the previous case, the fast reaction occurring ahead of the maximum pressure point rather prohibits formation of steep pressure gradient. This result indicates that the position of formation of steep pressure gradient becomes farther from the window with increasing radiation intensity. Although the result is not quantitatively comparable with the experimental results mentioned previously, it nevertheless shows the behaviour observed in the experiments using the rectangular box chamber.

The above results confirm that the radiation intensity is one of the important factors which govern the amplification of pressure waves. Furthermore, the results indicate the importance of the mode of combusion energy release in the non-uniformly reacting gas. Very high radiation intensity does not necessarily result in formation of steep pressure gradient field. Besides the results of numerical solution, one should notice that ideal homogeneous excitation of gas mixture results in uniform constant volume combustion, in which no shock wave is formed.

In order to illustrate the importance of the mode of energy release in non-uniformly reacting gases, the results of numerical analysis mentioned above are further examined. In Fig. 3 and Table 1, induction time of constant volume combustion in an equi-molar H_2-Cl_2 mixture at 100 torr initial pressure, has already been shown for different radiation intensities. Based on the Beer-Lambert photon-absorption law (see Fig. 11), for the three different incident radiation intensities, radiation intensity at a given distance x can be calculated. Thus, using the results shown in Fig. 3, as shown in the x-t diagram of Fig. 15, we can plot the induction time at different positions for the above-mentioned three cases of numerical analysis. Trajectories of the maximum pressure point are also plotted in

the figure. Although, in reality, the gasdynamic-chemical coupling effects become salient as the wave amplification proceeds, these effects can be neglected in the early stages.

It should be noted that relation between the induction time and the corresponding trajectory of the maximum pressure point differs for the three cases. For the case of the weakest incident radiation intensity, the maximum pressure point approaches the induction time curve. As shown in Fig. 12, this case corresponds to a weak wave amplification. Besides the fact that the chemical reaction rate is not sufficient for wave amplification, we see that the volume of photo-dissociating gas mixture is not sufficient to amplify the wave. For the case of the strongest radiation intensity, distance between the trajectory of the maximum pressure point and the induction time curve increases in the very early stages. This separation between the two curves is the reason for the relatively gentle slope of pressure profile in Fig. 14. For the case of the intermediate radiation intensity, the trajectory of the maximum pressure point is approximately parallel to the induction time curve. We see that this relation between the two curves is important in the wave amplification process. Indeed, one can recognize that the parallel motion of the curves makes the combustion energy release in phase with the pressure wave.

Although the above argument on the relation between induction time curve and pressure wave is valid only in the early stage of wave amplification process, it elucidates the important role of induction time gradient field in wave amplification phenomena.

5. Conclusions and Proposal of SWACER Mechanism

From the results presented in the preceding sections, we may conclude the following important remarks on a qualitative basis.

a) From the Experimental Records by Professor R. Knystautas

It is shown that direct detonation initiation is possible by the flash photolysis technique. In contrast with the blast initiation, where a sufficiently strong shock wave is generated externally by a powerful ignition source to initiate detonation directly, in the photochemical initiation, the direct initiation occurs primarily based on the combustion energy release of the gas mixture itself.

Radiation intensity is one of the important factors which govern the photochemical initiation. For direct initiation of detonation, a certain level of radiation intensity is required to induce sufficiently rapid chemical reactions in the irradiated mixtures.

The detonation initiation phenomenon observed involves two processes. In the first process, the strong reaction shock waves are formed in the non-uniformly reacting mixture. In the second process, the shock waves interact with each other to form a detonation wave. The rapid formation of the reaction shock waves plays an important role in the early stage of the photochemical detonation initiation.

b) Theoretical Results

The results of numerical analysis confirm that radiation intensity is one of the significant factors which govern the shock wave amplification. A certain level of radiation intensity is required for rapid shock wave amplification.

The results indicate that the combustion energy release in phase with the pressure wave can provide an effective means of wave amplification. In the early stages, an effective energy release is established by the induction time gradient field in the non-uniformly reacting gas, and the wave is amplified. In the later stages, the amplified wave itself is capable of enhancing rapid chemical heat release by the gasdynamic compression effects, and the wave is further amplified.

c) Proposal of SWACER Mechanism

The results of the present numerical analysis have suggested that one of the most effective processes for rapid shock wave amplification is such that the energy release from the combustion is in phase with the propagation of the shock wave. Such an effective amplification process can be sustained either by the induction time gradient field generated in non-uniformly reacting gas, or by the gasdynamic compression effects of the amplified wave itself. This shock wave amplification through the "coherent" energy release from the combustion is analogous to the principle of a laser, where a photon flux induces stimulated emission of radiation from excited molecules or atoms, and a very efficient amplification of the flux is obtained. Thus, we may refer to the shock wave amplification mechanism as the "SWACER" mechanism* representing "Shock Wave Amplification through Coherent Energy Release", in analogy to LASER which denotes "Light Amplification by Stimulated Emission of Radiation".

---

* A part of the results in this chapter have already been reported in the recent paper by Lee, Knystautas and the author (39), and the term SWACER mechanism has been proposed for the first time in the paper.

The SWACER mechanism can be one of the possible mechanisms which enhance detonation initiation. Effective shock wave amplification depends on whether or not a reacting flow-field maintains the SWACER mechanism for a sufficiently long duration. Various parameters, such as the induction time gradient, reactivity of gas mixture, or geometry of flow-field, should govern the SWACER mechanism. In the following chapters, the basic features of the SWACER mechanism are pursued through some numerical analyses.

CHAPTER 3

PRESSURE WAVES GENERATED BY MOVING ENERGY SOURCES

1. Introduction

In the preceding chapter, the concept of SWACER mechanism has been proposed. It has been shown that the induction time gradient field of the non-uniformly photo-dissociating gas mixture plays an important role in the shock wave amplification. Although the importance of the gradient field has emerged from the numerical analysis in the preceding chapter, the analysis has not fully illuminated the details of the amplification because of the complexity involved in the gasdynamic-chemical couplings.

Perhaps one of the most interesting questions is whether or not the gradient field can independently provide sufficiently strong shock wave amplification without any support of the gasdynamic-chemical coupling effects, which may also play a significant role in the shock wave amplification process. In this chapter, in order to resolve this interesting question and to illustrate the importance of the induction time gradient field, pressure waves generated in the gradient field are numerically analyzed by introducing a relatively simple theoretical model.

The basic idea of the theoretical model is illustrated by Sketch 1 below. We consider an inflammable mixture filled in a tube with a semi-infinite length. The heat release of the mixture is assumed to start right after the ignition. As shown in the x-t diagram of the sketch, we produce an induction time gradient field through such an ignition process. The induction time gradient is varied by changing the velocity of the igniter.

Using this theoretical model, we expect to investigate the basic aspects of the SWACER mechanism.

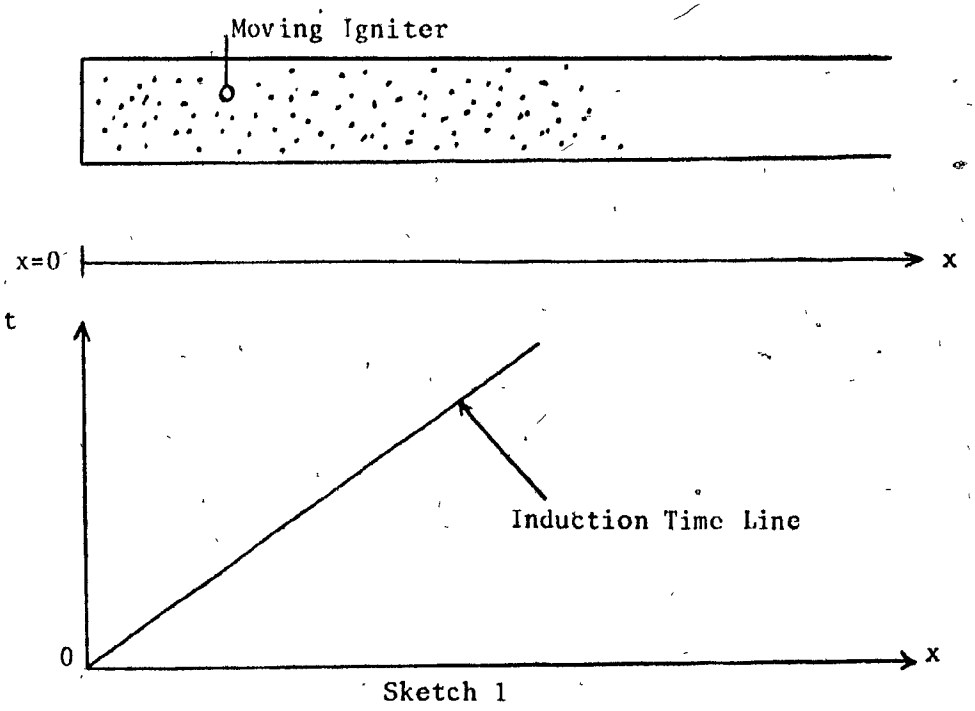

Sketch 1

The above theoretical model has already been considered in the book by Zeldovich and Kompaneets (40). However, since a similarity solution has been used in their analysis, gasdynamic profiles only in the steady propagation regime of shock wave have been obtained. In this chapter, the non-steady flow-fields generated by the moving energy sources are numerically analyzed using a finite difference method.

2. Theoretical Model

The theoretical model considered here is a one-dimensional system in which a fixed energy per unit mass Q_o is released at a rate $\dot{q}(x,t)$ by a moving energy source. Thermal conduction and viscosity effects are neglected. The gasdynamic equations are written in the following form:

Mass Conservation: $$\frac{\partial \rho}{\partial t} + \frac{\partial (\rho u)}{\partial x} = 0 \qquad (3\text{-}1)$$

Momentum Conservation: $$\frac{\partial u}{\partial t} + u \frac{\partial u}{\partial x} = -\frac{1}{\rho} \frac{\partial p}{\partial x} \qquad (3\text{-}2)$$

Energy Conservation: $$\frac{\partial p}{\partial t} + u \frac{\partial p}{\partial x} + \gamma p \frac{\partial u}{\partial x} = \rho(\gamma - 1)\dot{q} \qquad (3\text{-}3)$$

State of Gas: $$p = \rho R T \qquad (3\text{-}4)$$

where x is distance and t is time; ρ, u, p, and T denote density, velocity, pressure, and temperature respectively; and, γ and R represent the specific heat ratio and the gas constant respectively.

The solutions of the above equations depend on the particular form of the energy release function $\dot{q}(x,t)$, the initial state of the system, and the boundary conditions. In particular, a one-dimensional planar symmetric system, initially at rest, is considered (x=0 corresponds to the symmetry plane). Thus, the boundary condition and the initial conditions are written as follows:

Boundary Condition: $$u(0,t) = 0 \qquad (3\text{-}5)$$

Initial Condition: $$u(x,0) = 0$$

$$p(x,0) = p_o$$

$$\rho(x,0) = \rho_o \qquad (3\text{-}6)$$

$$T(x,0) = T_o = p_o/\rho_o R$$

where the variables with subscript "o" denote the initial states.

The energy release function is chosen in a form, which can simulate the energy release from the combustion zone travelling at a fixed and constant velocity V_o and depositing in each unit mass a total energy Q_o at a rate ω. It should be noted that the induction time gradient $d\tau_{ind}/dx$ is expressed in terms of the velocity V_o as

$$d\tau_{ind}/dx = 1/V_o$$

Consequently, $\dot{q}(x,t)$ may be written in the following form:

$$\dot{q}(x,t) = \omega(t - \frac{x}{V_o})\, H(t - \frac{x}{V_o}) \qquad (3\text{-}7)$$

where $\omega(\tau)(\tau = t - \frac{x}{V_o})$ satisfies the condition

$$\int_0^\infty \omega(\tau)\, d\tau = Q_o \qquad (3\text{-}8)$$

and where $H(\tau)$ is the Heaviside or step function

$$H(\tau) = 0 \qquad \tau < 0$$

$$= 1 \qquad \tau \geq 0 \qquad (3\text{-}9)$$

For mathematical convenience, we shall now select a functional form for $\omega(\tau)$ which may be integrated analytically and satisfies the condition (3-8). One such function is given as follows:

$$\omega(\tau) = \frac{Q_o\, \tau}{\tau_R^2} \exp\,(-\tau^2/2\tau_R^2) \qquad (3\text{-}10)$$

$$\tau = t - \frac{x}{V_o} \qquad (3\text{-}11)$$

and, as illustrated in Fig. 16, τ_R is the time required for $\omega(\tau)$ to reach its peak value. In analogy to the combustion problem, this characteristic time τ_R is referred to hereon as the "reaction time".

The total energy per unit cross-sectional area deposited by the energy source is denoted as E, and it is given as follows:

$$E = \int_0^\infty (\frac{p-p_o}{\gamma-1} + \frac{1}{2}\rho u^2)\, dx \qquad (3\text{-}12)$$

$$= \int_0^t \int_0^\infty \rho\,(x,t)\, \dot{q}\,(x,t)\, dx\, dt \qquad (3\text{-}13)$$

Using the characteristic time τ_R together with the initial conditions ρ_o, p_o, T_o, and c_o (initial sound velocity: $\sqrt{\gamma p_o/\rho_o}$), we can introduce the following dimensionless variables.

$$t^* = t/\tau_R, \qquad x^* = x/c_o\tau_R$$
$$p^* = p/p_o, \qquad u^* = u/c_o \qquad (3\text{-}14)$$
$$\rho^* = \rho/\rho_o, \qquad T^* = T/T_o$$

We obtain the following normalized equations by substituting the above variables into the equations (3-1)-(3-4).

$$\frac{\partial \rho^*}{\partial t^*} + \frac{\partial (\rho^* u^*)}{\partial x^*} = 0 \qquad (3\text{-}1')$$

$$\frac{\partial u^*}{\partial t^*} + u^* \frac{\partial u^*}{\partial x^*} = -\frac{1}{\gamma \rho^*} \frac{\partial p^*}{\partial x^*} \qquad (3\text{-}2')$$

$$\frac{\partial p^*}{\partial t^*} + u^* \frac{\partial p^*}{\partial x^*} + \gamma p^* \frac{\partial u^*}{\partial x^*} = \gamma(\gamma-1)\rho^* \dot{q}^* \qquad (3\text{-}3')$$

$$p^* = \rho^* T^* \qquad (3\text{-}4')$$

where

$$\dot{q}^* = Q^* (t^* - x^*/A) \exp\left(-\frac{1}{2}(t^* - \frac{x^*}{A})^2\right) \cdot H(t^* - \frac{x^*}{A})$$
$$Q^* = Q_o/c_o^2 \qquad (3\text{-}14)$$
$$A = V_o/c_o$$

In a similar manner, the boundary and initial conditions (3-5) and (3-6), and the total energy E in Eqs. (3-12) and (3-13) can be normalized as follows:

$$u^*(0,t^*) = 0 \qquad (3\text{-}5')$$
$$u^*(x^*,0) = 0$$
$$p^*(x^*,0) = 1 \qquad (3\text{-}6')$$
$$\rho^*(x^*,0) = 1$$
$$T^*(x^*,0) = 1$$

$$E^* = E/c_o p_o \tau_R = \int_0^\infty \left(\frac{p^*-1}{\gamma-1} + \frac{\gamma}{2}\rho^* u^{*2}\right) dx^* \qquad (3\text{-}15a)$$

$$= \int_0^{t^*}\int_0^\infty \gamma \rho^* \dot{q}^* \, dx^* \, dt^* \qquad (3\text{-}15b)$$

where E^* is the normalized total energy per unit cross-sectional area.

The above normalized governing equations show that the parameters, the specific heat ratio γ, the normalized energy release per unit mass Q^*, and the Mach number of the energy source A, determine the amplification process of pressure waves. In this analysis, $\gamma = 1.4$ and $Q^* = 10$ are assumed, and the flow-fields generated for different energy source Mach numbers are numerically analyzed, using a hybrid version of the Van Leer's finite difference scheme (42)* and the Boris-Book's antidiffusion method (44-46)**. Details of the numerical computation are given in Appendix IV.

For given values of Q^* and γ, we can calculate the pressures of the Chapman-Jouguet detonation wave and the constant volume combustion. Thus, we assess the strength of the pressure wave obtained through the numerical analysis, in comparison with these values. The Chapman-Jouguet detonation Mach number M_{CJ} and the shock pressure of the detonation (i.e. so-called von Neumann pressure) $p_{V.N.}$ are obtained using the Rankine-Hugoniot relations (41):

$$M_{CJ} = \sqrt{1 + \frac{\gamma^2-1}{2} Q^*} + \sqrt{\frac{\gamma^2-1}{2} Q^*} \qquad (3\text{-}16)$$

$$\frac{p_{V.N.}}{p_o} = \frac{2\gamma M_{CJ}^2 - \gamma + 1}{+1} \qquad (3\text{-}17)$$

The constant volume combustion pressure $p_{C.V.}$ is given by the following equation:

---

* The author is grateful to Professors Taki (Fukui University, Japan) and Fujiwara (Nagoya University, Japan) (43) for pointing out this finite difference scheme to him.

** The author would like to thank Professor G.G. Bach (McGill University) for helpful discussions and suggestions on this method.

$$\frac{p_{C.V.}}{p_o} = 1 + \gamma(\gamma-1)\, Q^* \qquad (3\text{-}18)$$

For $Q^* = 10$ and $\gamma = 1.4$, we obtain $M_{CJ} = 4.60$, $p_{V.N.}/p_o = 24.9$, and $p_{C.V.}/p_o = 6.6$.

3. Results and Discussions

The flow-fields generated for energy source Mach numbers $\Lambda = 0.5$, 1, 3, 3.5, 4, 4.25, 4.5, 5, and 6 were numerically analyzed. In particular, Figs. 17-26 display the pressure profiles and the x-t diagrams for $\Lambda = 0.5$, 1, 3, 4, and 5.

In Fig. 17, the development of pressure wave for $\Lambda = 0.5$ is illustrated. In the figure, the "energy source" represents the dominant region of energy release. More precisely, it covers from the front of energy source to the point where the volumetric energy release rate $(\rho\dot{q})$ is 10% of the maximum of $(\rho\dot{q})$. In the figure, we can notice the early formation of a shock wave which immediately runs away from the energy source. The third pressure profile shows that the peak pressure has decreased after the detachment of the shock wave from the energy source. The shock wave propagation soon approaches a steady state regime, and the quiescent field right behind the rear edge of the energy source is indicated by the flat pressure profile.* The interaction between the pressure wave and the energy release for this case is more clearly illustrated in the x-t diagram of Fig. 18, where the trajectories of the point of the maximum volumetric energy release rate $(\rho\dot{q})_{max}$ and the maximum pressure point (p_{max}) are shown. The coherent energy release to the pressure wave lasts only

* It was observed that $|u^*| \lesssim 10^{-2} \sim 10^{-3}$ right behind the rear edge of the energy source.

$t^* \sim 4$, and after the decoupling, the amplification immediately decreases. The trajectories of p_{max} and $(\rho\dot{q})_{max}$ show that the shock wave propagates at a constant velocity after $t^* \sim 8.5$. Figs. 19 and 20 correspond to the case of A = 1. The flow-field is similar to the previous case with the exception that the shock detachment occurs later and a larger peak pressure results. In both cases, weak shock wave amplification is observed with peak pressure far below that of the constant volume combustion ($p_{C.V.}/p_o = 6.6$)

In contrast with the above cases, the cases of A = 3 and 4 reveal strong shock wave amplification. Fig. 21 shows the pressure profiles for the case of A = 3, while Fig. 22 is the corresponding x-t diagram. We observe a strong shock wave amplification over a time $t^* \sim 8$. During this period, the energy source remains in close proximity of the shock wave to provide a coherent energy release. Furthermore, the shock wave produces a region of high density. Thus, the volumetric energy release rate ($\rho\dot{q}$) maintains a high magnitude, and a peak pressure far above that of the constant volume combustion results. After this amplification process, the shock wave starts to decouple from the energy source, and a steady propagation regime of the wave results. Figs. 23 and 24 corresponds to the case of A = 4. In this case, the shock wave travels closely with the energy source for a longer period than in the previous case, and this results in a higher peak pressure. As shown in the pressure profiles, the peak pressure is almost that of the Chapman-Jouguet detonation.

Figs. 25 and 26 show the development of pressure wave for the case of A = 5 in which the energy source Mach numer exceeds M_{CJ} (=4.6). In this case, no shock wave is formed but rather a broad compression wave propagates. Fig. 26 shows that $(\rho\dot{q})_{max}$ point is always ahead of the p_{max}

point, and this is in contrast with the previous cases of $A < M_{CJ}$. Since the energy release becomes less coherent in this case than in the previous case, a lower peak pressure results. As shown in Fig. 25, the compression wave broadens as the time goes on, and finally the compression wave starts to propagate in a steady state regime where the velocity of p_{max} point is less than the Chapman-Jouguet detonation velocity. As we increase A, the effect of the wave broadening becomes more salient, and the energy is distributed more evenly, thus the amplification decreases. In the limit $A \to \infty$, the energy release becomes, of course, completely uniform, and the constant volume combustion results.

In order to properly evaluate the efficiency of various energy sources for shock wave amplification, the following two parameters are considered. One is the peak pressure ratio p_{max}/p_o. The other is E^*, which is the normalized total energy deposited by energy source (see Eqs. (3-15a) and (3-15b)). Fig. 27 shows the variation of the peak pressure ratio p_{max}/p_o, with respect to the energy source Mach number A and the normalized total energy E^*. We can evaluate which energy source provides the maximum value of p_{max}/p_o for a given value of E^*. In other words, we can assess the relative efficiency of various energy sources. It is shown that the optimal source Mach number is in the range $1 < A < M_{CJ}$, and that its exact value obviously depends on the total energy deposited. The curves in this region intersect in such a way that a given source remains optimal only temporarily as it becomes immediately superseded by a faster source. Consequently, the optimal Mach number monotonically increases with E^* and approaches M_{CJ} as $E^* \to \infty$, indicating that the Chapman-Jouguet detonation itself is the most efficiently amplified wave in the steady propagation regimes.

The results of the present numerical analysis have illustrated the basic aspects of the SWACER mechanism. It is clearly shown that effective shock wave amplification requires that the energy source and the pressure wave travel in close proximity to each other. The unison between the two establishes the coherence and determines the resulting amplification process. Furthermore, due to the resulting local increase in density, the volumetric energy release is increased, which in turn further enhances the amplification process. If the decoupling of the pressure wave from the energy source occurs, the coherent energy release immediately breaks down, and the shock wave amplification ceases. Thus, the generation of strong shock wave depends on whether or not the coherent energy release can be maintained for a sufficiently long period.

Within the framework of the present theoretical model, the results have confirmed that the induction time gradient field has the potential of rapidly amplifying a shock wave to a strength above that of constant volume combustion to that of a Chapman-Jouguet detonation with comparable heat release. Thus, it is now obvious that a detonation initiation can be triggered in the gradient field if a non-uniformly reacting gas mixture can provide a coherent energy release to the shock wave for a sufficiently long duration. One may notice that the following conditions must be satisfied for detonation initiation. Firstly, inside the volume of the reacting gas mixture, a certain non-uniformity of reaction must provide a proper induction time gradient field as well as the coherence between the energy release and the resulting shock wave. Secondly, the volume of the gas must be sufficiently large to generate a shock wave which is strong enough to auto-ignite the gas outside the volume. The volume required for generating an auto-igniting shock wave depends on the

reactivity of the gas. The present results indicate that gas mixtures with larger reaction times, thus, weaker gas mixtures require a corresponding larger volume of the gas mixtures. It has been shown that the length of gas required for strong shock amplification is proportional to the reaction time τ_R. If these conditions are satisfied, an auto-igniting shock wave can be generated, and finally a detonation wave may propagate outside the volume.

CHAPTER 4

SHOCK WAVE AMPLIFICATION IN NON-UNIFORMLY PREHEATED GASES

1. Introduction

In the preceding chapter, the results have suggested that detonation initiation can be triggered in a non-uniformly reacting field if the SWACER mechanism is sustained for a sufficiently long time. Indeed, as mentioned in the introduction of this thesis, the recent experiments by Knystautas et al. (15) have demonstrated that, by means of obstacles, the non-uniformly reacting field of intense turbulent mixing can generate a rapid shock wave amplification, which leads to a formation of detonation.

There are some previous theoretical works which investigated the detonation initiation in non-uniformly reacting gas mixtures. Zeldovich et al. (47) have investigated the formation of detonation waves in non-uniformly preheated gases. In their analysis, a finite length of gas is considered, and at the end of this length a still adiabatic wall is assumed. The initial temperature distribution is assumed such that temperature decreases linearly from a high temperature at the wall with a constant gradient. The flow-fields for different initial temperature distributions have been numerically analyzed. They have demonstrated that, for certain initial temperature gradients, detonation waves are formed via a rapid shock wave amplification.

Barthel and Strehlow (48) have more recently studied the formation and propagation of spherical shock waves occurring when the reactivity of explosive gas is non-uniformly enhanced inside a sphere of gas mixture. Their analysis have shown that detonation transition is possible through a rapid shock wave amplification. Thus, it is shown that the detonation

initiation through a shock wave amplification occurs in three-dimensional geometry as well.

In this chapter, the shock wave amplification in non-uniformly preheated gases is numerically analyzed in connection with the detonation transition. A theoretical model similar to the above-mentioned model by Zeldovich et al. is pursued in the present study. The present analysis particularly emphasizes the important role of the gradient field in the wave amplification as well as the effects of important factors, such as reactivity of gas mixture or gasdynamic parameters. As mentioned in the previous chapter, the minimum volume of non-uniformly reacting gas required for detonation initiation should depend on the reactivity of gas. In the following analysis, the induction and exothermic processes of reacting gas mixtures are described by a relatively simple model. We shall investigate whether or not the coherent shock wave amplification is maintained in the preheated volume for different combinations of parameters which are involved in the chemical reactions and gasdynamics. Finally, we shall seek for the conditions for detonation initiation in terms of the dominant parameters.

2. Theoretical Model

We consider a non-uniformly preheated gas mixture in the space $x \geq 0$, in a one-dimensional planar symmetric system. The initial temperature distribution is assumed as follows: (see Sketch 1 below):

$$\begin{aligned} T(x,0) &= T_w - \frac{T_w - T_o}{L} x \qquad (0 \leq x \leq L) \\ &= T_o \qquad\qquad\qquad\quad (x > L) \end{aligned} \tag{4-1}$$

where T_w is the initial temperature of the gas at x=0; T_o is the temperature outside the preheated region; and L is the length of the preheated gas. The field is assumed to be quiescent initially, that is,

$$p(x,0) = p_o, \qquad u(x,0) = 0 \tag{4-2}$$

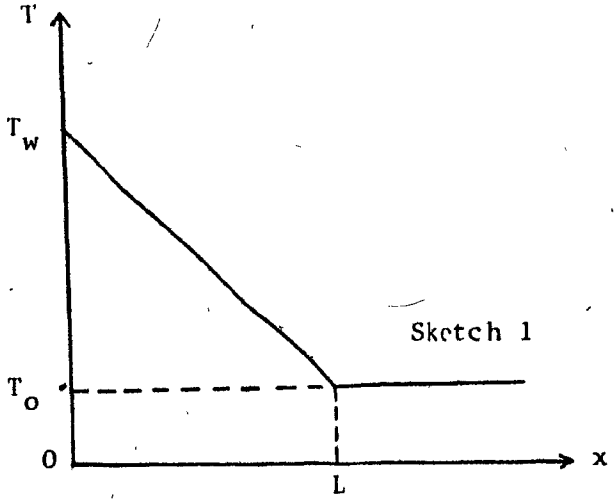

Sketch 1

The reaction of each gas particle is described by a simple Arrhenius induction time law and a heat release function. The induction process is expressed by the following equation:

$$\frac{d\lambda}{dt} = -k\rho \exp(-E_{act}/RT) \qquad (\text{if } T \geq T_{ig}) \tag{4-3}$$

where d/dt is the substantial derivative; λ represents the progress of induction process; λ = 1 and 0 correspond to the start and termination of induction process respectively; pre-exponential factor k and activation energy E_{act} are constants; and T_{ig} is the ignition temperature below which the induction process does not proceed. The above equation indicates that the induction process largely depends on the temperature of gas. From the initial temperature distribution, we see that the induction time of the particle at x=0 $t_{ind.w.}$ is the minimum. The induction time $\tau_{ind.w.}$ is given by the following equation:

$$\tau_{ind.w.} = \frac{1}{k\rho_w} \exp\left(E_{act}/RT_w\right) \qquad (4\text{-}4)$$

where ρ_w is the initial density at x=0. The induction times of other gas particles may deviate from the initial ones due to the development of the gas expansion starting at x=0.

The gas starts to liberate heat after the induction process. According to the heat release function used for the analysis in the preceding chapter, we express the exothermic reaction of each gas particle as follows:

$$\dot{q} = \frac{Q_o \tau}{\tau_R^2} \exp\left(-\tau^2/2\tau_R^2\right) \qquad (4\text{-}5)$$

$$\tau = t - t_{\lambda=0}$$

where τ_R is the characteristic reaction time at which $\dot{q}$ approaches the maximum heat release rate, and $t_{\lambda=0}$ is the time when the induction process terminates.

In order to follow the reaction of each gas particle, in the present numerical computation, the governing equations of gasdynamics are written in the following Lagrangian form:

Mass Conservation: $$\frac{\partial v}{\partial t} - \frac{\partial u}{\partial \xi} = 0 \qquad (4\text{-}6)$$

Momentum Conservation: $$\frac{\partial u}{\partial t} + \frac{\partial p}{\partial \xi} = 0 \qquad (4\text{-}7)$$

Energy Conservation: $$\frac{\partial e}{\partial t} + \frac{\partial (pu)}{\partial \xi} = \dot{q} \qquad (4\text{-}8)$$

State of Gas: $$p = \rho RT \qquad (4\text{-}9)$$

where $v = 1/\rho$ (4-10)

$$e = \frac{pv}{v-1} + \frac{1}{2}u^2 \qquad (4\text{-}11)$$

$$d\xi = \rho(dx - udt) \qquad (4\text{-}12)$$

and where ξ is the independent variable in the Lagrangian coordinates, and $\xi = 0$ corresponds to $x = 0$. The boundary condition at the wall ($\xi=0$) is given as follows:

$$u(0,t) = 0 \tag{4-13}$$

Using the initial conditions outside the preheated region, namely, ρ_o, p_o, T_o, and sound velocity c_o, together with the length L and the characteristic gasdynamic time τ_g ($=L/c_o$), we introduce the following dimensionless variables:

$$\begin{aligned} t^* &= t/\tau_g, & x^* &= x/L \\ v^* &= v/v_o (v_o = 1/\rho_o), & p^* &= p/p_o \\ T^* &= T/T_o, & u^* &= u/c_o \\ d\xi^* &= (dx^* - u^* dt^*)/v^* \end{aligned} \tag{4-14}$$

We can obtain the following normalized equations by substituting the above variables into the original dimensional equations.

$$\text{Mass Conservation:} \quad \frac{\partial v^*}{\partial t^*} - \frac{\partial u^*}{\partial \xi^*} = 0 \tag{4-15}$$

$$\text{Momentum Conservation:} \quad \frac{\partial u^*}{\partial t^*} + \frac{\partial}{\partial \xi^*}\left(\frac{p^*}{\gamma}\right) = 0 \tag{4-16}$$

$$\text{Energy Conservation:} \quad \frac{\partial e^*}{\partial t^*} + \frac{\partial}{\partial \xi^*}\left(\frac{p^* u^*}{\gamma}\right) = \dot{q}^* \tag{4-17}$$

$$\text{where } e^* = \frac{p^* v^*}{\gamma(\gamma-1)} + \frac{1}{2} u^{*2} \tag{4-18}$$

$$\dot{q}^* = \alpha \tau^* Q^* \exp\left(-\frac{1}{2} \alpha^2 \tau^{*2}\right) \tag{4-19}$$

and where $\alpha = \tau_g/\tau_R$, $\tau^* = t^* - t^*_{\lambda=0}$ and $Q^* = Q_o/c_o^2$.

$$\text{Induction Parameter:} \quad \frac{\partial \lambda}{\partial t^*} = -\frac{k^*}{v^*} \exp\left(-\frac{E^*_{act}}{T^*}\right) \tag{4-20}$$

$$(\text{if } T^* \geq T^*_{ig})$$

where $k^* = k\rho_o \tau_g$, $E^*_{act} = E_{act}/RT_o$, and $T^*_{ig} = T_{ig}/T_o$.

Position of Gas Particle: $x^*(\xi^*,t^*)=\int_0^{\xi^*} v^*(\xi^*,t^*)d\xi^*$ (4-21)

Initial Conditions: $T^* = T_w^* - (T_w^* - 1)x^* (x^* \leq 1)$ (4-22)

$= 0 \qquad (x^* \geq 1)$

$p^* = 1, \; u^* = 0$ (4-23)

where $T_w^* = T_w/T_o$.

Boundary Condition: $u^*(0,t^*) = 0,$ (4-24)

From the above normalized equations (4-14)-(4-24), we find the following dimensionless parameters, which govern the chemical-gasdynamic process occurring in the preheated gas mixture:

$$T_w^*, \; T_{ig}^*, \; Q^*, \; E_{act}^*, \; \gamma$$

$$\alpha(= \tau_g/\tau_R) \text{ and } \beta(= \tau_g/\tau_{ind.w.})$$

In the following analysis, the effects of the length of preheated gas and the reactivity of gas are particularly emphasized. For this reason, the first five of the above parameters are to be held constant throughout the numerical analysis: $T_w^* = 4$, $T_{ig}^* = 8/3$, $Q^* = 20$, $E_{act}^* = 50$ and $\gamma = 1.4$, while the remaining parameters α and β are varied so as to determine their relative influence on the shock wave amplification process. The parameter α denotes the ratio of the characteristic gasdynamic time to the characteristic heat release time, while the parameter β is the ratio of the characteristic gasdynamic time to the characteristic induction time.

For $Q^* = 20$ and $\gamma = 1.4$, the corresponding Chapman-Jouguet detonation Mach number M_{CJ} and the von Neumann pressure jump $p_{V.N.}/p_o$, are given by Eqs. (3-16) and (3-17): $M_{CJ} = 6.35$ and $p_{V.N.}/p_o = 46.9$.

The finite difference method employed in the present numerical analysis is a hybrid version of MacCormack's second-order explicit scheme (49,50) and Boris-Book's antidiffusion method (44-46). Details of the finite difference method and procedure of the numerical computation are given in Appendix V.

In most computer runs, the computational grids for ξ covered the length $0 \leq x^* \leq 1.0 \sim 1.3$ so as to discern whether or not the SWACER mechanism is sustained in the preheated length for various combinations of the parameters α and β.

3. Results and Discussion

Fig. 28 shows the pressure profiles for the case of $\alpha = 45.45$ and $\beta = 27.58$. We observe a strong shock wave amplification which has the potential of forming a detonation wave. In the figure, we can see that the reaction front propagating in phase with the pressure wave is responsible for such a strong amplification. Fig. 29 is the corresponding x-t diagram which shows that the amplification process is divided into three stages. In the early stage of the amplification process ($t^* \lesssim 0.06$), the reaction front follows the trajectory prescribed by the initial induction time curve (which is calculated based on the initial distributions of temperature and density). A compression wave is formed as described in the previous chapter. In the second stage ($0.06 \lesssim t^* \lesssim 0.15$), the wave then propagates into neighbouring hot gas which is under the induction process. Although the amplitude of the wave is relatively small, the induction time of the neighbouring hot gas is reduced by the compression effects. The resulting heat release, in turn, reinforces the amplification of the wave. Finally, a strong shock wave is established, and the perfect

coherence between the wave and the reaction front continues to accelerate the amplification further. The wave amplification in this stage may be called self-coherence, because the shock-heating of the wave itself becomes the most dominant. We can consider that the first two stages of the amplification process provide certain conditions for establishing the self-coherent amplification mechanism. When the shock passes through the edge of preheated region at $x^*=1$, the shock over-pressure is about 40% of the von Neumann spike. Since the shock wave is sufficiently strong inducing rapid heat release, the wave will eventually grow into a detonation wave.

Fig. 30 shows the pressure profiles for the case of $\alpha = 11.36$ and $\beta = 27.58$, and the corresponding x-t diagram is given in Fig. 31. In comparison with the previous case, this case has a smaller value of α and the same value of β. We can see that an increase in the characteristic reaction time relative to the characteristic gasdynamic time reduces the rate of wave amplification and results in a weaker amplification. A compression wave with a gentle slope is formed, and the wave propagates with increasing its strength. Although the initial induction time curve is identical to that of the previous case, due to a slower reaction rate (a larger ratio of the characteristic reaction time to the characteristic gasdynamic time), the distance between the wave front and the reaction front is relatively large. This prevents effective energy release to the wave. A shock wave is then established at time $t^* \lesssim 0.35$. However, the wave is not strong enough to rapidly induce heat release from the gas mixture ahead which is at a relatively low temperature. Thus, as a result, the reaction front starts to decelerate, and the distance between the shock and the reaction front progressively increases. As shown in the last

pressure profile of Fig. 30, the shock pressure ratio is only about 4, which is insufficient even to induce induction process of the gas mixture outside the preheated region. Therefore, the shock wave decays outside the preheated region.

Figs. 32 and 33 respectively show the pressure profiles and the x-t diagram for the case of $\alpha = 45.45$ and $\beta = 2.207$. In comparison with the case of $\alpha = 45.45$ and $\beta = 27.58$, in this case, β has been reduced to a lower value. We observe that the initial induction time gradient has become larger. It is shown that an increase in the characteristic induction time relative to the characteristic gasdynamic time prevents strong shock wave amplification. The trajectory of the reaction front deviates from the initial induction time curve in the very early stages. The reaction front and the maximum pressure point travel in unison for a relatively long duration ($0.5 \lesssim t^* \lesssim 0.7$). However, the effect of the large induction time becomes salient as the time goes on, and it prevents wave amplification. In particular, this is clearly shown in the noticeable deceleration of the reaction front after time $t^* \approx 0.8$. As a result, we observe a rapid increase of the distance between the shock wave and the reaction front.

From the above three cases, we see that increase in either of the parameters α or β enhances the shock wave amplification. For certain combinations of the parameters, the SWACER mechanism is maintained and rapidly amplifies a shock wave to a certain strength which is capable of triggering the onset of detonation. The amplification process is divided into three stages. In the first stage, a pressure wave is amplified primarily due to the energy release from the prescribed initial induction time gradient field. In the second stage, the amplified wave itself starts

to induce the heat release of neighbouring preheated gas. Finally, in the third stage, a shock wave is formed, and a self-coherent amplification is established by a strong shock-heating effect. We can consider that the establishment of the self-coherent stage depends on the first two stages. If a pressure wave is not developed to a certain strength in the first two stages, the self-coherent stage will never be established, and consequently the wave starts to decay.

Table 2 summarizes the results of computer runs for various combinations of the parameters α and β. In the table, for each computer run, the shock pressure ratio p_s/p_o near the edge of the preheated region, the position of the shock wave x_s/L, the position of the reaction front x_r/L, and the normalized time t/τ_g are given, and the criterion for the wave amplification is also provided*.

The criterion for the wave amplification is based on the fact that the shock wave and the reaction front must propagate in unison for sustaining the coherent energy release in the entire preheated region of gas mixture. Quantitatively speaking, though it may involve some arbitrariness, the case, in which a shock wave is followed by a reaction front within the distance of 0.02 L at the edge of the preheated region, is considered to have the potential of detonation formation through the coherent shock wave amplification. Such a case is referred to as "coupled" in the table, based on the relation between the shock wave and the reaction front. If

---

* The case of Run 20 is an exceptional one. Because the criterion could be easily obtained from a salient decoupling between the shock wave and the reaction front in the early stages, and because quite a large number of mesh points were required to resolve the reaction zone accurately, further computation was not carried out to avoid unnecessary cost of the computation.

the coherent shock wave amplification is not sustained, the shock decouples from the reaction front. This case is referred to as "decoupled".

In the above table, we notice that, in all the coupled cases, the shock pressure ratio is at least above 12.7. One may easily verify that the value is above that of the shock wave which has the minimum strength required for triggering induction process of the non-heated gas particles outside the preheated region. From the well-known Rankine-Hugoniot shock wave relation, we see that the shock Mach number for providing the ignition temperature T^*_{ig} is 2.99. The corresponding shock pressure ratio is 10.3. Thus the shock pressure ratios in all the coupled cases are certainly above this value.*

The criteria for shock wave amplification in Table 2 are plotted in the α-β plane of Fig. 34. The regime of the coupled cases is separated from that of the decoupled cases by the curve AB. In the range $2 \lesssim \beta \lesssim 140$, the minimum length of the preheated gas required for sustaining the coherent shock wave amplification increases from about 20 $c_o\tau_R$ to 45 $c_o\tau_R$ with decreasing the value of β. In the range $\beta \lesssim 2$, the minimum length required sharply increases, while, for very large value of β, we notice that the minimum length must be at least greater than about 10 $c_o\tau_R$.

The present relatively simple model has served well to elucidate the basic features of the shock wave amplification phenomena occurring in the preheated gas mixtures. The present parametric study has also emphasized

---

* Runs 9 and 12 are critical cases. Although the shock pressure ratios are above 10.3, the distance between the shock and the reaction front is greater than 0.02 L ($x_s/L - x_r/L > 0.02$) for both the cases. Thus, these cases are referred to as decoupled in Table 2.

the relative importance of the characteristic gasdynamic, induction, and reaction times in the amplification phenomena. The results show that the reactivity of explosive gases is one of the important factors involved in the shock wave amplification, which has already been pointed out by Meyer and Oppenheim (21). As mentioned in the introduction of the present thesis, the transition process induced by obstacles occurs in the non-uniformly reacting turbulent field which is similar to the preheated field considered in the present theoretical model. Thus, the present results suggest that the above-mentioned parameters are also significant in the transition phenomena.

CHAPTER 5

CONCLUDING REMARKS AND RECOMMENDATIONS FOR FUTURE WORK

The basic aspects of the rapid shock wave amplification, which occurs in non-uniformly reacting gases, have been the main theme of the present thesis. The important concept of the SWACER mechanism has emerged through the numerical analysis of the flow-field of photochemically ignited gas mixtures. The research has been extended to the theoretical analysis, which has aimed to elucidate the basic aspects of the SWACER mechanism and to show the importance of the amplification mechanism in some of the detonation initiation processes.

In the following, the important results of the present research are summarized (as numbered 1 to 5) and some recommendations for future work are also provided.

Chapter 2

In the preliminary investigations, the basic aspects of the photochemical constant volume combustion and the photochemical detonation initiation, have been studied (Appendices I and II). The schlieren photographs obtained by Professor R. Knystautas have shown that the rapid formation of the shock waves in the photochemically ignited gas mixture plays a significant role in the photochemical detonation initiation.

1. The results of the present numerical analysis have shown that the radiation intensity is one of the important factors which govern the shock wave amplification. If the radiation intensity is not strong enough to induce sufficiently fast chemical reactions, the pressure wave can not be amplified strongly, and the decoupling of the wave from the reaction zone results in a deflagration. The results have also suggested that very

high intensity of radiation does not necessarily result in rapid formation of shock wave. It is shown that the explosion rather approaches uniform constant volume combustion.

2. The examination of the results has suggested an important aspect of the shock wave amplification. It is shown that the coherence between the pressure wave and the energy release from the combustion is one of the most effective means of shock wave amplification. It is found that the coherent shock wave amplification can be established either by the induction time gradient field, or by the compression effects of the amplified wave itself. The concept of "SWACER" mechanism has been proposed.

Chapter 3

3. A theoretical study on the coherence phenomenon between energy release and pressure wave has been carried out. Such a study has stemmed from a consideration that the real gasdynamic-chemical coupled shock wave amplification is, in essence, the phenomenon of the interaction between the pressure wave and the temporal-spatial sequence of energy release. The flow-fields generated by moving energy sources, which are governed by the induction time gradient field, are numerically analyzed. Within the framework of the theoretical model, the optimum Mach number of the moving source has been searched so as to assess the strongest shock wave amplification. It is clearly shown that effective shock wave amplification requires that the energy source and the pressure wave travel in close proximity of each other. The optimum source Mach number A^* is in the range $1 < A^* < M_{CJ}$ and depends on the total energy deposited by the source. With increasing the total energy, A^* approaches M_{CJ} and the corresponding shock overpressure increases. If the source Mach number A is in the range $A > M_{CJ}$,

no shock wave is formed and a compression wave results. Therefore, at the steady propagation regime, the energy source travelling at the Chapman-Jouguet detonation velocity corresponds to the optimal condition for the pressure rise among all the possible energy sources.

Chapter 4

4. The shock wave amplification in non-uniformly preheated gases has been numerically analyzed in connection with the detonation transition. The results of the present numerical analysis emphasize the important roles of the characteristic gasdynamic time τ_g, the reaction time τ_R, and the induction time $\tau_{ind.w}$. Increase in either of the non-dimensional parameters $\alpha(= \tau_g/\tau_R)$ or $\beta(= \tau_g/\tau_{ind.w.})$ enhances the shock amplification process. Only certain combinations of these parameters allow the coherent shock wave amplification to be sustained. It is found that sufficient sustenance of the SWACER mechanism requires that the length of the preheated gas L must, roughly speaking, satisfy the condition $L \gtrsim 20\ c_o\tau_R$.

5. When the SWACER mechanism is maintained in the preheated region of gas mixture, the wave amplification process can be divided into three stages. In the first stage, the wave is amplified due to the energy release from the prescribed initial induction time gradient field. In the second stage, the wave deviates from the induction time curve and starts to trigger the heat release of neighbouring hot gas mixture. Finally, a strong shock wave is established in the third stage, and the shock wave is capable of providing the self-coherent amplification process, in which the shock wave and the reaction front travels in the perfect coherence by the strong shock-heating. The establishment of the self-coherent stage depends on whether or not a certain strength of the wave is ensured through the energy release in the first two amplification stages.

Recommendations for Future Work

1. In the numerical analysis of Chapter 2, the influence of the temporal variation of radiation intensity has not been considered. This should be investigated systematically. In the present study, hydrogen-chlorine mixtures are analyzed. Perhaps, more quantitative and refined investigation can be carried out by analyzing O_3-O_2 mixtures. The chemical kinetics of O_3-O_2 system is well-established, and the chemical species involved are only O, O_2, and O_3. Thus, we can expect to carry out the numerical analysis more easily. In addition to these theoretical works, some experimental works should also be performed. Detailed spectroscopic measurement of the flash radiation should be carried out as well as the schlieren photographic observations.

2. The theoretical study in Chapter 3 has been limited to the planar symmetric geometries. Studies should also be carried out for cylindrical and spherical symmetric geometries. Through such studies, we can obtain the important information concerning the effect of area divergence on the wave amplification process.

3. The analysis of the shock wave amplification in the temperature gradient field should be more systematically carried out. Studies for cylindrical and spherical symmetric geometries should yield some interesting results. Also, some improvement may be made concerning the modelling of the chemical reactions of gas mixture. A more realistic heat release function may be expressed in terms of an empirical formula which includes the thermodynamic parameters and the concentration of fuel, oxidizer, and radicals. Such an empirical formula may be obtained through a systematic study of the chemical kinetics of the real reaction systems such as O_3-O_2, H_2-Cl_2 or H_2-O_2 systems.

4. In addition to the above-mentioned theoretical works, some experimental works should also be carried out. We can generate a temperature gradient field, using an imploding cylindrical shock wave and a circular cylinder whose axis is at the implosion center. The imploding shock reflects at the surface of the cylinder, and the reflected shock wave starts to decay by the area divergence effect. Thus the temperature of the shocked gas decreases in the radial direction. The observation of the shock amplification phenomena in such a gradient field should yield some interesting results.

CHAPTER 6

STATEMENT OF ORIGINALITY AND CONTRIBUTION TO KNOWLEDGE

Prior to the present research, the basic features and mechanisms of the shock wave amplification in explosive gases have not been clearly elucidated. In fact, the rapid shock wave formation phenomena have been sometimes regarded as the phenomena governed solely by the expansion of the localized explosion center, and the process of the shock wave amplification has not been precisely analyzed.

The author believes that the concept of the SWACER mechanism introduced in the present research is quite important for a better understanding of the shock wave amplification phenomena. It is shown for the first time that the coherent energy release generated by the induction time gradient field plays a significant role in the shock wave amplification phenomena. The author expects that the results presented in this thesis are a distinct contribution to the knowledge in the field of gasdynamics of explosions.

APPENDIX I

PRELIMINARY EXPERIMENT AND DETAILS OF EXPERIMENT OF SCHLIEREN OBSERVATION OF PHOTOCHEMICAL DETONATION INITIATION

A. Preliminary Experiment

The main aim of the preliminary experiment was to confirm the feasibility of photochemical detonation initiation. Gas mixtures of C_2H_2-O_2, C_2H_2-O_2-NO_2 and H_2-Cl_2 were mainly tested. The relative feasibility of photochemical initiation for these mixtures was investigated by measuring the induction times for detonation initiation.

The photon-absorption and photo-dissociation of molecular oxygen and nitrogen dioxide are briefly described in the following, while those of molecular chlorine are given in Chapter 2.

A-1 Photon-Absorption and Photo-Dissociation of O_2 and NO_2*

The absorption spectrum of oxygen molecule in the range of 1200-2600 Å is given in Fig. 35. A salient photon-absorption starts at 2000 Å and below this wavelength the absorption coefficient noticeably increases. The absorption bands from 1759 to 1950 Å is called Schumann-Runge bands, where the dissociation of one oxygen molecule generates two normal oxygen atoms:

$$O_2\ (^3\Sigma_g^-) + h\nu \rightarrow 2\ O(^3P) \qquad (I\text{-}1)$$

The photo-dissociation process changes below the Schumann-Runge bands. In the continuum absorption range of 1290-1750 Å, one photo-dissociating oxygen molecule generates one excited $O(^1D)$ and normal $O(^3P)$ atoms.

$$O_2(^3\Sigma_g^-) + h\nu' \rightarrow O(^1D) + O(^3P) \qquad (I\text{-}2)$$

---

* The details of the molecular physics of the photo-dissociation processes are provided in the book by Calvert and Pitts (35).

Although molecular oxygen has strong photon-absorption below 1800 Å, it can not be easily achieved to generate a sufficient amount of oxygen atoms, due to the difficulty in producing intense far ultra-violet radiation. In fact, the maximum radiation strength of most light sources lies in the range above 2000 Å. The available far ultra-violet radiation is quite weak. Thus, some photo-sensitizers are sometimes added to the fuel-oxygen mixtures in the flash photolysis experiments. In particular, NO_2 is one of the strongest photo-sensitizers.

The absorption coefficient of NO_2 is shown in Fig. 36. The bond energy of NO_2 is about 71.8 Kcal/mole corresponding to 3945 Å. Below this wavelength, the photo-dissociation becomes possible. Between 2537 and 3945 Å, the dissociation of one NO_2 molecule generates one oxygen atom in ground state and one nitric oxide in ground state:

$$NO_2 + h\upsilon \rightarrow NO\ (X^2\Pi) + O(^3P) \qquad (I\text{-}3)$$

Below 2537 Å the dissociation process changes, and one excited oxygen atom is generated instead of normal one:

$$NO_2 + h\upsilon \rightarrow NO\ (X^2\pi) + O(^1D) \qquad (I\text{-}4)$$

A-2 Details of Experimentation

A-2-1 Flash Cavity

The essential part of the experimental apparatus is illustrated in Fig. 37. An existing solid state laser cavity was easily converted into the flash cavity for the experiment. The upper photograph in the figure displays the inside of the double elliptical silver-coated flash cavity (16.5 cm long and 11 cm wide) wherein a quartz explosion tube (14 mm ID, 1 mm wall thickness and 42.5 cm long) was inserted along the central axis. The tube was irradiated by two xenon flash tubes (EG & C FX47C). The lower schematic diagram illustrates the cross-section of the flash cavity. A

large portion of the energy discharged in the flash tubes is converted into thermal energy. A water-cooling system was used to protect the explosion tube, the flash tubes, and the silver coated surface of the flash cavity from the heat. The flow of nitrogen gas was used to avoid loss of far ultra-violet radiation of the flash tube, otherwise oxygen in air would have completely absorbed the far ultra-violet. The photon transmission of the quartz explosion tube used in the experiment cuts off sharply at about 1650 Å. Thus, due to the nitrogen flow, the far ultra-violet down to 1650 Å was available to dissociate oxygen molecules. In fact, although the available far ultra-violet radiation intensity was supposed to be relatively small, it was found that C_2H_2-O_2 mixtures detonate without any addition of NO_2.

A-2-2 Flash Tube

The flash tubes were connected to an energy supply system (Maser Optics Inc.) which consisted of a 2250 μF capacitor bank, a DC power supply, and a trigger unit. The capacitor bank could be charged to about 4 KV, and the corresponding maximum energy was about 18 KJ. Fig. 38 shows the radiation output of the flash tubes for different flash energies (energy stored in the capacitor bank). This was monitored by a photo-tube (RCA 929). The tube was charged with a +150 V DC supply. The outputs were measured across a 2 MΩ resistor. It was found that the irradiation duration is about 2 msec irrespectively of the flash energy. The trace of the flash irradiation was sometimes smeared with the noise caused by the strong electron discharge in the flash tubes. Since the experiment aimed only to investigate the relative feasibility of photochemical detonation initiation for some different gas mixtures, the actual radiation intensity of the flash

irradiation was not measured. The relative radiation intensity was expressed in terms of the flash energy.

A-2-3 Diagnostic Techniques

A detailed schematic diagram of the entire experimental system is illustrated in Fig. 39. A pressure transducer was placed at one end of the quartz explosion tube so as to detect the abrupt pressure jump by a detonation wave. The above-mentioned photo-tube monitored the flash irradiation. A sodium-chloride plate was placed in front of the photo-tube to reduce the radiation intensity to the tube. The outputs from the pressure transducer and the photo-tube were plugged in one channel of an oscilloscope (Tektronix Type 555). In the resulting superimposed trace, the induction time for detonation initiation is defined as the time lag between the start of the flash irradiation and the abrupt jump of the pressure output.

The pressure transducer used was designed by Knystautas (51) and is shown in Fig. 40. It consisted of a barium titanate-zinc rod combination and a brass housing case. The positive face of the barium titanate element (6 mm long and 6 mm diameter) was jointed to the zinc rod (4 cm long and 6 mm diameter) with silver epoxy glue, while the negative face was grounded by soldering a copper wire between the element and the brass housing case. The output from the pressure transducer was directly connected to the oscilloscope without any emitter follower circuit.

The quartz explosion tube was connected with a pyrex glass tube (14 mm ID, 1 mm wall thickness and 120 cm long), and a streak camera was employed to observe the propagation of detonation wave for C_2H_2-O_2 or C_2H_2-O_2-NO_2 mixtures. The luminosity from these gases was strong enough

to be recorded on a film. Streak records were obtained on Kodak Tri-X type 475 70 mm film. The writing speed of the camera was kept about 6cm/msec. The contact switch of the camera could provide a signal to the trigger unit for the flash tubes, so that the flash tubes were fired simultaneously with the shutter opening of the camera. The duration of the shutter opening was set at 2 msec or 5 msec.

A-2-4 Preparation of Test Gas Mixtures

Gases of commercial purity were used without any additional purification. The gas mixtures were prepared in two 5 liter capacity stainless steel tanks by the method of partial pressures. The tanks were filled to 300-500 torr of the mixture. Adequate mixing was obtained by allowing the gases to diffuse for 12-24 hours prior to the experiments. Oxy-acetylene mixtures were sometimes sensitized with nitrogen dioxide (NO_2) which was made by mixing nitric oxide (NO) and oxygen. Due to the rapid reaction $NO + \frac{1}{2} O_2 \rightarrow NO_2$ at room temperatures, NO_2 could be obtained within an hour after the mixing of the gases.

A-2-5 Test Procedure

To prepare for an experiment, the explosion tube and the lines connecting the tube with the storage tanks of the test mixtures were first evacuated to a pressure lower than about 0.02 torr. The explosion tube was then filled with the gas mixture at a higher pressure than the desired initial pressure. The tube was then slowly evacuated until the required pressure was obtained. Thereafter, all the valves were closed. The lines between the valves of the explosion tube and the storage tanks were evacuated again to prevent any possible danger of detonation feedback.

The range of initial pressures of the gas mixtures was between 20 to 100 torr. The upper limit was determined by safety considerations from detonation overpressures in the explosion tube. Since the wall thickness of the tube was only 1 mm, a higher initial pressure would have caused damage to the experimental system.

The oscilloscope and the photo-tube circuit were switched on at least 20 minutes before the experiment, so that the measurement systems were sufficiently warmed up. The streak camera was kept running about 1 minute before the experiment so as to ensure a steady rotation of the drum.

A-3 Experimental Results

Rapid detonation initiation was observed for the mixtures of C_2H_2-O_2, C_2H_2-O_2-NO_2 and H_2-Cl_2 in the initial pressure range 20 - 100 torr. The top photograph in Fig. 41 is a typical pressure trace superimposed on the photo-tube output recording the radiation of the flash tubes. The sudden pressure jump indicates that a detonation wave is formed with an induction time of about 600 μsec (as indicated by t_i in the figure). The bottom photograph is the streak record for the same experimental condition. The record shows that a fully developed detonation wave emerges directly from the flash cavity after the delay time of about the same as that from the pressure record. This result indicates that the direct initiation is achieved inside the flash cavity. Fig. 42 shows the pressure record for an H_2-Cl_2 mixture. It is also shown that a fully developed detonation wave is already established at 10 cm from the flash cavity.

The induction time was found to depend on the particular mixture used, its initial pressure and composition, as well as the flash energy and NO_2 concentration. The induction times measured by the combination of the

pressure transducer and the photo-tube are plotted in Fig. 43. The results show that the induction time decreases with (1) increasing initial pressure, (2) increasing flash energy and (3) increasing NO_2 concentration. These behaviours are to be expected. In addition, in comparing the induction times for the test gas mixtures at the flash energy of 6 KJ, we may notice that, as the mixture becomes less feasible to detonate, the dependence of induction time on the initial pressure as well as the fluctuation of induction time increase.

β. Details of Experiment of Schlieren Observation of Photochemical Detonation Initiation

B-1 Flash Tube

Fig. 44 shows the schematic diagram of the radiation source system. Powerful xenon flash tubes (Xenon Corp. FPA-8-100C) were employed. The flash energy was supplied from an 8 μF capacitor (Tobe Deutschmann Lab. Model ESC-248 B, 5 nano Henry inductance, maximum allowable energy 2.5KJ), which was charged with a high voltage DC power supply (0-60 KV DC, Hipotronix). The flash tubes were fired by a "home-made" switch and a trigger module (EG & G TM11-A). The electrodes of the switch were of polished stainless steel 2.5 cm in diameter with a flat face. One of the electrodes had a central hole to accomodate the trigger pin through which a +30 KV pulse from the trigger module to the electrode induces the main discharge between the electrodes. The distance between the electrodes was adjustable, and the inside of the switch was pressurized with dry nitrogen gas, so that the discharge was controlled to provide a reliable switching function. The electron discharge inside the switch could be detected by a current transformer

(Pearson Electronics, Model 1025, 0.025 v/amp). The signal from the transformer was used to trigger an oscilloscope (Tektronix 556) which recorded the pressure inside the explosion chamber. The spark light unit for the schlieren photography was also triggered by the signal.

Fig. 45 shows a typical oscilloscope record of the radiation from the flash tube. This was monitored by an RCA 929 photo-tube which was charged with a +150 V DC, and the output was measured across a 2 MΩ resistor. It was found that the flash duration is about 250 μsec irrespectively of the flash energy.

B-2 Pressure Transducer

In the experiments using the rectangular box chamber, two calibrated piezoelectric pressure transducers (PCB 113A24, 1 V output/200 psi) were mounted on the stainless steel plates which were about 12 mm apart from both the end sides of the chamber. Each pressure transducer had a built-in amplifier and was powered by a battery unit (PCB Model 480A). The output from the unit was plugged into the oscilloscope and recorded on Polaroid type 47 film.

B-3 Spark Schlieren System

The spark schlieren system consisted of a spark light unit, two schlieren mirrors, and a camera. Fig. 46 shows the schematic diagram of the spark light unit. The signal from the current transformer in the radiation source system was sent to a delay pulse generator (Rutherford Electronics Co., Model A2). Two capacitors (Condenser Products Corp., EB 502-50 MP, 0.005 μF) in parallel connection were charged to 20-25 KV with a DC power supply (Hipotronix). The main discharge was triggered

inside a switch (EG & G Model GP 12-B) by a +30 KV pulse from the trigger module with a desired delay time, and the spark light was generated in a 5 mm gap between two electrodes. The spark light was focused at a pin hole on a metal plate by a 75 mm focal length lens, and a point light source was obtained for the schlieren photography.

The schlieren mirrors were parabolic mirrors of 1.5 m focal length and provided a undistorted field of view of 15 cm diameter. In front of the camera, a razor-knife edge was placed. The camera itself consisted of an integral iris diaphragm and shutter, a 180 mm focal length lens, an extensible bellows (up to 1.5 m), and a Polaroid film holder. The alignment of the schlieren system was obtained using a steady light source (Tungsten arc lamp) placed near the schlieren light source.

B-4 Preparation of Test Gas

Hydrogen and chlorine gases of commercial purity were used to make equimolar hydrogen-chlorine mixtures. The mixture was prepared in a 20 stainless steel tank by the method of partial pressures. The mixture at 1-2 atm filled the storage tank, and the mixture was stored at least 24 hours prior to the experiment so as to obtain a sufficient mixing by the diffusion.

B-5 Test Procedure

Prior to the loading of the mixture into the explosion chamber, first the switching functions in the radiation source and spark light systems were checked. After a sufficient evacuation of the explosion chamber and the lines connecting the chamber with the storage tank, the gas mixture at a higher pressure than the desired initial pressure was

introduced to the chamber. The chamber was then slowly evacuated till the required pressure was obtained. Thereafter the mixture between the valve of the chamber and that of the storage tank was evacuated to avoid any possible danger of detonation feedback. The explosion chambers were found to be sufficiently strong to endure the detonation pressures of equimolar H_2-Cl_2 mixture initially at 100 torr.

APPENDIX II

NUMERICAL ANALYSIS OF H_2-Cl_2 EXPLOSION

A. Constant Volume Combustion

A-1. Governing Equations and Computation Techniques

The governing equations for H_2-Cl_2 constant volume explosion are expressed as follows:

Chemical Kinetic Equations:

$$\frac{d[i]}{dt} = W_i \qquad (i = H_2, Cl_2, H, Cl, \text{ and } HCl) \qquad \text{(II-1)}$$

Energy Conservation Equation:

$$\{\sum_i ([i]\ (C_{pi} - Ro))\}\ \frac{dT}{dt} = -\sum_i W_i\ (h_i - RoT) + \varepsilon I[Cl_2] \qquad \text{(II-2)}$$

Conservation of Atoms:

$$\frac{1}{2}[H] + \frac{1}{2}[HCl] + [H_2] = [H_2]_o \qquad \text{(II-3)}$$

$$\frac{1}{2}[Cl] + \frac{1}{2}[HCl] + [Cl_2] = [Cl_2]_o \qquad \text{(II-4)}$$

where $[i]$: concentration of chemical species i

W_i : production rate of species i

C_{pi} : constant pressure specific heat of species i (energy/mole/deg)

Ro : universal gas constant

T : temperature

h_i : specific enthalpy of species i (energy/mole)

$\varepsilon I[Cl_2]$: radiation energy absorbed by Cl_2 per unit time per unit volume (see Eq. (2-3) in Chapter 2)

$[i]_o$: initial concentration of species i

In the above governing equations, W_{H_2} and W_{Cl_2} in Eq. (II-2) can be expressed by the following equations using Eqs. (II-3) and (II-4):

$$W_{H_2} = -\frac{1}{2} W_{H} - \frac{1}{2} W_{HCl} \qquad \text{(II-5)}$$

$$W_{Cl_2} = -\frac{1}{2} W_{Cl} - \frac{1}{2} W_{HCl} \qquad \text{(II-6)}$$

The concentration $[H_2]$ and $[Cl_2]$ can be obtained using Eq. (II-3) and (II-4). Thus, by the elimination, we have now four non-linear differential equations, which are three chemical kinetic equations for H, Cl and HCl, and the energy conservation equation.

In the present study, the chemical reaction rates were mainly taken from the paper by Cohen et al. (36), and the data are summarized in Table 3. In Eq. (II-2), C_{pi} and h_i are the functions of temperature and expressed in terms of the polynomials of temperature. The coefficients of the polynomials were taken from the report by Gordon and McBride (53), and those are listed in Table 4.

The fourth-order Runge-Kutta method has been used to integrate the differential equations. In each iteration procedure between t and t+Δt, the time step Δt is repeatedly adjusted to satisfy the following condition imposed on the increase of temperature:

$$\left| \frac{T(t+\Delta t) - T(t)}{T(t)} \right| \leq 5 \times 10^{-4} \qquad \text{(II-7)}$$

If the above condition is not satisfied, the computation is redone by reducing the time step size to 75% of the previous one.

The above criterion was set based on the following results: when the time step is about 10 times larger than that obtained by the above criterion, some numerical instabilities are observed. On the other hand, when the time step is further reduced by a factor of 2 — 5 from that obtained by the above criterion, very little change in the results is

found. (For example, the relative error of the temperature is less than about 0.1%). Thus, the above criterion for the time step is sufficient for obtaining reasonably accurate results.

A-2 Distinctions Between Photochemical and Thermal Explosions

The main purpose of the numerical analysis in Chapter 2 has been to elucidate the basic features of the shock wave amplification in photochemically reacting gas mixtures. In this section, the basic aspects of the photochemical explosion mode are discussed in comparison with the thermal explosion mode.

Rice (55) has calculated the induction times of photochemically ignited H_2-O_2-Cl_2 reactions. Cerkanowicz and Stevens (38) have also theoretically studied the reactions of photochemically ignited H_2-O_2 mixtures. However, the distinctions between the photochemical and thermal explosions have not been studied in their works. In the present research, the distinctions between the two explosion modes in H_2-Cl_2 reaction system have been studied through a numerical analysis.

Equi-molar H_2-Cl_2 mixtures initially at 298°K have been considered throughout the numerical computations. The basic premise of the theoretical thermal explosion model is that the mixture is instantaneously heated up to a higher temperature, and the subsequent chemical reactions are calculated. For photochemical explosion, two theoretical models have been considered. In the first model, the photo-dissociation process of Cl_2 has not been considered, and it is assumed that a certain amount of chlorine atoms is instantaneously produced. In the second model, a 3300 Å monochromatic light beam has been assumed, and the photo-dissociation process has been taken into account. One typical result obtained for this model has already been presented in Section 2 of Chapter 2.

Fig. 47 shows one of the results for the first model of photochemical explosion. It is assumed that about 9% of Cl_2 is instantaneously dissociated into chlorine atoms. The figure shows the changes of chemical species concentration and temperature. The chlorine atom concentration decreases during the initial 12 μsec, due to its rapid consumption in the chain-carrying steps (i.e. $H_2 + Cl \rightarrow HCl + H$ and $H + Cl_2 \rightarrow HCl + Cl$), and at the same time temperature is increasing due to the exothermicity of the chain-carrying steps. After passing the minimum point in the early stage of the reaction, the chlorine atom concentration increases due to the thermally enhanced chain-carrying reactions. In the present study, the induction time is determined by taking the intercept of the tangent to the maximum slope of the temperature-time curve with the initial temperature line. The induction times so calculated for different degree of Cl_2 dissociation in equi-molar H_2-Cl_2 intially at 100 torr are summarized in Table 5-A.

Fig. 48 shows one of the results for the thermal explosion. It is assumed that an equi-molar H_2-Cl_2 mixture initially at 100 torr and 298°K is instantaneously heated up to 1800°K. In contrast with the previous case, the concentration of HCl is always much greater than those of H and Cl atoms in the entire process of the reaction. Right after the very early stage of the reaction, where a very small amount of H and Cl atoms is produced via the thermal dissociation of H_2 and Cl_2, the chain-carrying steps are extremely accelerated due to the higher temperature, and they are dominant in the entire combustion process. The induction time is determined as before, and the results obtained for different initial conditions are summarized in Table 5-B.

In order to further elucidate the basic distinctions between the thermal and photochemical explosions, the results of numerical analysis (computer runs A-2 through A-7, and B-1 through B-3 in Table 5) are plotted in the T-log[Cl] plane of Fig. 49. Such a phase plane analysis was introduced for the first time by Yang and Gray (56, 57) in their studies on the oxidation of hydrocarbons. Berlad (58) discussed the distinctions between the thermal and photochemical explosions on a qualitative basis, using this phase plane. In the figure, the curves show how the reaction proceeds in the phase plane for different initial conditions. One can see that the phase plane is sharply divided into the domains of the thermal and the photochemical explosions by the separation curve S.

The effects of initial pressure on the induction time for both the thermal and photochemical ignition modes are also studied. For the photochemical intiation, radiation intensity of 1.5 KW/cm^2 at 3300 Å is considered; and the induction times determined as before are summarized in Table 5-C. The results of the thermal explosions have already been given in Table 5-B for the comparison (computer runs B-2 and B-4 through B-7). Fig. 50 displays the calculated induction times as a function of initial pressure. The figure shows that the induction time increases with decreasing initial pressure for both the ignition modes, and that the induction time sharply increases for initial pressures less than 100 torr. The induction times have been normalized with respect to the induction time at 1 atm in order to make both the modes compatible for comparison. The result is shown in Fig. 51. The normalized induction time for the photochemical explosion becomes much less than that for the thermal explosion with decreasing initial pressures. This indicates that the photochemical ignition is capable of providing more stable ignition than the thermal one. In fact, Cerkanowicz et al. (59-61) have demonstrated experimentally that

the relative minimum ignition energy in sub-atmospheric fuel-air mixtures is much less with the photochemical ignition than with the spark (thermal) ignition.' Moreover, the experiments of detonation induction time measurements for H_2-Cl_2 mixtures in the present research (Appendix I-A) have shown that the dependence of the induction time on the initial pressure is relatively small in the photochemical initiation mode. Thus, from the results of the present study and the above-mentioned Cerkanowicz's work, we can conclude that the photochemical ignition technique is more efficient and stable than the thermal ignition technique.

B. A Modified Version of Leap-Frog Finite Difference Method

The governing equations of one-dimensional flow-field of the reacting H_2-Cl_2 mixture are expressed as follows:*

Mass Conservation: $$\frac{\partial \rho}{\partial t} + \frac{\partial (\rho u)}{\partial x} = 0 \qquad \text{(II-8)}$$

Momentum Conservation: $$\frac{\partial u}{\partial t} + u\frac{\partial u}{\partial x} = -\frac{1}{\rho}\frac{\partial p}{\partial x} \qquad \text{(II-9)}$$

Energy Conservation: $$\rho\frac{\partial U}{\partial t} + \rho u\frac{\partial U}{\partial x} = -p\frac{\partial u}{\partial x} + \varepsilon I[Cl_2] \qquad \text{(II-10)}$$

Chemical Kinetic Equations: $$\rho\frac{\partial Y_i}{\partial t} + \rho u\frac{\partial Y_i}{\partial x} = M_i W_i \qquad \text{(II-11)}$$

$$(i = H_2,\ H,\ Cl_2,\ Cl, \text{and } HCl)$$

Equation of State: $$p = \rho R_0 T \sum_i \frac{Y_i}{M_i} \qquad \text{(II-12)}$$

Boundary Condition: $$u(o,t) = 0 \qquad \text{(II-13)}$$

where U is the specific internal energy of the mixture (energy/mass);

---

* For mathematical simplicity of the boundary conditions, the symmetric flow-field is assumed.

$\varepsilon I[Cl_2]$ is the radiation energy absorbed by chlorine molecules (see Eq. (2-2)); Y_i is the weight or mass fraction of the species i; M_i is the molecular weight of the species i; W_i is the molar production rate of the species i (mole per unit volume per unit time); and Ro is the universal gas constant.

The leap-frog scheme has been applied to the above mass, momentum, and energy conservation equations. The scheme has second-order accuracy. In this finite difference method, both the time and spatial differentials are approximated by the centered differences, and the unknown values at time $t = t_o + t$ are obtained from the values at $t = t_o$ and $t = t_o - t$, as shown below:

Mass Conservation:

$$\rho_m^{n+1} = \rho_m^{n-1} - \frac{\Delta t}{\Delta x}\left[(\rho u)_{m+1}^n - (\rho u)_{m-1}^n\right] \qquad \text{(II-14)}$$

Momentum Conservation:

$$u_m^{n+1} = u_m^{n-1} - \frac{\Delta t}{\Delta x} u_m^n \left(u_{m+1}^n - u_{m-1}^n\right) - \frac{\Delta t}{\Delta x} \frac{1}{\rho_m^n}\left(p_{m+1}^n - p_{m-1}^n\right) \qquad \text{(II-15)}$$

Energy Conservation:

$$U_m^{n+1} = U_m^{n-1} - \frac{\Delta t}{\Delta x} u_m^n \left(U_{m+1}^n - U_{m-1}^n\right) - \left(\frac{p}{\rho}\right)_m^n \frac{\Delta t}{\Delta x}\left(u_{m+1}^n - u_{m-1}^n\right) + 2\Delta t \left(\frac{\varepsilon I\, Y_{Cl_2}}{M_{Cl_2}}\right)_m^n \qquad \text{(II-16)}$$

where the subscript m denotes the m^{th} spatial mesh point, while the superscript n denotes the n^{th} time mesh point; and, Δx and Δt denote the spatial mesh size and the time step size, respectively. The radiation intensity I at a given mesh point $x = m\,\Delta x$ can be obtained by numerically integrating the following equation:

$$I = I_o \exp\left(-\varepsilon \int_0^x \frac{\rho Y_{Cl_2}}{M_{Cl_2}} dx\right) \qquad \text{(II-17)}$$

where I_o is the radiation intensity at x=0, and the above integration has been approximated by the trapezoidal rule.

The chemical kinetic equations (II-11) are rearranged as follows:

$$\frac{\partial Y_i}{\partial t} = \frac{1}{\rho} M_i W_i - u \frac{\partial Y_i}{\partial x} \qquad \text{(II-11')}$$

Since it was found that the time integration by the leap-frog method is inappropriate to integrate the rapid chemical reactions, it was necessary to use a scheme that can evaluate the time change of the chemical species more accurately. The following scheme has been employed to integrate the above equation.

First, only the under-lined part of the equation is considered, and the third-order Runge-Kutta scheme is applied to the part. With the assumption that the temperature and the density are unchanged during the time interval between time t_o and $t_o + \Delta t$, the increment at m^{th} spatial mesh point $\Delta Y_{i,m}$ is obtained. The spatial differential in Eq. (II-11') is then approximated by the centered difference. Finally, the solution $Y^{n+1}_{i,m}$ is obtained as follows:

$$Y^{n+1}_{i,m} = Y^n_{i,m} + \Delta Y_{i,m} - \frac{1}{2} \frac{\Delta t}{\Delta x} u^n_m \left(Y^n_{i,m+1} - Y^n_{i,m-1}\right)$$

$$(i = H_2,\ H,\ Cl_2,\ Cl,\ \text{and } HCl) \qquad \text{(II-18)}$$

The values ρ, u, U, and Y_i at the boundary x=0 were computed by the following equations, based on the symmetric conditions of the flow-field:

$$\rho(\Delta x,t) = \rho(-\Delta x,t),\ p(\Delta x,t) = p(-\Delta x,t)$$

$$U(\Delta x,t) = U(-\Delta x,t),\ Y_i(\Delta x,t) = Y_i(-\Delta x,t)$$

$$u(\Delta x,t) = -u(-\Delta x,t) \qquad \text{(II-19)}$$

In each iteration of the computation, the temperature and the pressure at each mesh point are evaluated from ρ, Y_i, and U. First, the temperature is obtained using the following relations:

$$U = \sum_i (h_i \cdot Y_i/M_i) - RoT \sum_i \frac{Y_i}{M_i} \qquad \text{(II-20)}$$

where h_i is the enthalpy of the species i, and whose polynomial fitting coefficients are listed in Table 4. Equation (II-20) is rearranged into the following form

$$T = \frac{\sum_i (h_i(T) \cdot Y_i/M_i) - U}{Ro \sum_i \frac{Y_i}{M_i}} \qquad \text{(II-20')}$$

The temperature was evaluated by an iteration method, in which the temperature calculated on the right hand side of the above equation is being re-substituted until the following convergence condition is satisfied:

$$\left| \frac{T^{\ell+1} - T^{\ell}}{T^{\ell}} \right| \leq 0.1\% \qquad \text{(II-21)}$$

where ℓ denotes the number of the iteration. The pressure is then obtained using the equation of state (II-12):

$$p = \rho RoT \sum_i \frac{Y_i}{M_i} \qquad \text{(II-12)}$$

In the present research, about 70 spatial mesh points were used to cover the length of 3.5 cm. Through a preliminary estimation on the time step, it was found that the minimum time step required for the integration of the chemical kinetic equations is much smaller than the time step determined by the standard Courant-Friedrich-Lewy criterion for the non-reacting flow-fields. Thus, the time step is determined by the chemical kinetic equations, and the step size has been $0.01 \sim 0.05$ μsec in most computer runs.

The finite difference method presented here has worked reasonably well for analyzing the reacting non-steady flow-fields. Perhaps, one of the defects involved in the computation method is that the method is unstable to the discontinuity waves such as detonation waves or shock waves. However, since the research has aimed only to analyze the early stage of the shock wave amplification phenomena, the numerical instabilities have not saliently appeared in the results of the computation.

APPENDIX III

REFLECTED PRESSURE BEHIND SYMMETRICALLY COLLIDING CHAPMAN-JOUGUET DETONATION WAVES

In Chapter 2, the reflected pressure behind the photochemically initiated detonation waves has been measured. In order to check the experimental results, the reflected pressure is theoretically calculated.

The basic assumptions of the theoretical model are as follows: Two symmetrically colliding Chapman-Jouguet detonation waves are considered; the waves are assumed to be simple discontinuity waves (i.e. the structure of the wave is not considered); and the chemical reaction is neglected behind the reflected waves.

The condition for the symmetrical reflection of two Chapman-Jouget detonation waves is equivalent to that for the reflection of one detonation wave at the wall. Sketch 1 below illustrates the condition:

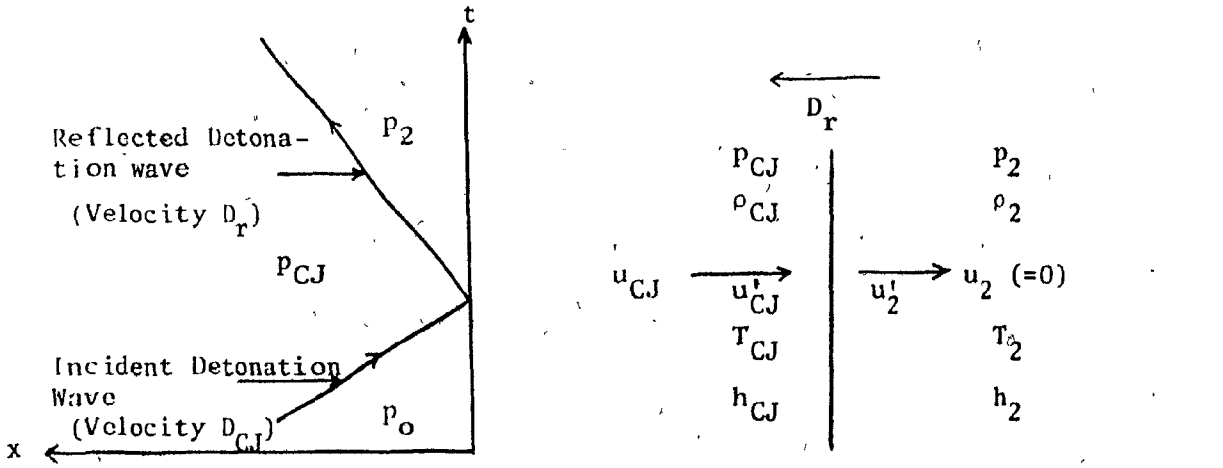

a) x-t Diagram

b) Condition across the reflected wave (in wave co-ordinate)

Sketch 1

where the subscripts "0", "CJ", and "2" denote the initial conditions, the conditions for the Chapman-Jouguet detonation wave, and the conditions for the reflected wave, respectively; D_{CJ} is the velocity of the incident detonation wave in the laboratory co-ordinates, while D_r is the velocity of the reflected wave in the same co-ordinates; u_{CJ} and u_2 represent the particle velocities in the laboratory co-ordinates, while u'_{CJ} and u'_2 are the velocities in the wave co-ordinates; and h is the specific enthalpy (energy/mass).

The relations between the velocities in the laboratory co-ordinates and those in the wave co-ordinates are given by the following equations:

$$u'_{CJ} = D_r + u_{CJ} \qquad \text{(III-1)}$$

$$u'_2 = D_r \quad (u_2 = 0) \qquad \text{(III-2)}$$

where the boundary condition at the wall provides $u_2=0$.

The conservation equations across the reflected wave are given as follows:

Mass Conservation: $$\rho_{CJ}u'_{CJ} = \rho_2 u'_2 \qquad \text{(III-3)}$$

Momentum Conservation: $$p_{CJ} + \rho_{CJ}u'^2_{CJ} = p_2 + \rho_2 u'^2_2 \qquad \text{(III-4)}$$

Energy Conservation: $$h_{CJ} + \frac{1}{2}u'^2_{CJ} = h_2 + \frac{1}{2}u'^2_2 \qquad \text{(III-5)}$$

Assuming an ideal gas with the constant specific heat ratio γ, we can express the specific enthalpy h by the following equation

$$h = \frac{\gamma}{\gamma-1}\frac{p}{\rho} \qquad \text{(III-6)}$$

The energy conservation equation (III-5) is now given by the following equation:

$$\frac{\gamma}{\gamma-1}\frac{p_{CJ}}{\rho_{CJ}} + \frac{1}{2}u_{CJ}'^2 = \frac{\gamma}{\gamma-1}\frac{p_2}{\rho_2} + \frac{1}{2}u_2'^2 \qquad \text{(III-5')}$$

Eliminating u_{CJ}' and u_2' in Eqs. (III-3), (III-4), and (III-5), we obtain the relation between ρ_2/ρ_{CJ} and p_2/p_{CJ}, as shown below:

$$\frac{\rho_2}{\rho_{CJ}} = \frac{\frac{\gamma+1}{\gamma-1}\frac{p_2}{p_{CJ}} + 1}{\frac{\gamma+1}{\gamma-1} + \frac{p_2}{p_{CJ}}} \qquad \text{(III-7)}$$

On the other hand, by substituting Eqs. (III-1) and (III-2) into Eq. (III-3), ρ_2/ρ_{CJ} is also expressed as follows

$$\frac{\rho_2}{\rho_{CJ}} = \frac{D_r + u_{CJ}}{D_r} \qquad \text{(III-8)}$$

Thus, from Eqs. (III-7) and (III-8), the following equation for p_2/p_{CJ} is obtained

$$\frac{p_2}{p_{CJ}} = \frac{\frac{\gamma+1}{\gamma-1}(D_r + u_{CJ}) - D_r}{\frac{2}{\gamma-1}D_r - u_{CJ}} \qquad \text{(III-9)}$$

Using Eqs. (III-8) and (III-9), we can eliminate p_2 and ρ_2 in the momentum conservation equation (III-4). The rearranged Eq. (III-4) includes u_{CJ}' and u_2'. Using Eqs. (III-1) and (III-2), we finally obtain the equation for D_r.

$$\frac{2}{\gamma-1}D_r^2 + u_{CJ}\frac{3-\gamma}{\gamma-1}D_r - \left(u_{CJ}^2 + \frac{2\gamma}{\gamma-1}\frac{p_{CJ}}{\rho_{CJ}}\right) = 0 \qquad \text{(III-10)}$$

Solving the above equation, we can express D_r in terms of γ, u_{CJ}, p_{CJ}, and ρ_{CJ}:

$$D_r = \frac{\frac{\gamma-3}{\gamma-1}u_{CJ} + \sqrt{\left(\frac{\gamma-3}{\gamma-1}u_{CJ}\right)^2 + \frac{8}{\gamma-1}\left(u_{CJ}^2 + \frac{2}{\gamma-1}\frac{p_{CJ}}{\rho_{CJ}}\right)}}{\frac{4}{\gamma-1}} \qquad \text{(III-11)}$$

where the other solution provides a negative value. Thus, once D_r is obtained, the reflected pressure p_2 can be obtained using Eq. (III-9).

The properties of the Chapman-Jouguet detonation wave have been obtained using the computer program written by Gordon and McBride (53). For an equi-molar H_2-Cl_2 mixture initially at 100 torr and 298.15 °K (i.e. the gas mixture tested in the experiments), the results are summarized below.

p_{CJ} = 2.52 atm, T_{CJ} = 2886°K

ρ_{CJ} = 3.5653 x 10^{-4} g/cc,

D_{CJ} (detonation velocity) = 1656.1 m/sec,

$u_{CJ} = D_{CJ} - C_{CJ}$ (C_{CJ}: sound velocity; C_{CJ} = 910.9 m/sec)

= 745.2 m/sec

Mole Fraction

H : 0.01746, H_2 : 0.06455,

HCl: 0.77228, Cl : 0.14485,

Cl_2: 0.00086

Since the computer program has not provided the specific heat ratio γ, the polynomial fittings for C_{pi} shown in Table 4 are used to obtain the value of γ. Since the mole fractions of the chemical species as well as the temperature have already been provided, we can calculate the value of γ. The result obtained by the calculation has shown that γ = 1.36. Substituting the values of γ, u_{CJ}, p_{CJ}, and ρ_{CJ} into Eq. (III-11), we obtain D_r. Thus we can get the reflected pressure by substituting the value of D_r into Eq. (III-9).

The results have shown that D_r = 774.1 m/sec, p_2/p_{CJ} = 2.57, and p_2 = 6.46 atm (94.9 psi).

In addition to the above theoretical calculation, a detailed calculation, in which the chemical equilibrium is taken into account, has been made in the present research. The results are summarized below.*

$p_2 = 6.213$ atm $(p_2/p_{CJ} = 2.47)$

$\rho_2 = 7.5711 \times 10^{-4}$ g/cc

$T_2 = 3199°K$, $D_r = 663.3$ m/sec

Mole Fraction

H : 0.03244, H_2 : 0.08377

HCl : 0.70119, Cl : 0.18143,

Cl_2 : 0.00117

The reflected pressure calculated shows a good agreement with the value obtained by the simple theoretical model mentioned previously.

The reflected pressures calculated by both the theoretical models are lower than the pressure recorded in the experiments. This may be attributed to the following effects: the effect of the von-Neumann spike of the detonation wave; the three-dimensional structure of the detonation front; asymmetric collision of the deontation waves; and the effect of the intense radiation.

* The details of the computation technique are not shown here.

APPENDIX IV

A HYBRID VERSION OF VAN LEER'S FINITE DIFFERENCE SCHEME AND BORIS-BOOK's ANTIDIFFUSION METHOD

The finite difference method employed for the analysis in Chapter 3 is a hybrid version of Van Leer's scheme (42) and Boris-Book's antidiffusion method (44,46). The Van Leer's scheme is a simple one-step explicit method with first-order accuracy. Taki and Fujiwara (43) have analyzed two-dimensional nonsteady detonations using this finite difference scheme, and their results show that the scheme works quite well for the supersonic problems involving shock waves. The Boris-Book's antidiffusion method can provide accurate resolution of steep pressure gradient fields such as shock waves.

The normalized mass, momentum, and energy conservation equations (3-1')-(3-3') are rearranged in the following flux forms for the numerical computations:

$$\frac{\partial f}{\partial t^*} + \frac{\partial g}{\partial x^*} = S \qquad \text{(IV-1)}$$

where $f = \begin{bmatrix} \rho^* \\ \rho^* u^* \\ \frac{p^*}{\gamma} + \frac{1}{2}(\gamma-1)\rho^* u^{*2} \end{bmatrix}$, $g = \begin{bmatrix} \rho^* u^* \\ \rho^* u^{*2} + \frac{p^*}{\gamma} \\ u^*(p^* + \frac{1}{2}(\gamma-1)\rho^* u^{*2}) \end{bmatrix}$

$$S = \begin{bmatrix} 0 \\ 0 \\ \rho^*(\gamma-1)\,\dot{q}^* \end{bmatrix} \qquad \text{(IV-2)}$$

and where $\dot{q}^* = Q^*(t^*-x^*/A)\exp(-\frac{1}{2}(t^*-x^*/A)^2)\,H(t^*-x^*/A)$

$$Q^* = Q_o/c_o^2$$
$$A = V_o/c_o \qquad \text{(3-14)}$$

The above differential equations are first approximated by the Van Lerr's scheme as follows:

$$\tilde{f}_m^{n+1} = f_m^n - \frac{1}{2}\frac{\Delta t^*}{\Delta x^*}(g_{m+1}^n - g_{m-1}^n) + \frac{1}{2}\lambda_{m+1/2}^n (f_{m+1}^n - f_m^n)\left(\frac{\Delta t^*}{\Delta x^*}\right)^2$$

$$- \frac{1}{2}\lambda_{m-1/2}^n (f_m^n - f_{m-1}^n)\left(\frac{\Delta t^*}{\Delta x^*}\right)^2 + \frac{\Delta t^*}{4}(S_{m+1}^n + 2S_m^n + S_{m-1}^n) \qquad \text{(IV-3)}$$

$$\lambda_{m\pm1/2}^n = \frac{1}{2}\left[\{(c^* + |u^*|)_{m\pm1}^n\}^2 + \{(c^* + |u^*|)_m^n\}^2\right] \qquad \text{(IV-4)}$$

$$c^* = c/c_o \qquad \text{(IV-5)}$$

where Δx^* and Δt^* are the spatial mesh size and the time step size, respectively; m denotes the distance $m\Delta x^*$; and n denotes the n^{th} iteration.

The Boris-Book's antidiffusion method is then applied to $\tilde{f}_m^{n+1}$ as shown below:

$$\bar{f}_m^{n+1} = \tilde{f}_m^{n+1} + \{\eta_{m+1/2}(f_{m+1}^n - f_m^n) - \eta_{m-1/2}(f_m^n - f_{m-1}^n)\} \qquad \text{(IV-6)}$$

$$\Delta_{m+1/2} = \bar{f}_{m+1}^{n+1} - \bar{f}_m^{n+1} \qquad \text{(IV-7)}$$

$$\phi_{m+1/2} = \eta_{m+1/2}\,\Delta_{m+1/2} \qquad \text{(IV-8)}$$

$$\kappa_{m+1/2} = \text{sgn}\,\Delta_{m+1/2}\,\max\{0, \min[\Delta_{m-1/2}\,\text{sgn}\,\Delta_{m+1/2}, |\phi_{m+1/2}|, \Delta_{m+3/2}\,\text{sgn}\,\Delta_{m+1/2}]\} \qquad \text{(IV-9)}$$

$$f_m^{n+1} = \bar{f}_m^{n+1} - \kappa_{m+1/2} + \kappa_{m-1/2} \qquad \text{(IV-10)}$$

where $\eta_{m\pm1/2}$ is the diffusion-antidiffusion coefficient, and f_m^{n+1} is the solution.

In all the computer runs, Δx^* and $\eta_{m\pm1/2}$ have been kept 0.2 and 1/8 respectively, while Δt^* has been determined by the Courant-Friedrich-Lewy criterion:

$$\Delta t^* = \Lambda \frac{\Delta x^*}{(c^* + |u^*|)_{max}} \qquad \text{(IV-11)}$$

where Λ is the Courant number, which has been set at 0.85 in the present computation.

In order to check the accuracy of the computation, the normalized total energy deposited by the energy source E^* in Eqs. (3-15a) and (3-15b) was calculated by the integration of both the equations. The relative error, as defined by Eq. (IV-12), was found to be less than 0.2% in all the computer runs.

$$\% \text{ error} = \frac{\left| \int_0^\infty \left(\frac{p^*-1}{\gamma-1} + \frac{\gamma}{2} \rho^* u^{*2} \right) dx^* - \int_0^{t^*} \int_0^\infty \gamma \rho^* \dot{q}^* \, dx^* \, dt^* \right|}{\int_0^{t^*} \int_0^\infty \gamma \rho^* \, \dot{q}^* \, dx^* \, dt^*} \qquad \text{(IV-12)}$$

This indicates that the time step Δt^* is sufficiently small to accurately integrate the heat release function $\dot{q}^*$ at each mesh point.

The actual computation procedures in each iteration between t^* and $t^* + \Delta t^*$ are as follows:

i) The mass conservation equation is first solved by the Van Leer's scheme and the Boris-Book's antidiffusion method;

ii) Similarly, the momentum and energy conservation equations are solved;

iii) From the solution, g and S in Eq. (IV-2) are computed for the next iteration step;

iv) The time step Δt^* is determined by Eq. (IV-11), and the total energy E^* is also calculated.

The computational method has worked quite well. In particular, the Boris-Book's antidiffusion method has provided excellent resolution of shock wave profiles. The shock discontinuity has been successfully resolved

into two or three mesh points without any numerical instabilities, and it was found that the Rankine-Hugoniot shock relations are satisfied across the few mesh points. Since no complicated chemical reactions are involved in the theoretical model, the Van Leer's first-order scheme has also accurately integrated the gasdynamic equations with the heat release term.

APPENDIX V

A HYBRID VERSION OF MACCORMACK'S FINITE DIFFERENCE SCHEME AND BORIS-BOOK'S ANTIDIFUSSION METHOD

The MacCormack's second-order explicit finite difference method (49,50) has been used with the Boris-Book's antidiffusion method for the analysis in Chapter 4. The MacCormack's scheme is a predictor-corrector type two-step scheme with non-centered spatial differences.

The normalized governing equations are expressed in the following flux form.

$$\frac{\partial f}{\partial t^*} + \frac{\partial g}{\partial \xi^*} = S \qquad \text{(V-1)}$$

$$f = \begin{bmatrix} v^* \\ u^* \\ e^* \\ \lambda \end{bmatrix} \qquad g = \begin{bmatrix} u^* \\ p^*/\gamma \\ p^*u^*/\gamma \\ 0 \end{bmatrix} \qquad S = \begin{bmatrix} 0 \\ 0 \\ \dot{q}^* \\ -\frac{k^*}{v^*} \exp\left(-\frac{E^*_{act}}{T^*}\right) \end{bmatrix} \qquad \text{(V-2)}$$

In the predictive step of the MacCormack's scheme, the forward spatial difference is calculated, as shown in the following:

$$\tilde{f}^{n+1}_{m,1} = f^n_m - \frac{\Delta t^*}{\Delta \xi^*} (g^n_{m+1} - g^n_m) + S^n_m \Delta t^* \qquad \text{(V-3)}$$

where m denotes $m\Delta\xi^*$, and n denotes the n^{th} iteration. The predicted value of $\tilde{f}^{n+1}_{m,1}$ is then corrected in the second step of the scheme with the backward spatial difference:

$$\tilde{f}^{n+1}_{m,2} = \frac{1}{2} \{f^n_m + \tilde{f}^{n+1}_{m,1} - \frac{\Delta t^*}{\Delta \xi^*} (\tilde{g}^{n+1}_{m,1} - \tilde{g}^{n+1}_{m-1,1}) + \tilde{S}^{n+1}_{m,1} \Delta t^*\} \qquad \text{(V-4)}$$

where $\tilde{g}^{n+1}_{m,1}$ and $\tilde{S}^{n+1}_{m,1}$ have already been obtained from the predicted value $\tilde{f}^{n+1}_{m,1}$.

The Boris-Book's antidiffusion method is then applied to the mass, momentum, and energy conservation equationsso as to obtain accurate pressure profile of shock wave. The method does not apply to the differential equation for the induction parameter.

$$\bar{f}_m^{n+1} = \tilde{f}_{m,2}^{n+1} + \eta_{m+1/2}\,(f_{m+1}^n - f_m^n) - \eta_{m-1/2}\,(f_m^n - f_{m-1}^n) \qquad (V\text{-}5)$$

$$\Delta_{m+1/2} = \bar{f}_{m+1}^{n+1} - \bar{f}_m^{n+1} \qquad (V\text{-}6)$$

$$\phi_{m+1/2} = \eta_{m+1/2} \cdot \Delta_{m+1/2} \qquad (V\text{-}7)$$

$$\kappa_{m+1/2} = \operatorname{sgn} \Delta_{m+1/2} \max \{0, \min [\Delta_{m-1/2} \operatorname{sgn} \Delta_{m+1/2}, |\phi_{m+1/2}|, \Delta_{m+3/2} \operatorname{sgn} \Delta_{m+1/2}]\} \qquad (V\text{-}8)$$

$$f_m^{n+1} = \bar{f}_m^{n+1} - \kappa_{m+1/2} + \kappa_{m-1/2} \qquad (V\text{-}9)$$

where f_m^{n+1} is the solution, and the diffusion-antidiffusion coefficient $\eta_{m\pm1/2}$ is given by the following equation:

$$\eta_{m\pm1/2} = \frac{1}{12}\left(\left|\frac{u^{*n}_{m\pm1}}{c^{*n}_{m\pm1}}\right| + \left|\frac{u^{*n}_{m}}{c^{*n}_{m}}\right|\right) \quad (\text{if } \eta_{m\pm1/2} \leq \frac{1}{6})$$

$$= \frac{1}{6} \qquad (\text{if } \eta_{m\pm1/2} > \frac{1}{6}) \qquad (V\text{-}10)$$

where c^* is the normalized local sound velocity ($c^* = c/c_0$).

In the present analysis, the mesh size $\Delta\xi^*$ has been chosen small enough to cover the reaction zone with at least 10~20 mesh points. The number of mesh points inside the region of preheated gas has been from 200 to 500. The criterion for the time step Δt^* is given as follows:

$$\Delta t^* = \Lambda \min \left(\frac{v^* \Delta \xi^*}{c^*}, 0.05\,\frac{\tau_R}{\tau_g}\right) \qquad (V\text{-}11)$$

where the first value in the bracket of the equation provides the Courant-Fredrich-Lewy stability criterion, while the second value corresponds to

5% of the characteristic reaction time, which ensures sufficient time resolution of the heat release function. The Courant number Λ has been kept 0.75 throughout the computation.

The computation procedures in each iteration between t^* and $t^* + \Delta t^*$ have been carried out in the following manner:

i) The predictive step of the MacCormack's scheme is applied to the mass, momentum, and energy conservation equations as well as the equation for the induction parameter λ (Eq. (V-1)), and $\tilde{f}^{n+1}_{m,1}$ is obtained;

ii) $\tilde{g}^{n+1}_{m,1}$ and $\tilde{S}^{n+1}_{m,1}$ are calculated from the predicted value $\tilde{f}^{n+1}_{m,1}$;

iii) The diffusion-antidiffusion coefficient $\eta_{m+1/2}$ is calculated from f^n_m;

iv) $\tilde{f}^{n+1}_{m,2}$ is obtained by the corrective step of the MacCormack's scheme;

v) The Boris-Book's antidiffusion scheme is applied to the mass, momentum, and energy conservation equations, and the solution f^{n+1}_m is obtained ($f^{n+1}_m = \tilde{f}^{n+1}_{m,2}$ for the induction parameter λ);

vi) The position of each gas particle is obtained by the integration of the specific volume v^* using the trapezoidal rule (Eq. (4-20));

vii) For the next iteration step, g^{n+1}_m and S^{n+1}_m are calculated from f^{n+1}_m, and the time step Δt^* is determined by the criterion equation (V-11).

The Boris-Book's antidiffusion method has worked well for the resultion of shock wave discontinuity. The reason for using the second-order MacCormack's scheme is that the induction and heat release processes of the reaction must be accurately integrated. In fact, in a preliminary

test, a few numerical schemes were tested, and it was found that the first-order scheme presented in Appendix IV fails in solving the theoretical model. This is not only because of its accuracy, but because the first-order method is not applicable to the initial temperature gradient field in the theoretical model. Through the preliminary test, the second-order MacCormack's scheme was found to be the most reliable one among the computational methods tested. The accuracy of the computation has been evaluated by calculating the energy integral, which is similar to the evaluation mentioned in Appendix IV (see Eq. (IV-2)). The results have shown that the error is less than 1%, indicating that the computational method is sufficiently accurate.

REFERENCES

1. Bach, G.G., Knystautas, R., and Lee, J.H. — "Direct Initiation of Spherical Detonations in Gaseous Explosives" 12th Symposium (International) on Combustion, p. 853, The Combustion Institute, Pittsburgh (1969)

2. Bach, G.G., Knystautas, R., and Lee, J.H. — "Initiation Criteria for Diverging Gaseous Detonations" 13th Symposium (International) on Combustion, p. 1097, The Combustion Institute, Pittsburgh (1971)

3. Lee, J.H., and Ramamurthi, K. — "On the Concept of the Critical Size of a Detonation Kernel" Combustion and Flame, Vol. 27, p. 331, 1976

4. Laderman, A.J., and Oppenheim, A.K. — "Initial Flame Acceleration in an Explosive Gas" Proceedings of the Royal Society of London, Series A, Vol. 268, p. 153, 1962

5. Urtiew, P.A., and Oppenheim, A.K. — "Experimental Observations of the Transition to Detonation in an Explosive Gas" Proceedings of the Royal Society of London, Series A, Vol. 295, p. 13, 1966

6. Meyer, J.W., Urtiew, P.A., and Oppenheim, A.K. — "On the Inadequacy of Gasdynamic Processes for Triggering the Transition to Detonation" Combustion and Flame, Vol. 14, p. 13, 1970

7. Oppenheim, A.K. — "Novel Insights into the Structure and Development of Detonation" Astronautica Acta, Vol. 11, No. 6, p. 391, 1966

8. Strehlow, R.A. — "Gas Phase Detonations: Recent Development" Combustion and Flame, Vol. 27, No. 2, p. 81, 1968

9. Lee, J.H., Soloukhin, R.I., and Oppehheim, A.K. — "Current Views on Gaseous Detonations" Astronautica Acta, Vol. 14, p. 565, 1969

10. Lee, J.H. — "Initiation of Gaseous Detonations" Annual Review of Physical Chemistry, Vol. 28, p. 75, 1977

11. Strehlow, R.A. — "Unconfined Vapor-Cloud Explosions - An Overview" 14th Symposium (International) on Combustion, p. 1189, The Combustion Institute, Pittsburgh, 1973

12. Strehlow, R.A., and Baker, W.E. — "The Characterization and Evaluation of Accidental Explosions" Prog. Energy Combust. Sci., Vol. 2, p. 27, 1976

13. Lee, J.H., Pangritz, D., and Wagner, H.Gg. — "Some General Considerations of the Initiation of Unconfined Detonations" Max-Planck-Institute fur Stromungsforschung, Gottingen, Report No. 26, 1976.

14. Dorge, K.J., Pangritz, D., and Wagner, H.Gg. — "Experiments on Velocity Augmentation of Spherical Flames by Grids" Acta Astronautica, Vol. 3, p. 1067, 1976

15. Knystautas, R., Lee, J.H., Moen, I., and Wagner, H.Gg. — "Direct Initiation of Spherical Detonation by a Hot Turbulent Gas Jet" 17th Symposium (International) on Combustion, p. 1235, The Combustion Institute, Pittsburgh, 1979

16. Toong, T.Y. — "Chemical Effects on Sound Propagation" Combustion and Flame, Vol. 18, p.207, 1972

17. Toong, T.Y., Arbeau, P., Garris, C.A., and Patureau, J.P. — "Acoustic-Kinetic Interactions in an Irreversibly Reacting Medium" 15th Symposium (International) on Combustion, p.87, The Combustion Institute, Pittsburgh, 1975

18. Patureau, J.P., Toong, T.Y., and Garris, C.A. — "Experimental Investigation of Acoustic-Kinetic Interactions in Non-Equilibrium H_2-Cl_2 Reactions" 16th Symposium (International) on Combustion, p. 929, The Combustion Institute, Pittsburgh, 1977

19. Abouseif, G.E., Toong, T.Y., and Converti, J. — "Acoustic- and Shock-Kinetic Interactions in Non-Equilibrium H_2-Cl_2 Reactions" 17th Symposium (International) on Combustion, p. 1341, The Combustion Institute, Pittsburgh, 1979

20. Zajac, L.J., and Oppenheim, A.K. — "Dynamics of an Explosive Reaction Center" AIAA Journal, Vol. 9, p. 545, 1971

21. Meyer, J.W., and Oppenheim, A.K. — "Coherent Theory of the Strong Ignition Limit" Combustion and Flame, Vol. 17, p. 65, 1971

22. Norrish, R.G.W. — "The Study of Combustion by Photochemical Methods - Plenary Lecture" 10th Symposium (International) on Combustion, p. 1, The Combustion Institute, Pittsburgh, 1965

23. Norrish, R.G.W., Porter, G., and Thrush, B.A. "Studies of the Explosive Combustion of Hydrocarbons by Kinetic Spectroscopy - I. Free Radical Absorption Spectra in Acetylene Combustion" Proceedings of the Royal Society of London, Ser. A, Vol. 216, p. 165, 1953

24. Norrish, R.G.W., Porter, G., and Thrush, B.A. "Studies of the Explosive Combustion of Hydrocarbons by Kinetic Spectroscopy - II. Comparative Investigations of Hydrocarbons and a Study of the Continuous Absorption Spectra" Proceedings of the Royal Society of London, Ser. A., Vol. 227, p.423, 1955

25. Norrish, R.G.W., and Thrush, B.A. "Flash Photolysis and Kinetic Spectroscopy" Quarterly Reviews, Vol. 10, p. 149, 1956

26. Norrish, R.G.W., Porter, G., and Thrush, B.A. "Kinetic Studies of Gaseous Explosions" 5th Symposium (International) on Combustion, p. 651, The Combustion Institute, Pittsburgh, 1955

27. Thrush, B.A. "The Homogeneity of Explosions Initiated by Flash Photolysis" Proceedings of the Royal Society of London, Series A, Vol. 233, p. 147, 1955

28. Birkby, C., and Hutton, E. "Gaseous Explosions Initiated by Flash Photolysis - An Investigation of Radical and Ion Formation" 13th Symposium (International) on Combustion, p. 767, The Combustion Institute, Pittsburgh, 1971

29. Kinbara, T., and Noda, K. "Ion Formation in the Photochemically Initiated Combustion of the Mixture C_2H_2-O_2-NO_2. /I: The Ion Current and the Absorption Spectra" 12th Symposium (International) on Combustion, p. 395, The Combustion Institute, Pittsburgh, 1969

30. Kinbara, T., and Noda, K "Ion Formation in the Photochemically Initiated Combustion of C_2H_2-O_2-NO_2 Mixtures. Part II. Ion Current and Emission Spectra" 13th Symposium (International) on Combustion, p. 333, The Combustion Institute, Pittsburgh, 1971

31. Kinbara, T., and Noda, K. "Relation Between Ion Creation and C_2, CH, and OH Formation in the Combustion of Hydrocarbonds" 14th Symposium (International) on Combustion, p. 321, The Combustion Institute, Pittsburgh, 1973

32. Takahashi, T., Yoshida, E., and Masuko, A. — "A Study of Hydrocarbon Combustion by Flash Photolysis - Measurement of Absorption Spectra of Free Radicals and Explosion Pressure" Kogyo Kagaku Zasshi (Journal of Industrial Chemistry), Vol. 63, No. 8, p. 86, 1960 (in Japanese)

33. Takahashi, T., Yoshida, E., and Masuko, A. — "A Study of Hydrocarbon Combustion by Flash Photolysis - Induction Time and Explosion Limit of C_2H_2-O_2 and H_2-O_2 Mixtures" Kogyo Kagaku Zasshi (Journal of Industrial Chemistry), Vol. 63, No. 12, p. 62, 1960 (in Japanese)

34. Wadsworth, J. — "Use of Flash Photolysis to Initiate Detonation in Gaseous Mixtures" Nature, Vol. 190, p. 623, 1961

35. Calvert, J.G., and Pitts, J.N. — "Photochemistry" John Wiley & Sons, Inc., Chapter 3, pp. 126-239, 1966

36. Cohen, N., Jacobs, T.A., Emanuel, G., and Wilkins, R.L. — "Chemical Kinetics of Hydrogen Halide Lasers. 1. The H_2-Cl_2 System" International Journal of Chemical Kinetics, Vol. 1, p. 551, 1969 also erratum, ibid., Vol. 2, p. 339, 1970

37. Kondratiev, V.N. — "Rate Constants of Gas Phase Reactions" Academy of Sciences of the USSR, Order-of-Lenin Institute of Chemical Physics (Edited by R.M. Fristrom), National Bureau of Standards, U.S. Department of Commerce, COM-72-10014, 1972

38. Cerkanowicz, A.E., and Stevens, J.G. — "Radiative Augmentation of Combustion: Modeling" 1978 Fall Technical Meeting, Eastern Section of the Combustion Institute, Miami Beach, Florida, Paper No. 71, 1978

39. Lee, J.H., Knystautas, R., and Yoshikawa, N. — "Photochemical Initiation of Gaseous Detonations" Acta Astronautica, Vol. 5, p. 971, 1978

40. Zeldovich, Ya.B., and Kompaneets, A.S. — "Theory of Detonation" Academic Press, Chapter II, Section 11, 1960

41. Williams, F.A. — "Combustion Theory" Addison-Wesley, Inc., Chapter 2, pp. 18-36, 1965

42. Van Leer, B. — "Stabilization of Difference Schemes for the Equations of Inviscid Compressible Flow by Artificial Diffusion" Journal of Computational Physics, Vol. 3, p. 473, 1969

43. Taki, S., and Fujiwara, T. — "Numerical Analysis of Two-Dimensional Nonsteady Detonations" AIAA Journal, Vol. 16, No. 1, p. 73, 1978

44. Boris, J.P., and Book, D.L. — "Flux-Corrected Transport. I. SHASTA, a Fluid Transport Algorithm that Works" Journal of Computational Physics, Vol. 14, p. 38, 1973

45. Book, D.L., Boris, J.P., and Hain, K. — "Flux-Corrected Transport II: Generalizations of the Method" Journal of Computational Physics, Vol. 18, p. 248, 1975

46. Boris, J.P., and Book, D.L. — "Flux-Corrected Transport. III. Minimal-Error FCT Algorithms" Journal of Computational Physics, Vol. 20, p. 397, 1976

47. Zeldovich, Ya.B., Librovich, V.B., Makhviladze, G.M., and Sivashinsky, G.I. — "On the Development of Detonation in a Non-Uniformly Preheated Gas" Astronautica Acta, Vol. 15, p. 313, 1970

48. Barthel, H.O., and Strehlow, R.A. — "Direct Detonation Initiation by Localized Enhanced Reactivity" 17th Aerospace Sciences Meeting, New Orleans, LA., Paper No. 79-0286, 1979

49. Hung, C.M., and MacCormack, R.W. — "Numerical Solutions of Supersonic and Hyperbolic Laminar Compression Corner Flows" AIAA Journal, Vol. 14, No. 4, p. 475, 1976

50. MacCormack, R.W. — "Numerical Solution of the Interaction of a Shock Wave with a Laminar Boundary Layer" Lecture Notes in Physics, Springer-Verlag, Vol. 8, p. 151, 1972

51. Knystautas, R. — Private Communication

52. Benson, S.W., Cruickshank, F.R., and Shaw, R. — "Iodine Monochloride as a Thermal Source of Chlorine Atoms: The Reaction of Chlorine Atoms with Hydrogen" International Journal of Chemical Kinetics, Vol. 1, p. 29, 1969

53. Gordon, S., and McBride, B.J. — "Computer Program for Calculation of Complex Chemical Equilibrium Compositions, Rocket Performance, Incident and Reflected Shocks, and Chapman-Jouguet Detonations" NASA-SP-273, 1971

54. Stull, D.R., and Prophet, H. et al. "JANAF THERMOCHEMICAL TABLES" U.S. National Bureau of Standards, NSRDS-NBS-37, 1971

55. Rice, E.E. "A Study of Photochemically Initiated Weak Detonation Waves in Hydrogen-Oxygen-Chlorine Mixtures" Ph.D. Thesis, Ohio State University, 1972

56. Yang, C.H., and Gray, B.F. "On the Slow Oxidation of Hydrocarbon and Cool Flames" Journal of Physical Chemistry, Vol. 73, No. 10, p. 3395, 1969

57. Yang, C.H. "Two-Stage Ignition and Self-Excited Thermo-kinetic Oscillation in Hydrocarbon Oxidation" Journal of Physical Chemistry, Vol. 73, No. 10, p. 3407, 1969

58. Berlad, A.L. "Photochemical Effects on Explosive Instability" Combustion and Flame, Vol. 11, p. 445, 1967

59. Cerkanowicz, A.E. "Photochemical Enhancement of Combustion and Mixing in Supersonic Flows". AFOSR Scientific Report, AFOSR-TR-74-0153, 1973

60. Levy, M.E., Cerkanowicz, A.E., and McAlevy III, R.F. "Photochemical Ignition of Gaseous Fuel - Oxidizer Mixtures at Subatmospheric Pressures" AFOSR Scientific Report 68-1553, 1968

61. Levy, M.E., Cerkanowicz, A.E., and McAlevy III, R.F. "Photochemical Ignition of Gaseous Fuel - Oxidizer Mixtures at Subatmospheric Pressures" AFOSR Scientific Report, AFOSR 69-2153TR, 1969

TABLE 1

VARIATION OF INDUCTION TIME WITH RESPECT TO THE RADIATION INTENSITY (3300Å) IN EQUI-MOLAR H_2 - Cl_2 at 100 TORR (CONSTANT VOLUME EXPLOSION)

RADIATION INTENSITY (w/cm^2)	INDUCTION TIME (μsec)
1×10^2	168.0
2×10^2	117.5
3×10^2	95.2
4×10^2	80.9
5×10^2	72.7
7.5×10^2	57.8
1×10^3	49.4
1.25×10^3	43.2
1.5×10^3	38.8
2×10^3	32.9
2.5×10^3	28.9
3×10^3	26.1
4×10^3	21.8
5×10^3	19.0
6×10^3	16.9
7×10^3	15.2

TABLE 2

INFLUENCE OF α AND β ON SHOCK WAVE AMPLIFICATION

Run No.	α	β	(P_s/P_o,	x_s/L,	x_r/L,	t/τ_g)	Shock & Reaction Front
1	11.36	6.90	2.70	1.006	0.675	0.730	Decoupled
2	11.36	27.58	5.89	1.004	0.837	0.519	"
3	11.36	137.9	5.87	1.009	0.929	0.422	"
4	11.36	2.758×10^{12}	3.56	1.018	0.955	0.313	"
5	18.18	55.16	7.03	1.009	0.972	0.502	"
6	18.18	137.9	10.2	1.025	0.999	0.357	"
7	22.73	6.90	5.99	1.003	0.852	0.585	"
8	22.73	13.79	9.46	1.004	0.954	0.453	"
9	22.73	27.58	10.8	1.013,	0.984	0.394	"
10	22.73	137.9	12.7	1.011	1.001	0.327	Coupled
11	30.30	4.137	6.23	1.011	0.843	0.680	Decoupled
12	30.30	6.895	12.7	1.016	0.985	0.512	"
13	30.30	27.58	15.0	1.011	1.003	0.358	Coupled
14	36.36	6.895	15.6	1.008	0.995	0.479	"
15	45.45	1.379	1.88	1.001	0.389	1.320	Decoupled
16	45.45	2.207	4.24	1.006	0.656	0.925	"
17	45.45	2.758	18.3	1.004	0.994	0.733	Coupled
18	45.45	27.58	20.0	1.008	1.008	0.319	"
19	45.45	2.758×10^{12}	18.2	1.002	0.993	0.732	"
20	90.91	1.379	1.65	0.494	0.305	0.974	Decoupled

TABLE 3

REACTION RATE CONSTANTS OF H_2-$C\ell_2$ SYSTEM

Elementary Step	REACTION RATE CONSTANT $k = AT^n \exp(-E_{act}/RT)$*	A	n	E_{act}	Third Body Efficiencies	
$H_2 + M \underset{k-}{\overset{k+}{\rightleftharpoons}} 2H + M$	k+	(4.072×10^{18})	(-1.008)	(104.13)	M = ($C\ell$, $C\ell_2$, $HC\ell$)	1
	k-	10^{18}	-1	0.0	M = (H_2)	2.5
					M = (H)	20
$C\ell_2 + M \underset{k-}{\overset{k+}{\rightleftharpoons}} 2C\ell + M$	k+	6.15×10^{21}	-2.087	57.08	M = ($HC\ell$, H, H_2, $C\ell_2$)	1
	k-	(4.168×10^{19})	(-1.691)	(-0.020)	M = ($C\ell_2$)	1
$H + C\ell + M \underset{k-}{\overset{k+}{\rightleftharpoons}} HC\ell + M$	k+	(1.896×10^{21})	(-1.942)	(1.134)	M = (H, $C\ell$, H_2, $C\ell_2$, $HC\ell$)	1
	k-	6.776×10^{21}	-2	102.2		
$H_2 + C\ell \underset{k-}{\overset{k+}{\rightleftharpoons}} HC\ell + H$ **	k+	4.8×10^{13}	0.0	5.26		
	k-	(5.88×10^{13})	(-0.088)	(4.528)		
$C\ell_2 + H \underset{k-}{\overset{k+}{\rightleftharpoons}} HC\ell + C\ell$	k+	1.6×10^{12}	-0.05	2.62		
	k-	(5.17×10^{10})	(0.258)	(48.13)		

* k is in cc/mole/sec or $(cc/mole)^2$/sec, T in °K and E_{act} in Kcal/mole.

k+ has been obtained from the paper by Benson et al. (52), and other reaction rates and the third body efficiencies have been obtained from the paper by Cohen et al. (36)

Numbers in parentheses have been computed using the relation k+/k- = K_c, where K_c is equilibrium constant and has been calculated from the data of JANAF Thermochemical Tables (54).

TABLE 4

COEFFICIENTS OF POLYNOMIAL FITTING FOR C_p and h OF H_2-$C\ell_2$ SYSTEM (from Reference 53)

$$\frac{C_P}{R_o} = a_1 + a_2T + a_3T^2 + a_4T^3 + a_5T^4$$

$$\frac{h}{R_oT} = a_1 + a_2/2\ T + a_3/3\ T^2 + a_4/4\ T^3 + a_5/5\ T^4 + a_6/T \qquad (R_o: \text{universal gas constant})$$

Chemical Species	a_1	a_2	a_3	a_4	a_5	a_6
H_2	.30574 E+01	.26765 E-02	-.58099 E-05	.55210 E-08	-.18123 E-11	-.98890 E+03
	.31001 E+01	.51119 E-03	.52644 E-07	-.34910 E-10	.36945 E-14	-.87738 E+03
H	.25000 E+01	.0	.0	.0	.0	.25472 E+05
	.25000 E+01	.0	.0	.0	.0	.25472 E+05
$C\ell_2$	.31317 E+01	.48998 E-02	-.69411 E-05	.44786 E-08	-.10622 E-11	-.10980 E+04
	.43078 E+01	.31183 E-03	-.15311 E-06	.44512 E-10	-.43058 E-14	-.13458 E+04
$C\ell$	.20888 E+01	.28676 E-02	-.41906 E-05	.22409 E-08	-.33259 E-12	.13836 E+05
	.29595 E+01	-.41900 E-03	.15981 E-06	-.28103 E-10	.18674 E-14	.13659 E+05
$HC\ell$	.35248 E+01	.29985 E-04	-.86222 E-06	.20980 E-08	-.98658 E-12	-.12151 E+05
	.27666 E+01	.14382 E-02	-.46993 E-06	.73499 E-10	-.43731 E-14	-.11917 E+05

* The values in the upper column is for $300 \leq T \leq 1000$ °K, while the lower column represents the values for $1000 \leq T \leq 5000$ °K.

TABLE 5

INDUCTION TIMES OF H_2-$C\ell_2$ CONSTANT VOLUME EXPLOSION

A. Ideal Photochemical Ignition

Run No.	Initial Condition	Cℓ Atom Concentration	Induction Time
A-1	Equi-molar H_2-$C\ell_2$ (100 torr, 298 °K)	2.5×10^{-3} mole/liter (46.5% of initial $[C\ell_2]$)	0.6 μsec
A-2	"	1×10^{-3} mole/liter (18.6% of initial $[C\ell_2]$)	3.6 "
A-3	"	5×10^{-4} mole/liter (9.3% of initial $[C\ell_2]$)	9.7 "
A-4	"	1×10^{-4} mole/liter (1.9% of initial $[C\ell_2]$)	48.6 "
A-5	"	6×10^{-5} mole/liter (1.1% of initial $[C\ell_2]$)	75.4 "
A-6	"	1.5×10^{-5} mole/liter (0.28% of initial $[C\ell_2]$)	160 "
A-7	"	1×10^{-5} mole/liter (0.19% of initial $[C\ell_2]$)	370 "

TABLE 5

INDUCTION TIMES OF H_2-$C\ell_2$ CONSTANT VOLUME EXPLOSION

B. Ideal Thermal Ignition

Run No:	Initial Condition	Temperature	Induction Time
B-1	Equi-molar H_2-$C\ell_2$ (100 torr, 298 °K)	1400 °K	78.5 μsec
B-2	"	1600 °K	23.8 "
B-3	"	1800 °K	9.2 "
B-4	" (20 torr, 298 °K)	1600 °K	123 "
B-5	" (50 torr, 298 °K)	1600 °K	46.2 "
B-6	" (380 torr, 298 °K)	1600 °K	6.3 "
B-7	" (760 torr, 298 °K)	1600 °K	3.1 "

TABLE 5

INDUCTION TIMES OF H_2-$C\ell_2$ CONSTANT VOLUME EXPLOSION

C. Photochemical Ignition

Run No.	Initial Condition	Radiation Intensity	Induction Time
C-1	Equi-molar H_2-$C\ell_2$ (20 torr, 298 °K)	1.5 KW/cm^2 (3300 Å)	83.2 μsec
C-2	" (50 torr, 298 °K)	"	57.6 "
C-3	" (100 torr, 298 °K)	"	38.8 "
C-4	" (380 torr, 298 °K)	"	23.7 "
C-5	" (760 torr, 298 °K)	"	17.7 "

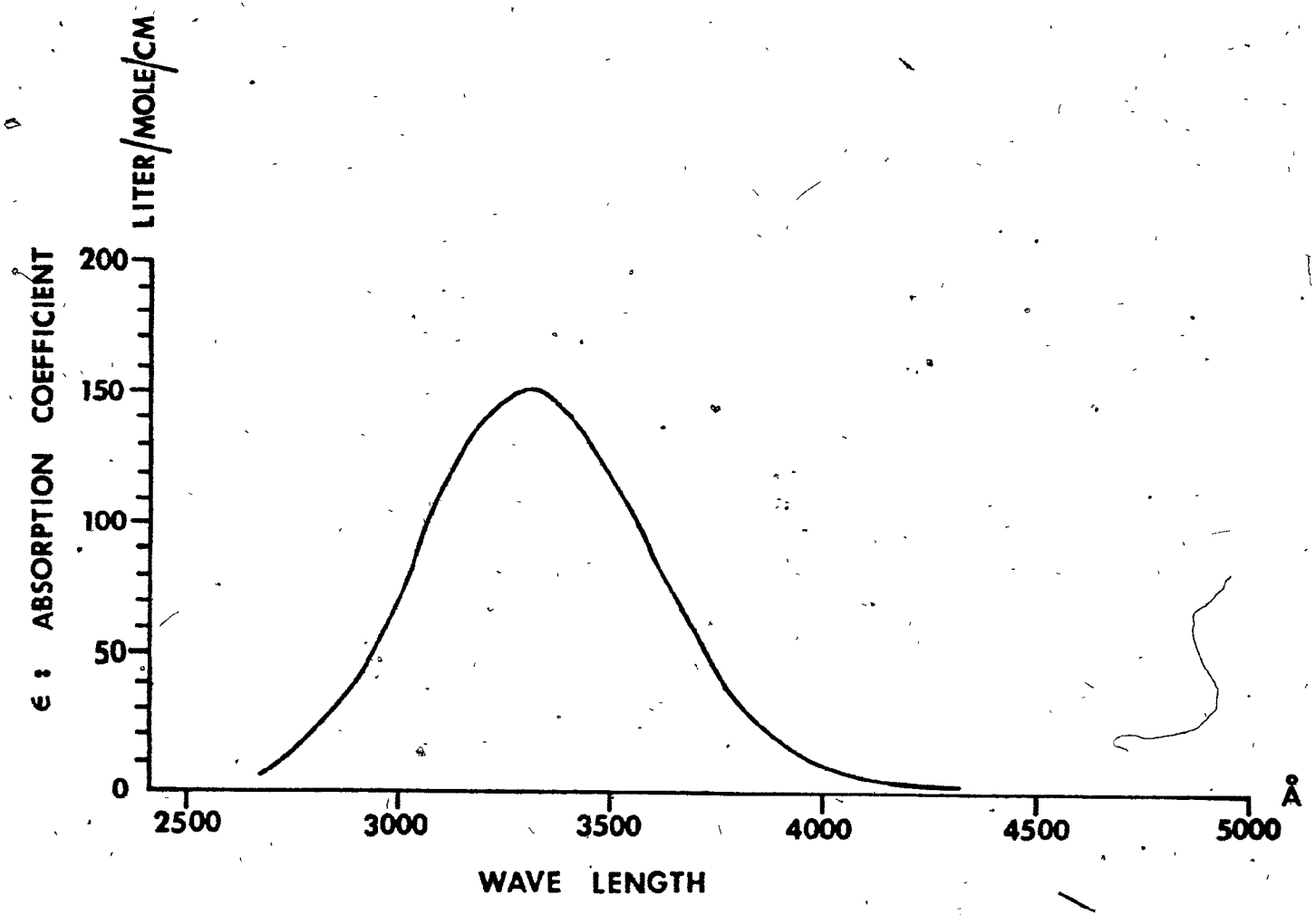

FIG. 1 ABSORPTION SPECTRUM OF Cl_2 AT 291°K (REF. 35)

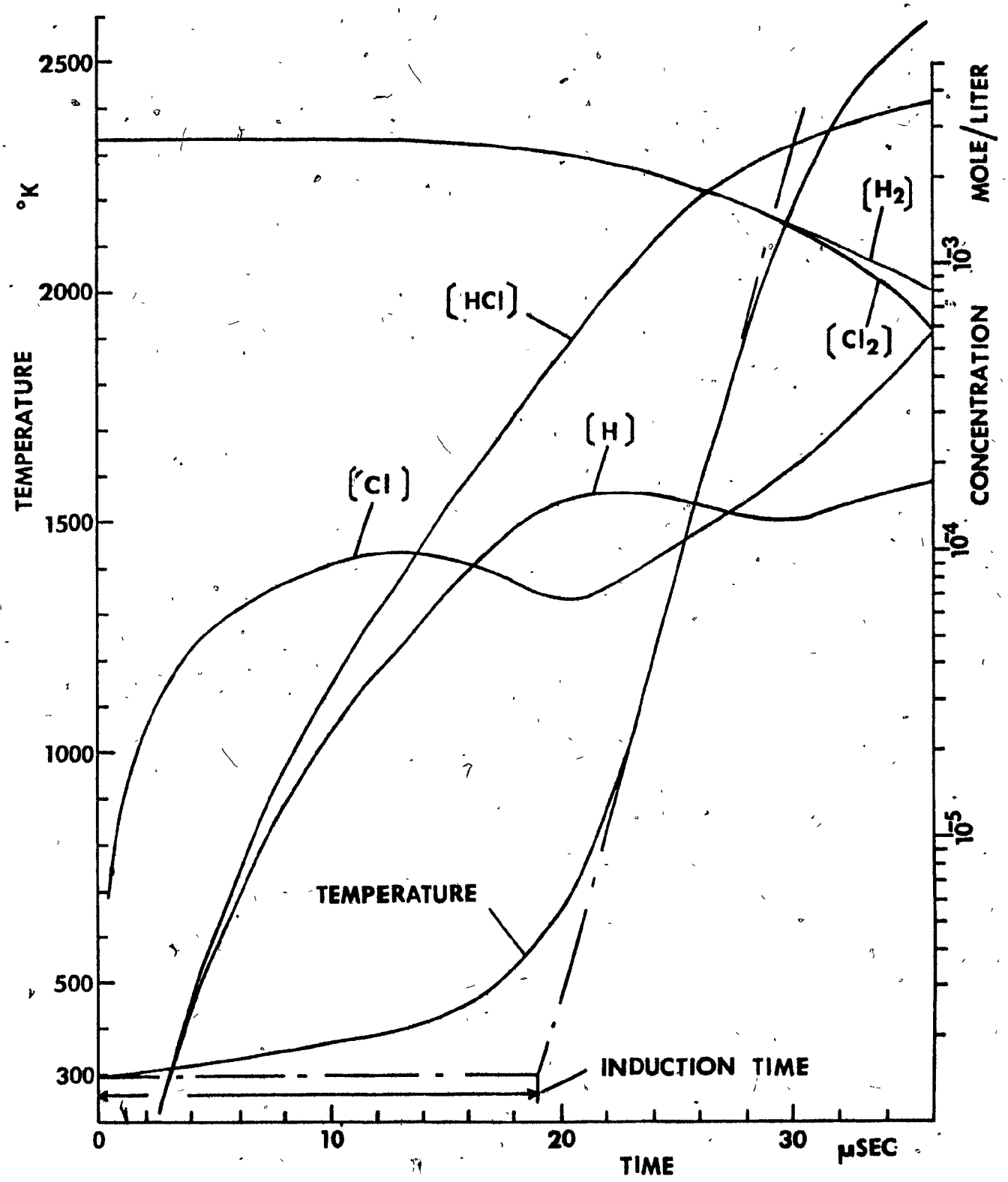

FIG. 2 PHOTOCHEMICAL CONSTANT VOLUME EXPLOSION OF H_2-Cl_2 (EQUI-MOLAR H_2-Cl_2 AT 100 TORR AND 298°K, 3300 Å LIGHT BEAM, RADIATION INTENSITY 5 KW/CM^2)

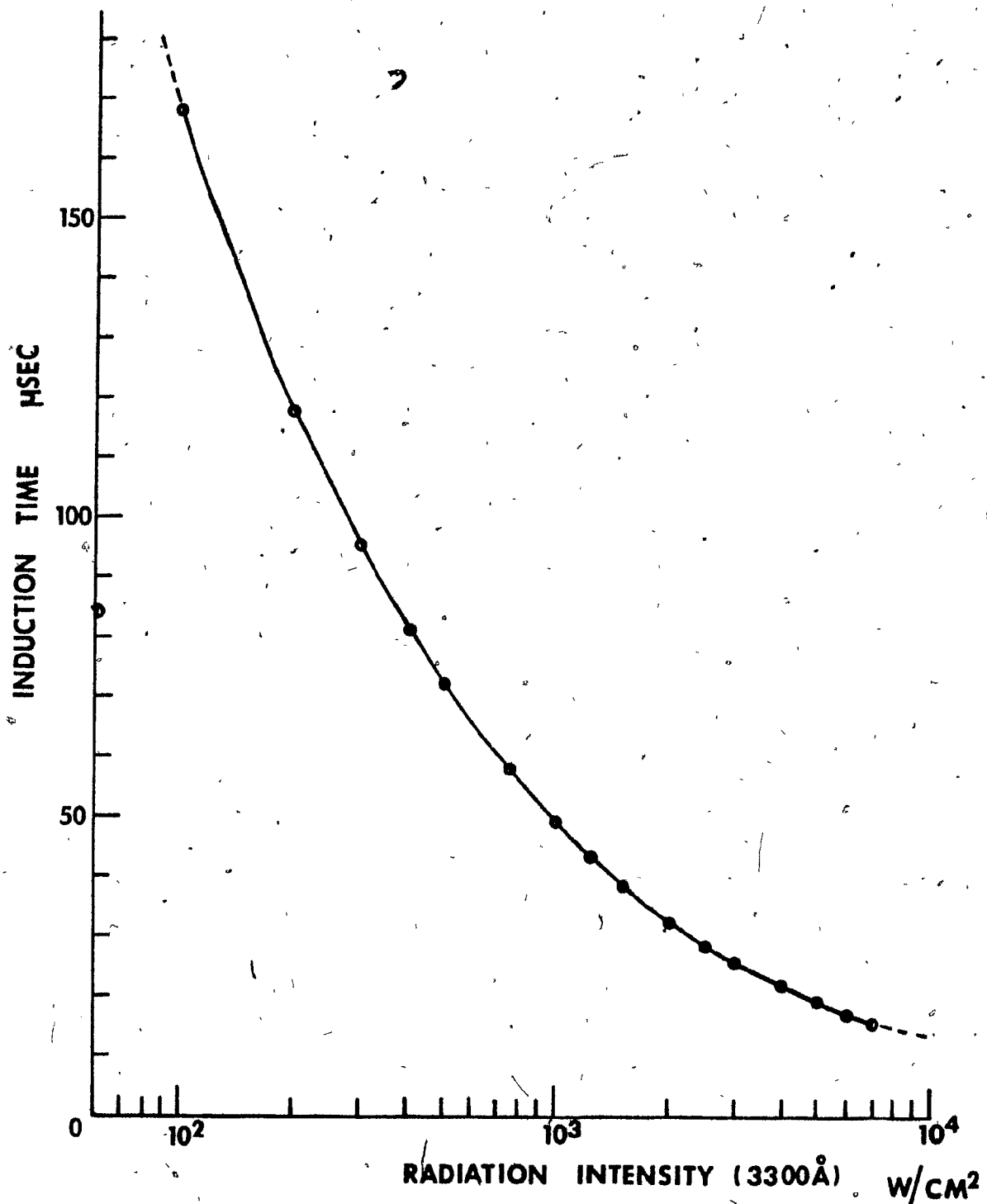

FIG. 3 VARIATION OF INDUCTION TIME WITH RESPECT TO RADIATION INTENSITY IN EQUI-MOLAR H_2-Cl_2 AT 100 TORR

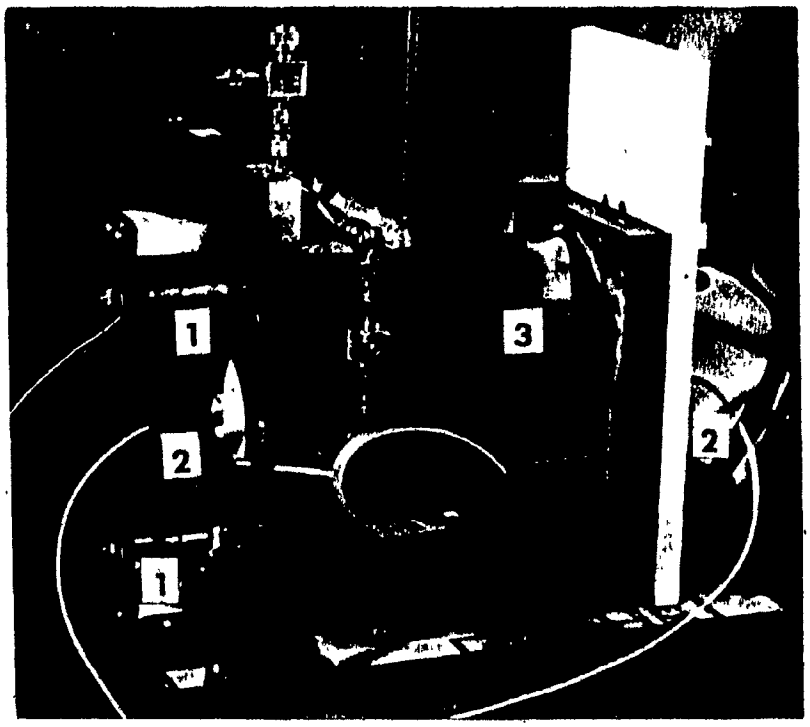

1 FLASH TUBE

2 PRESSURE TRANSDUCER

3 EXPLOSION CHAMBER

FIG.4 EXPERIMENTAL SETUP OF RECTANGULAR EXPLOSION CHAMBER

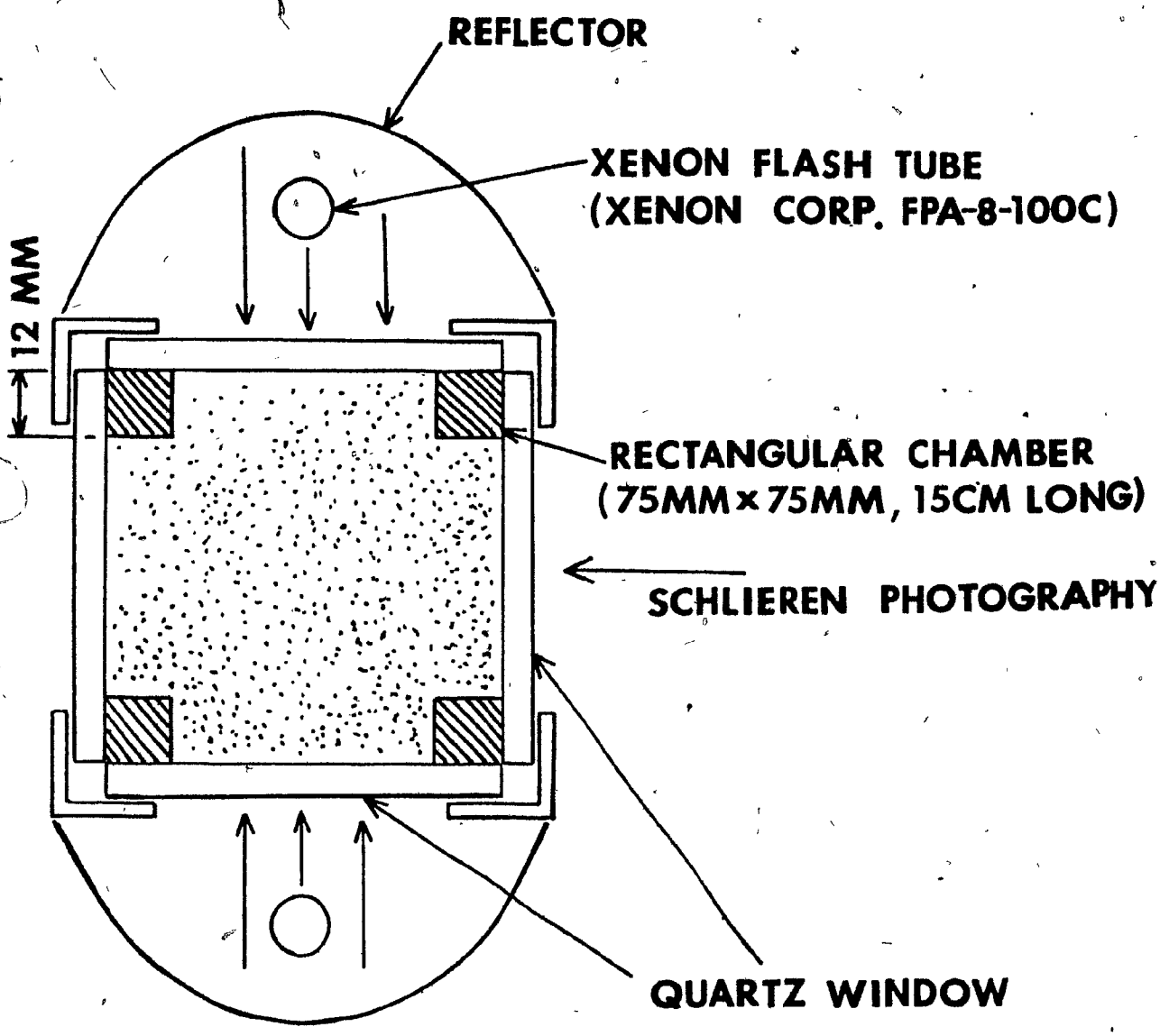

FIG. 5 SCHEMATIC DIAGRAM OF CROSS-SECTION OF RECTANGULAR EXPLOSION CHAMBER

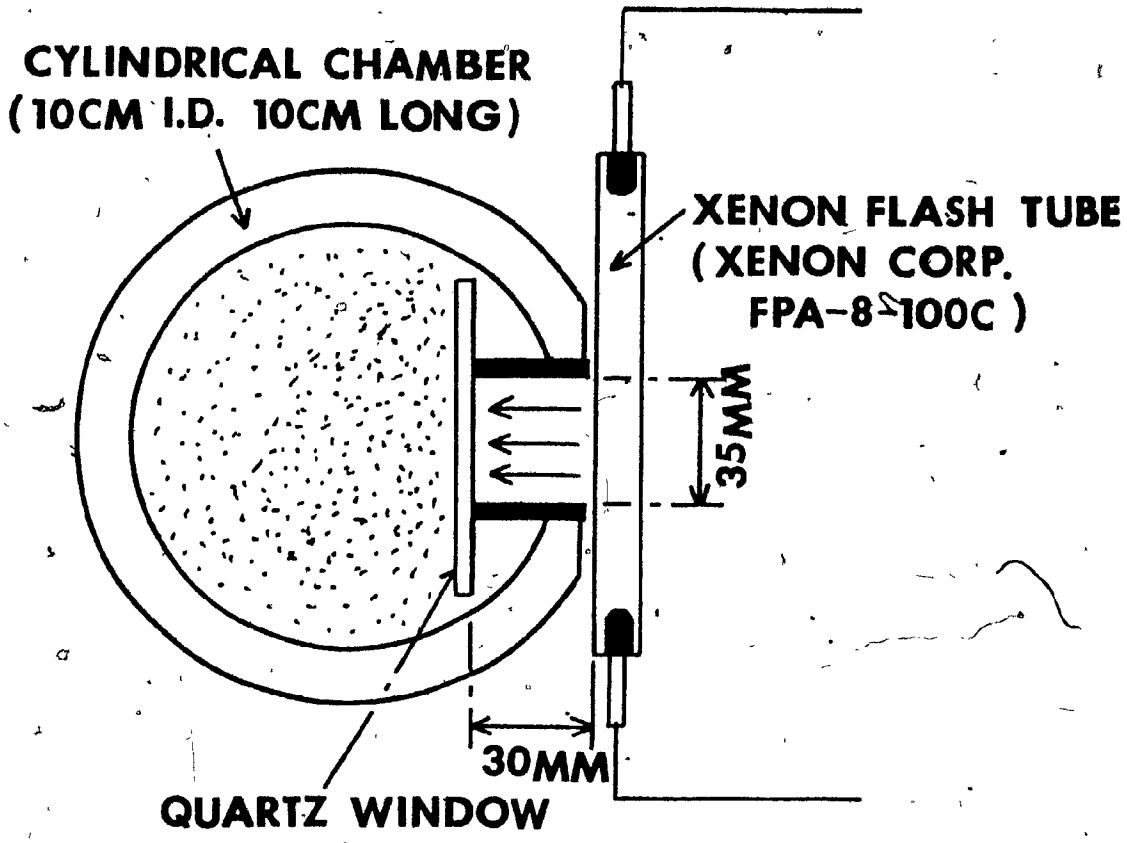

FIG. 6 SCHEMATIC DIAGRAM OF CYLINDRICAL EXPLOSION CHAMBER

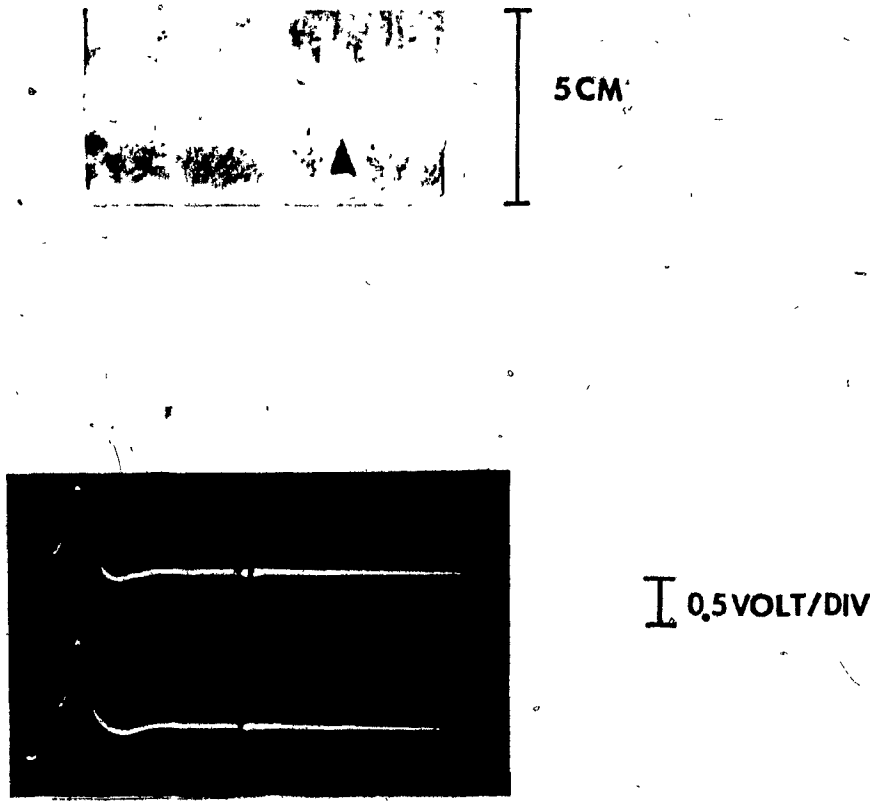

FIG. 7 PHOTOIRRADIATION OF Cl_2 AT 100 TORR
(FLASH ENERGY 1.6 KJ)

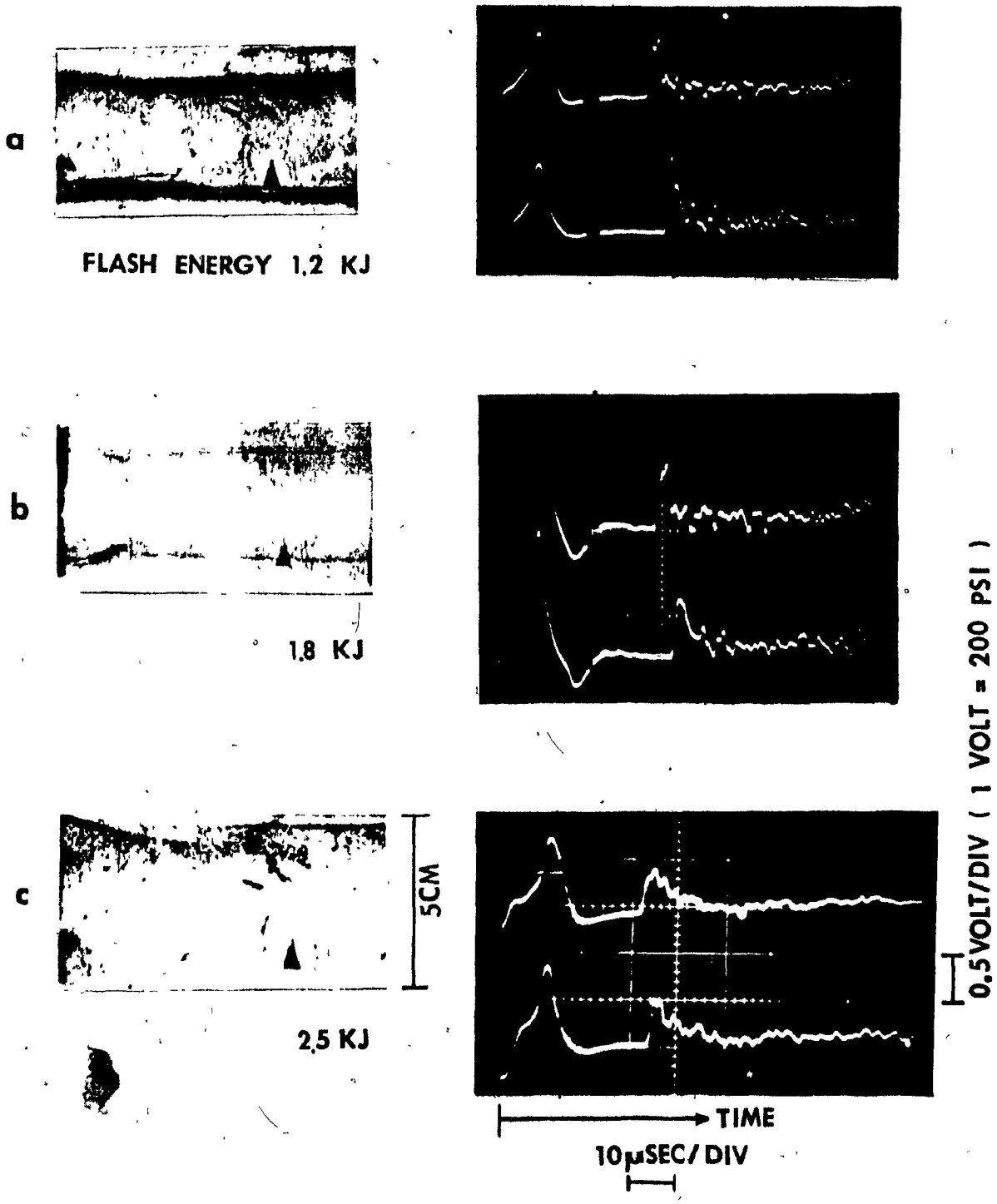

FIG. 8 EFFECT OF FLASH INTENSITY ON DETONATION INITIATION

(EQUI—MOLAR H_2—Cl_2 AT 100 TORR)

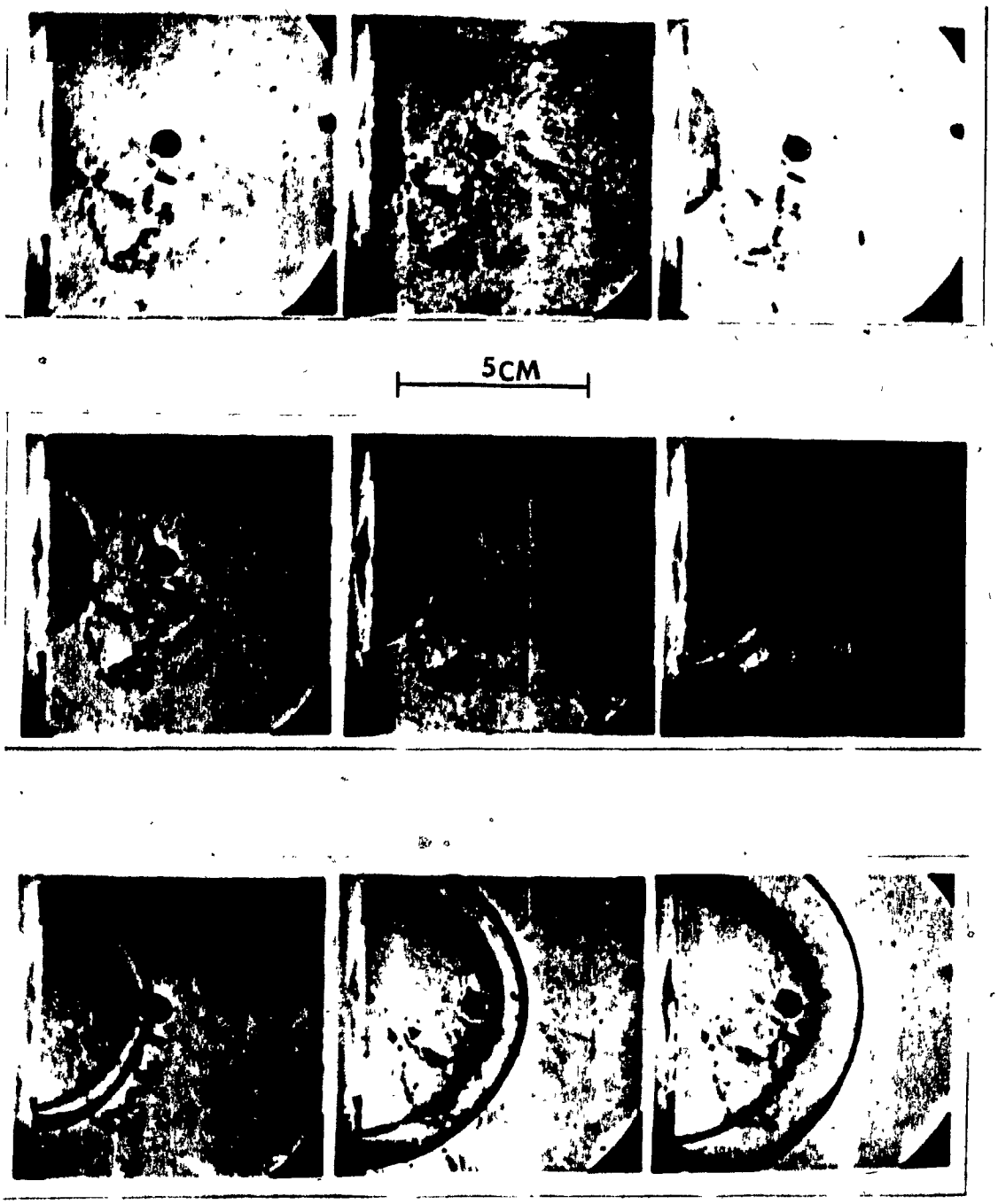

FIG. 9 PHOTOCHEMICAL INITIATION OF DEFLAGRATION

(EQUI-MOLAR H_2-Cl_2 AT 100 TORR, FLASH ENERGY 580 J)

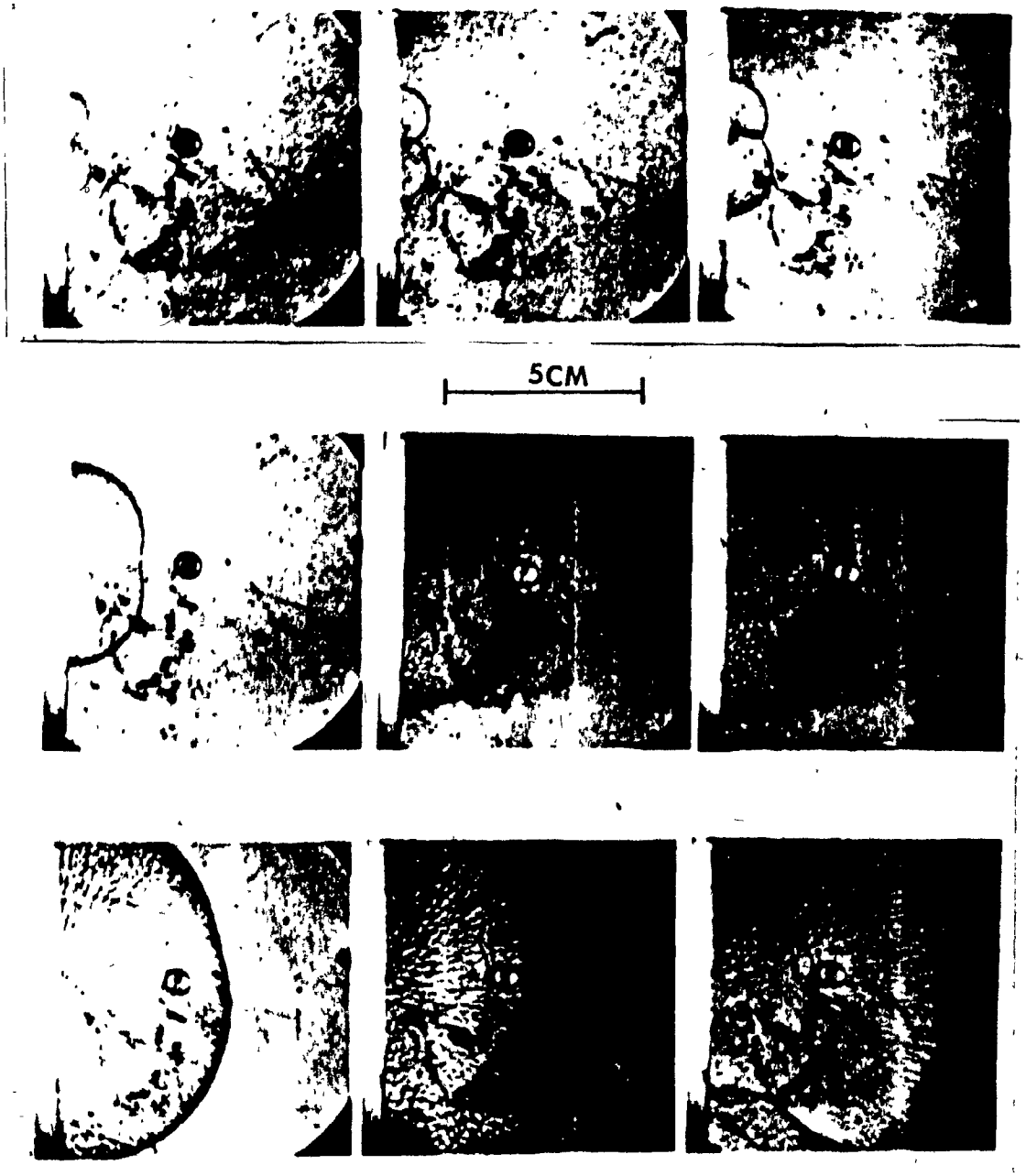

FIG. 10 PHOTOCHEMICAL INITIATION OF DETONATION

(EQUI-MOLAR H_2-Cl_2 AT 100 TORR, FLASH ENERGY 700 J)

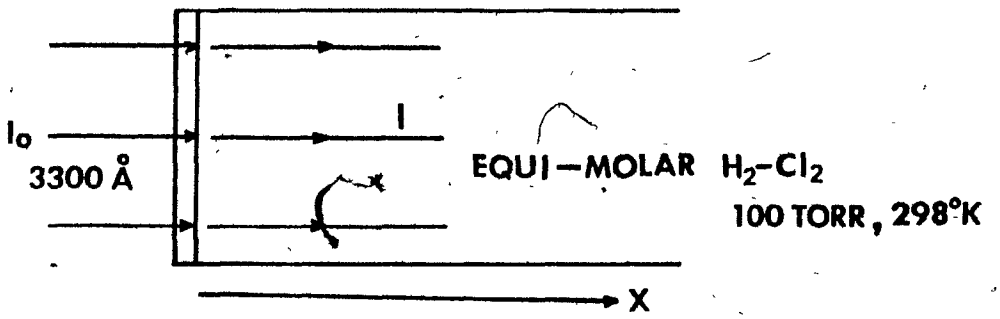

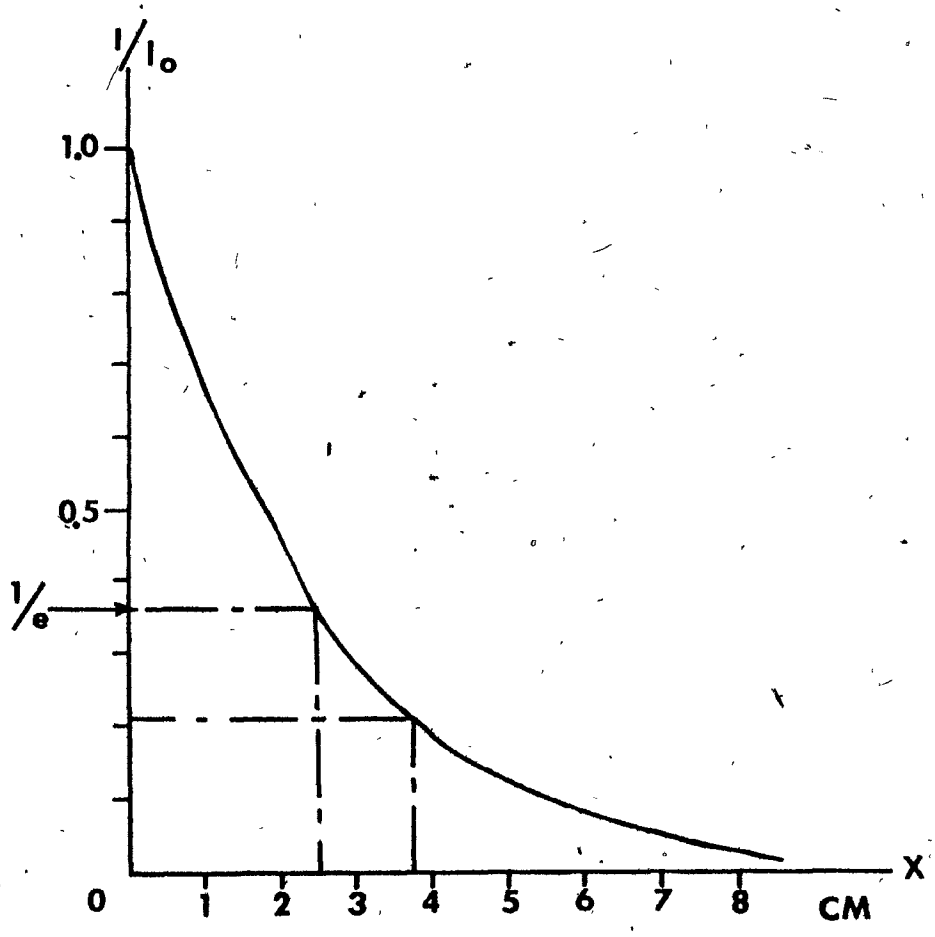

FIG. 11 DECAY OF 3300 Å RADIATION INTENSITY IN EQUI-MOLAR H_2–Cl_2 AT 100 TORR (ESTIMATED BY BEER-LAMBERT LAW)

AT MAXIMUM PRESSURE POINT

	(TIME	TEMPERATURE	HCl MOLE FRACTION)
1	(101.0 μSEC	1007°K	18.8%)
2	(106.8	1013	18.3)
3	(111.1	976	16.6)
4	(115.6	1024	17.6)
5	(118.3	798	9.6)

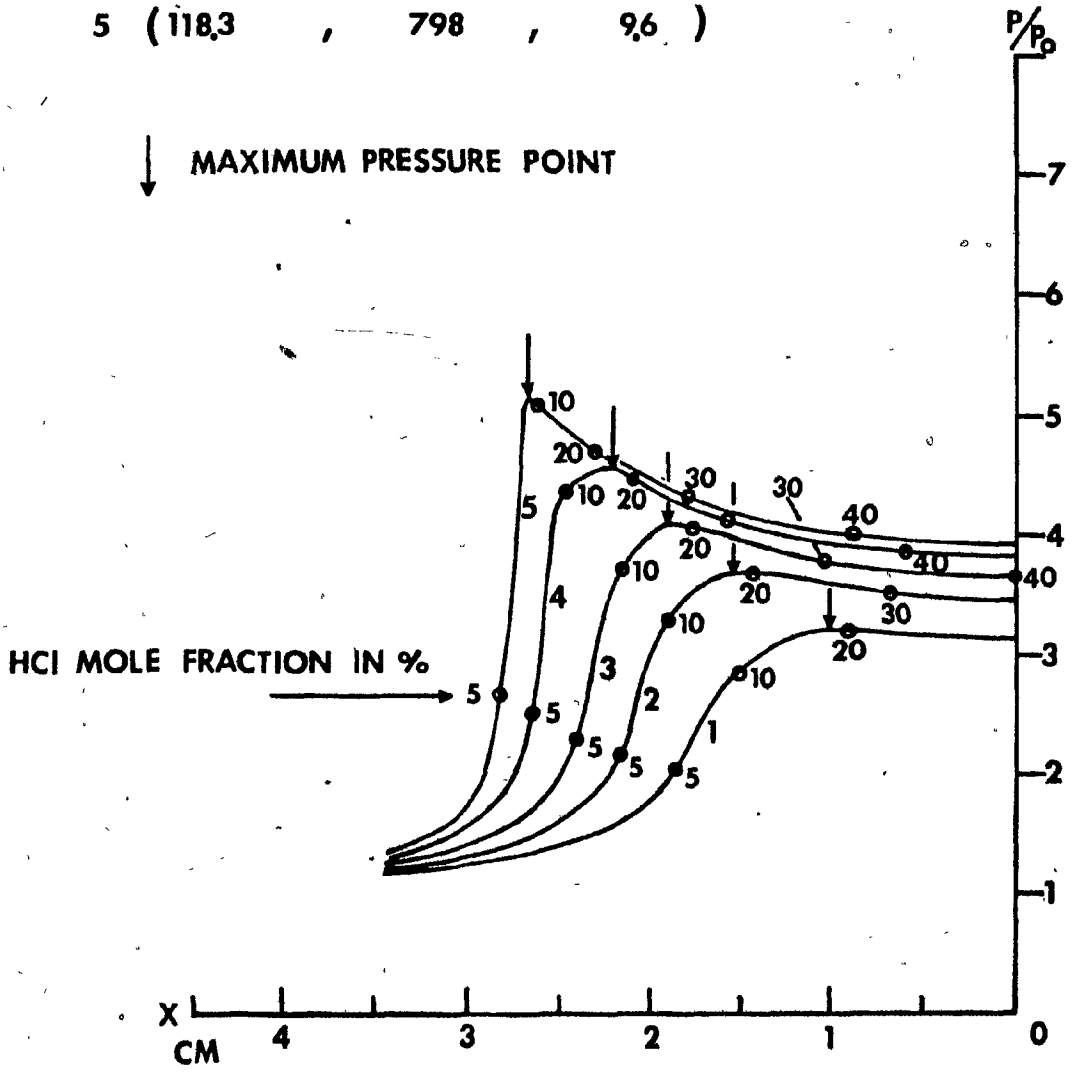

FIG. 12 DEVELOPMENT OF PRESSURE WAVE FOR WEAK RADIATION INTENSITY (EQUI-MOLAR H_2-Cl_2 AT 100 TORR, 3300 Å 5×10^2 W/CM^2 RADIATION)

AT MAXIMUM PRESSURE POINT

	(TIME	, TEMPERATURE	, HCl MOLE FRACTION)
1	(42.5 μSEC	, 1305°K	, 26.1 %)
2	(46.6	, 1441	, 29.0)
3	(50.2	, 1534	, 30.6)
4	(55.1	, 1619	, 31.2)
5	(59.9	, 1756	, 33.2)

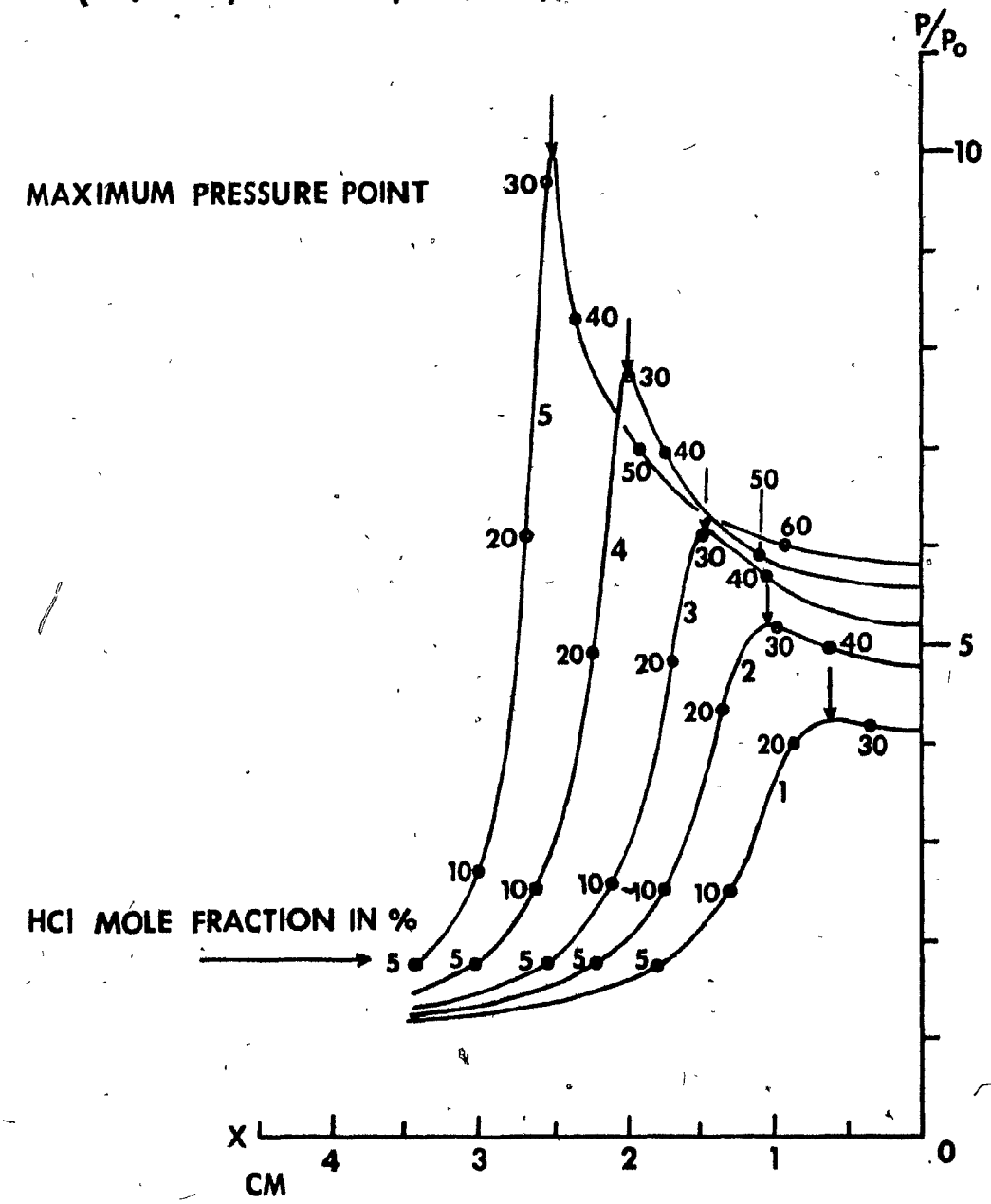

FIG. 13 DEVELOPMENT OF PRESSURE WAVE FOR STRONG RADIATION INTENSITY (EQUI-MOLAR H_2-Cl_2 AT 100 TORR, 3300 Å 2.5×10^3 W/CM^2 RADIATION)

AT MAXIMUM PRESSURE POINT

	(TIME	, TEMPERATURE	, HCl MOLE FRACTION)
1	(21.3 μSEC	, 1175 °K	, 22.5 %)
2	(24.8	, 1563	, 32.0)
3	(29.2	, 1927	, 41.1)
4	(33.2	, 2168	, 47.7)
5	(37.2	, 2315	, 52.2)

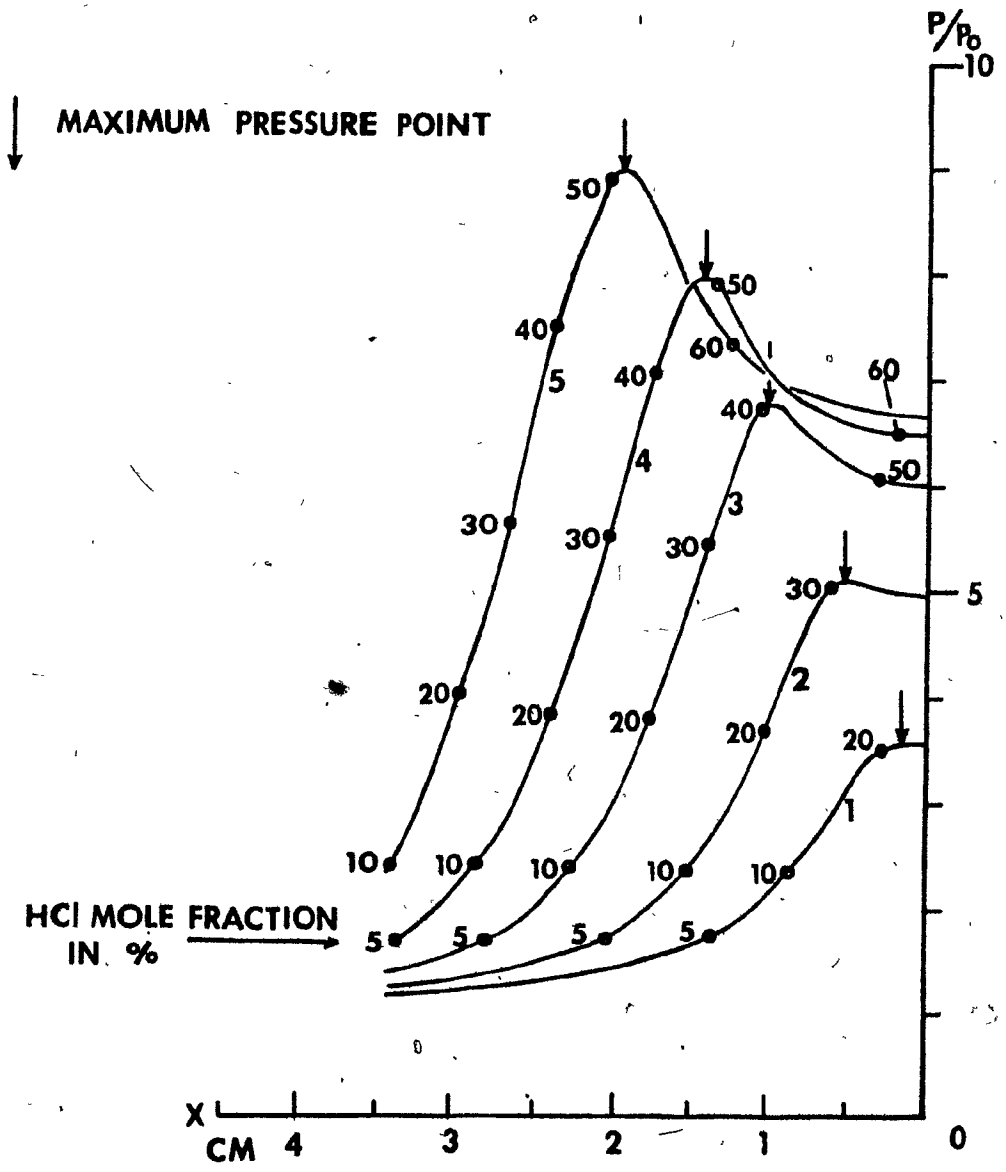

FIG. 14 DEVELOPMENT OF PRESSURE WAVE FOR VERY STRONG RADIATION (EQUI-MOLAR H_2-Cl_2 AT 100 TORR, 3300 Å 7×10^{-3} W/CM^2)

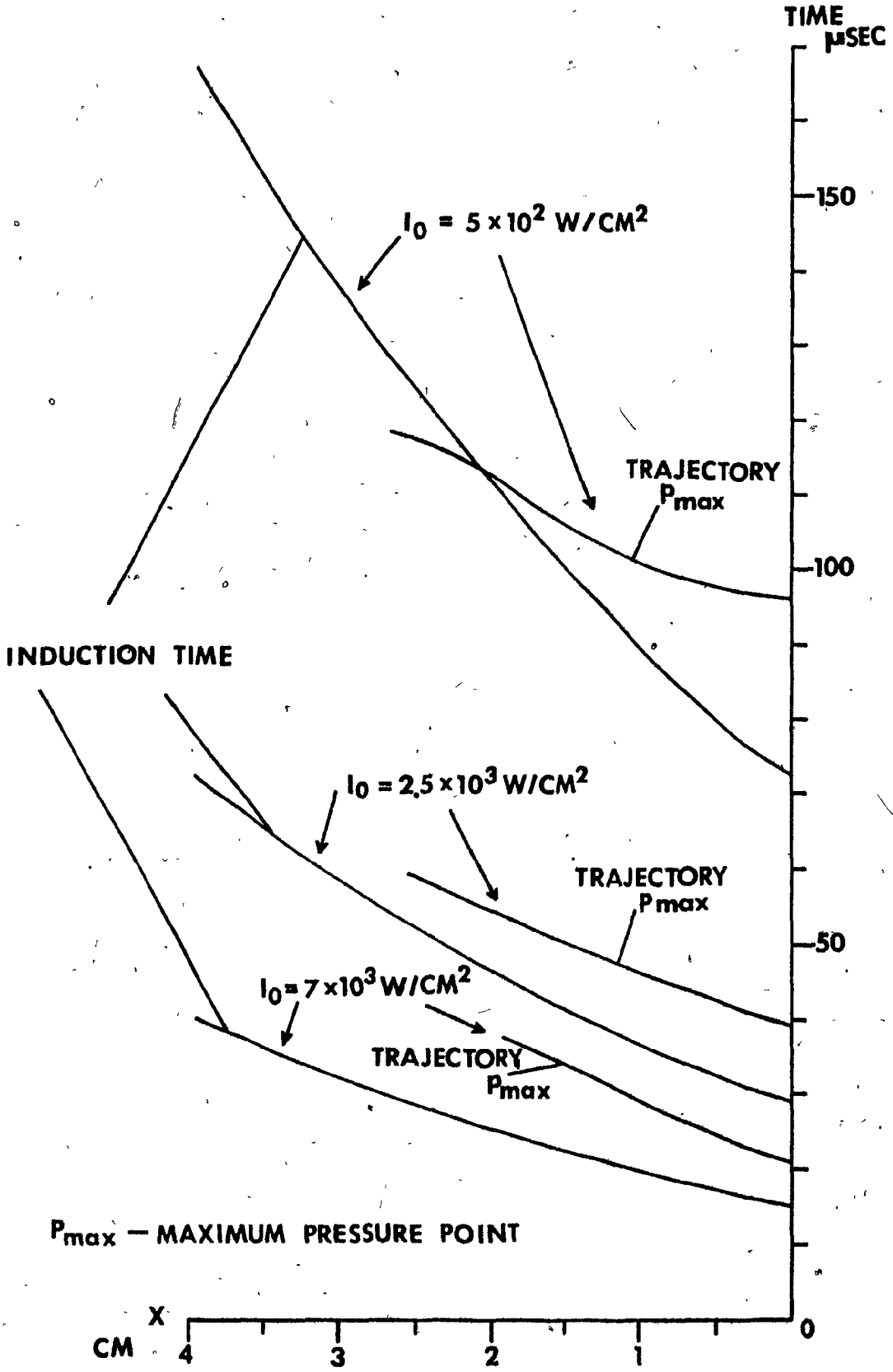

FIG.15 RELATION BETWEEN INDUCTION TIME GRADIENT AND WAVE AMPLIFICATION

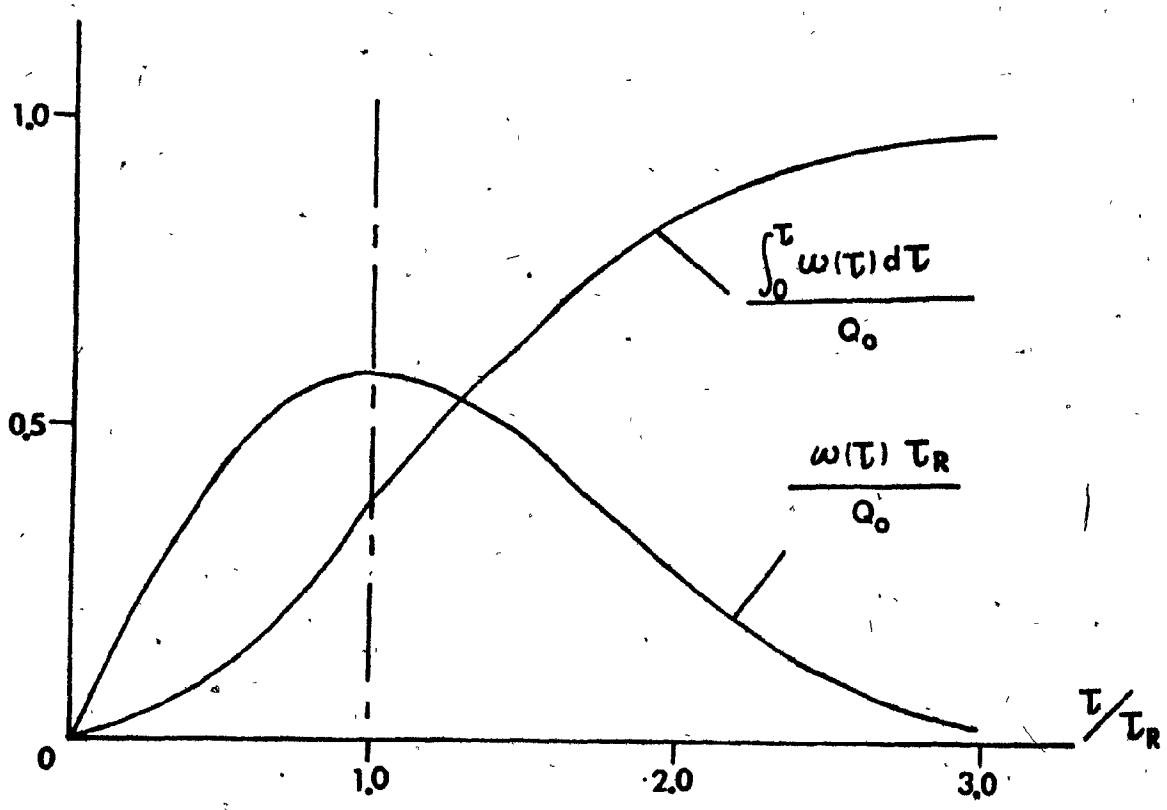

FIG. 16 ENERGY RELEASE FUNCTION

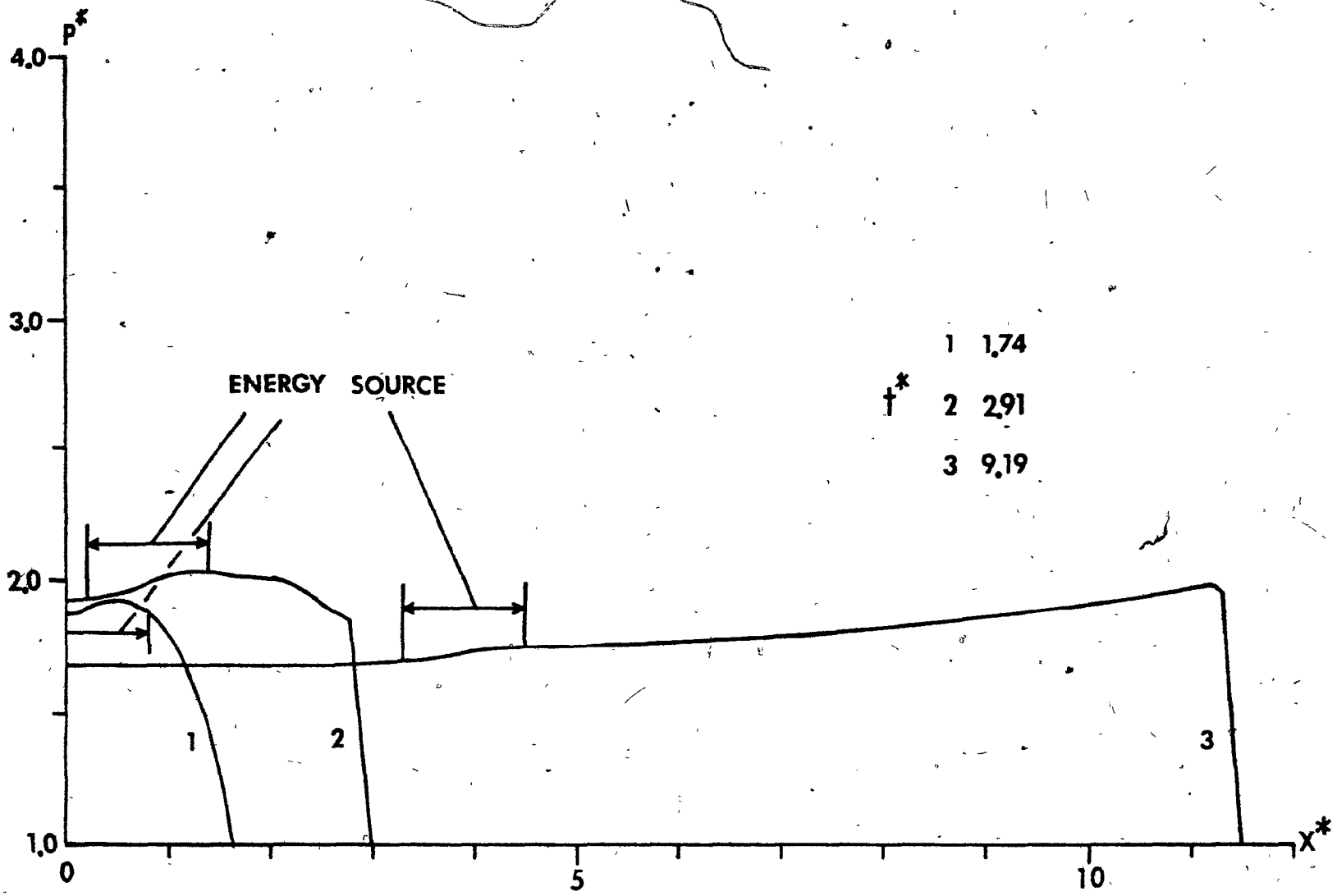

FIG. 17 PRESSURE PROFILE FOR $\gamma=1.4, Q^*=10$ and $A=0.5$

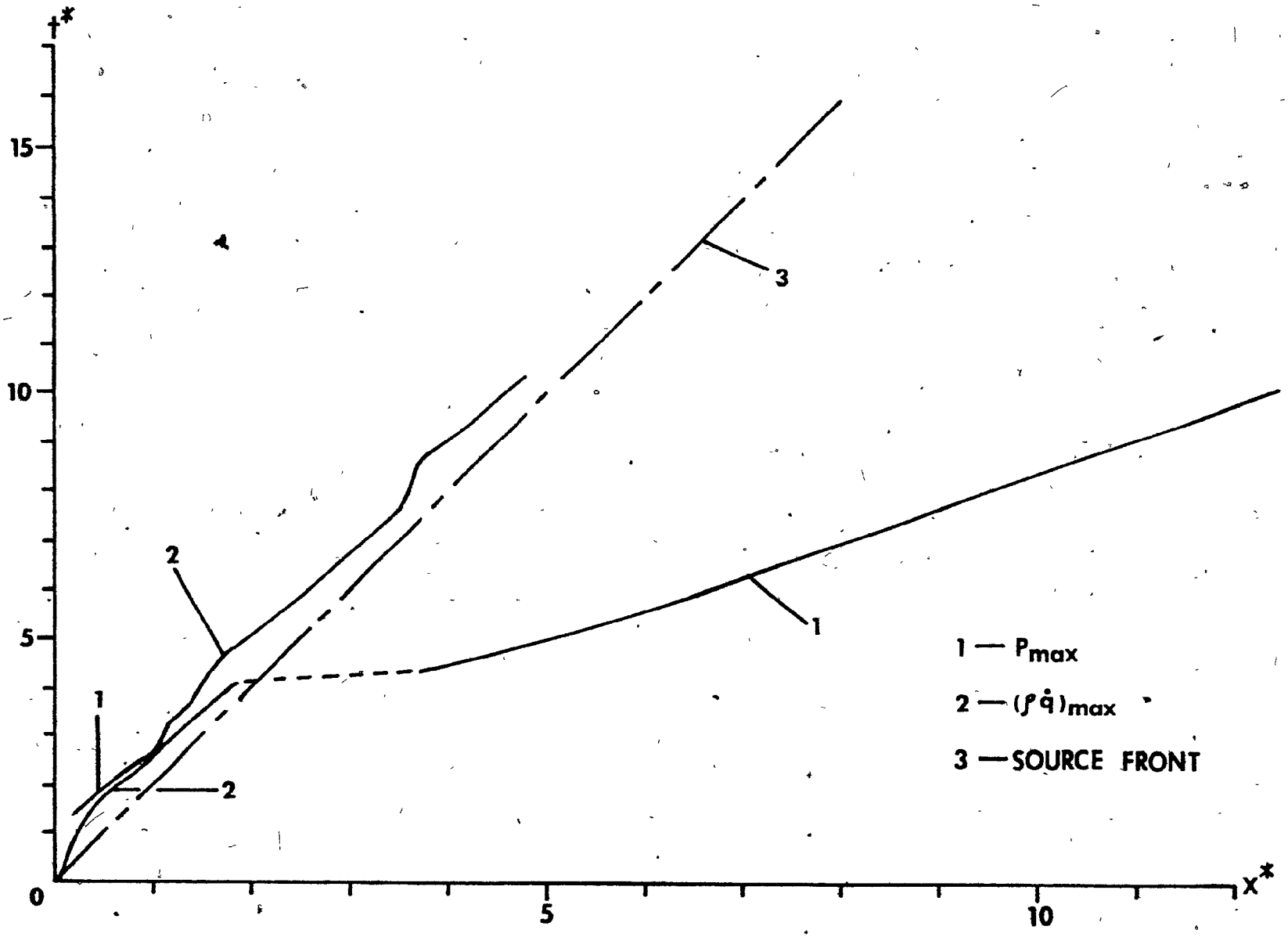

FIG. 18 X - t DIAGRAM FOR $\gamma = 1.4$, $Q^* = 10$ and $A = 0.5$

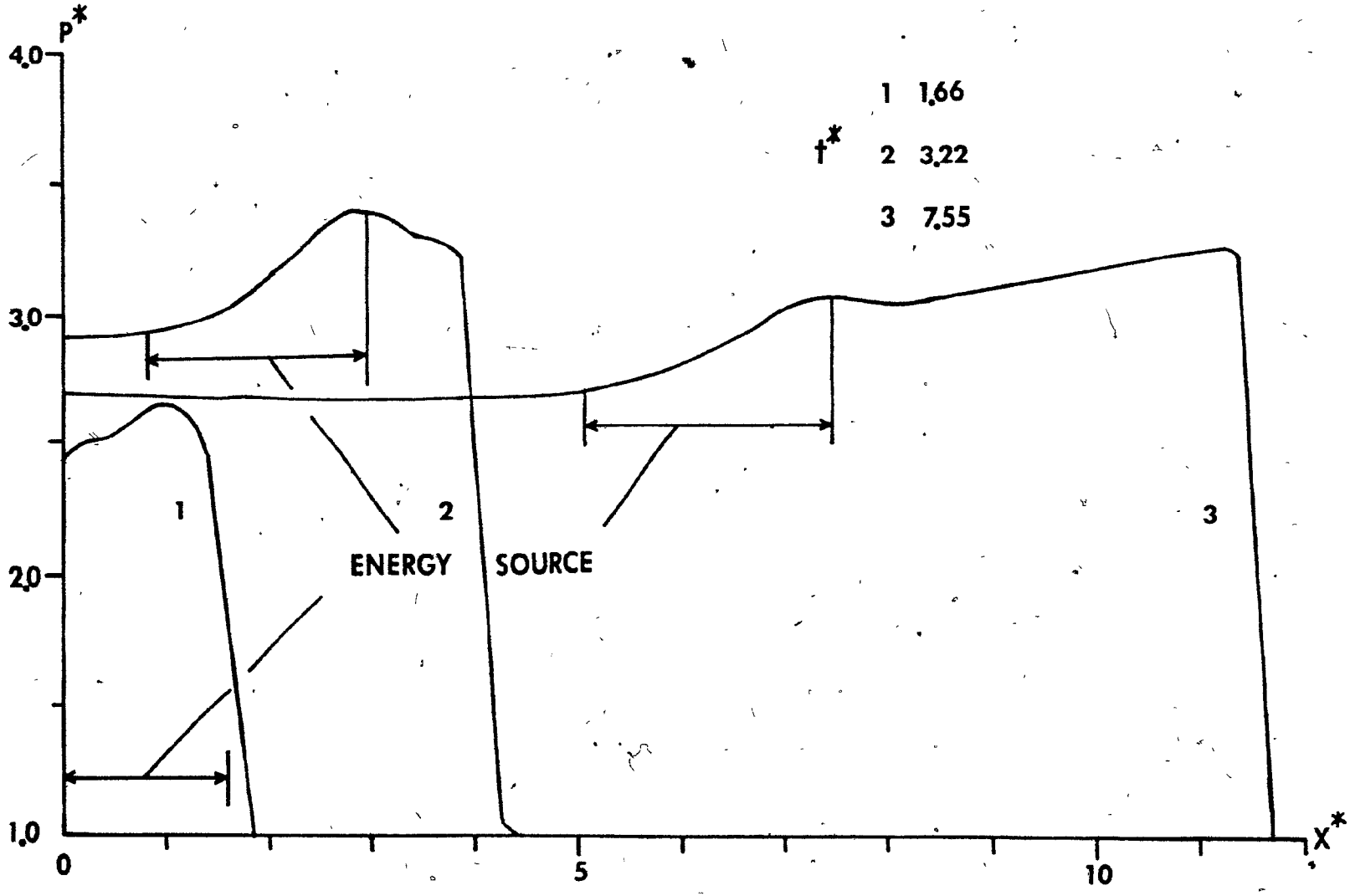

FIG. 19 PRESSURE PROFILE FOR $\gamma = 1.4$, $Q = 10^*$ and $A = 1.0$

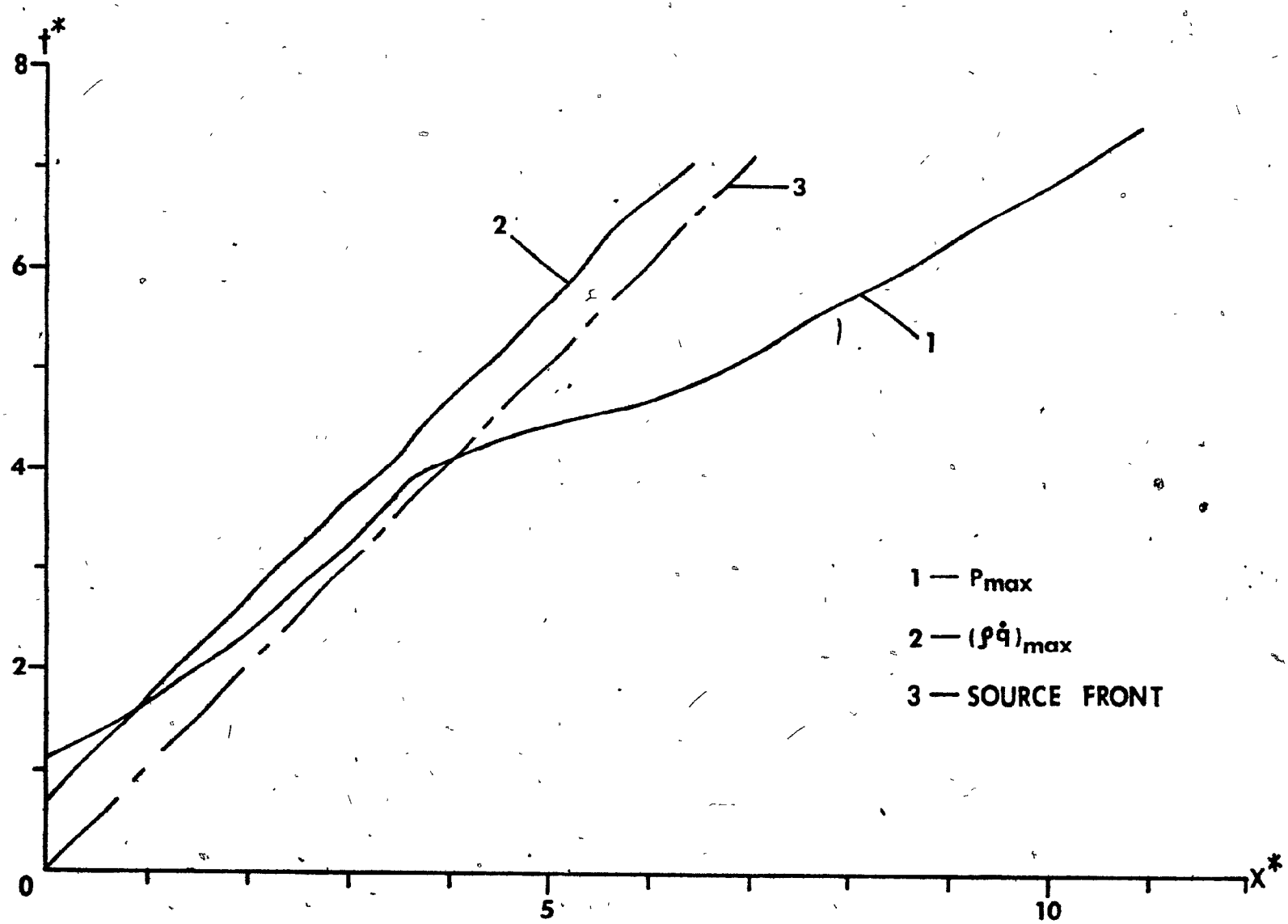

FIG.20 X-t DIAGRAM FOR $\gamma = 1.4$, $Q^* = 10$ and $A = 1.0$

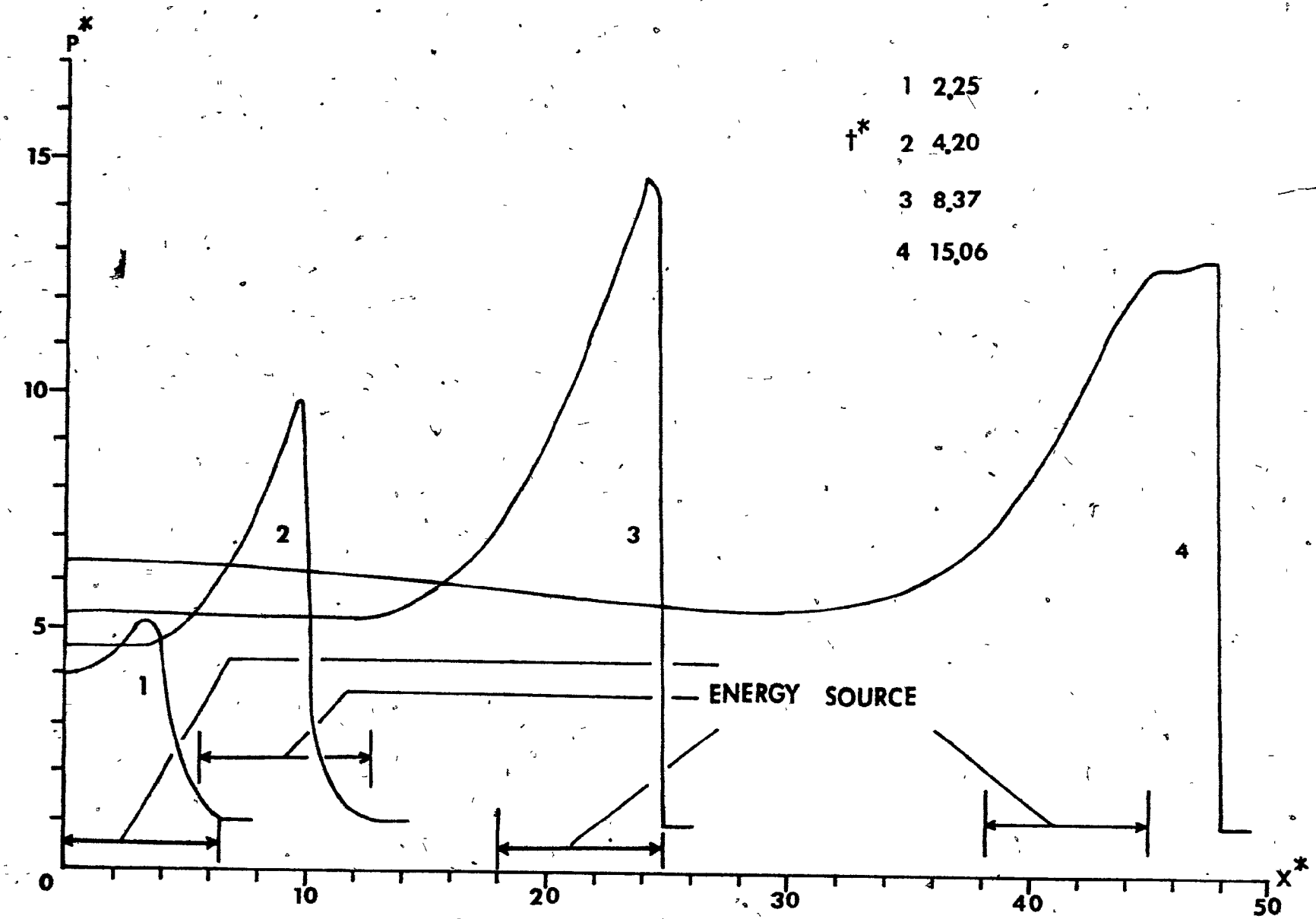

FIG.21 PRESSURE PROFILE FOR $\gamma = 1.4$, $Q^* = 10$ and $A = 3.0$

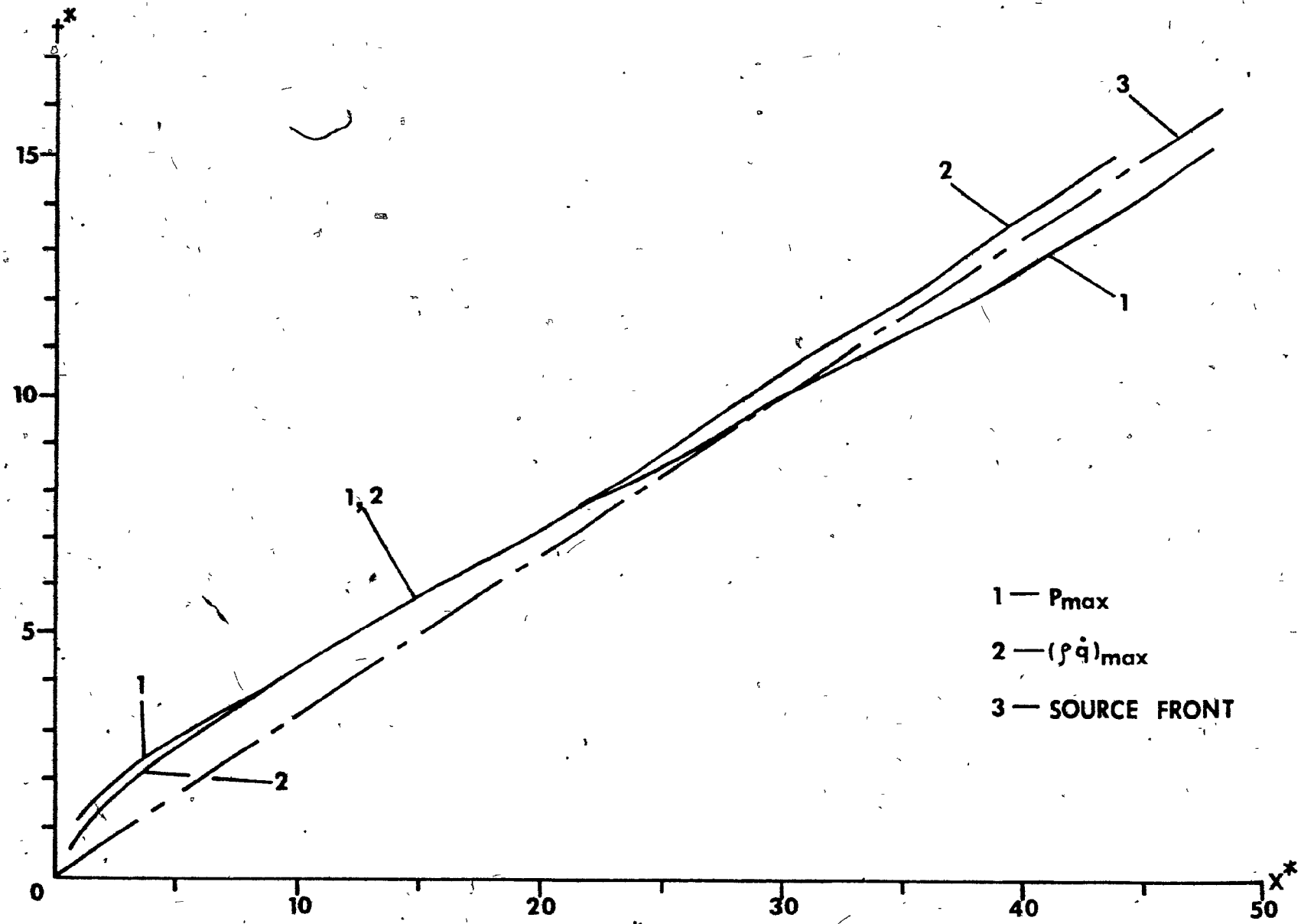

FIG. 22 X–t DIAGRAM FOR $\gamma=1.4$, $Q^*=10$ and $A=3.0$

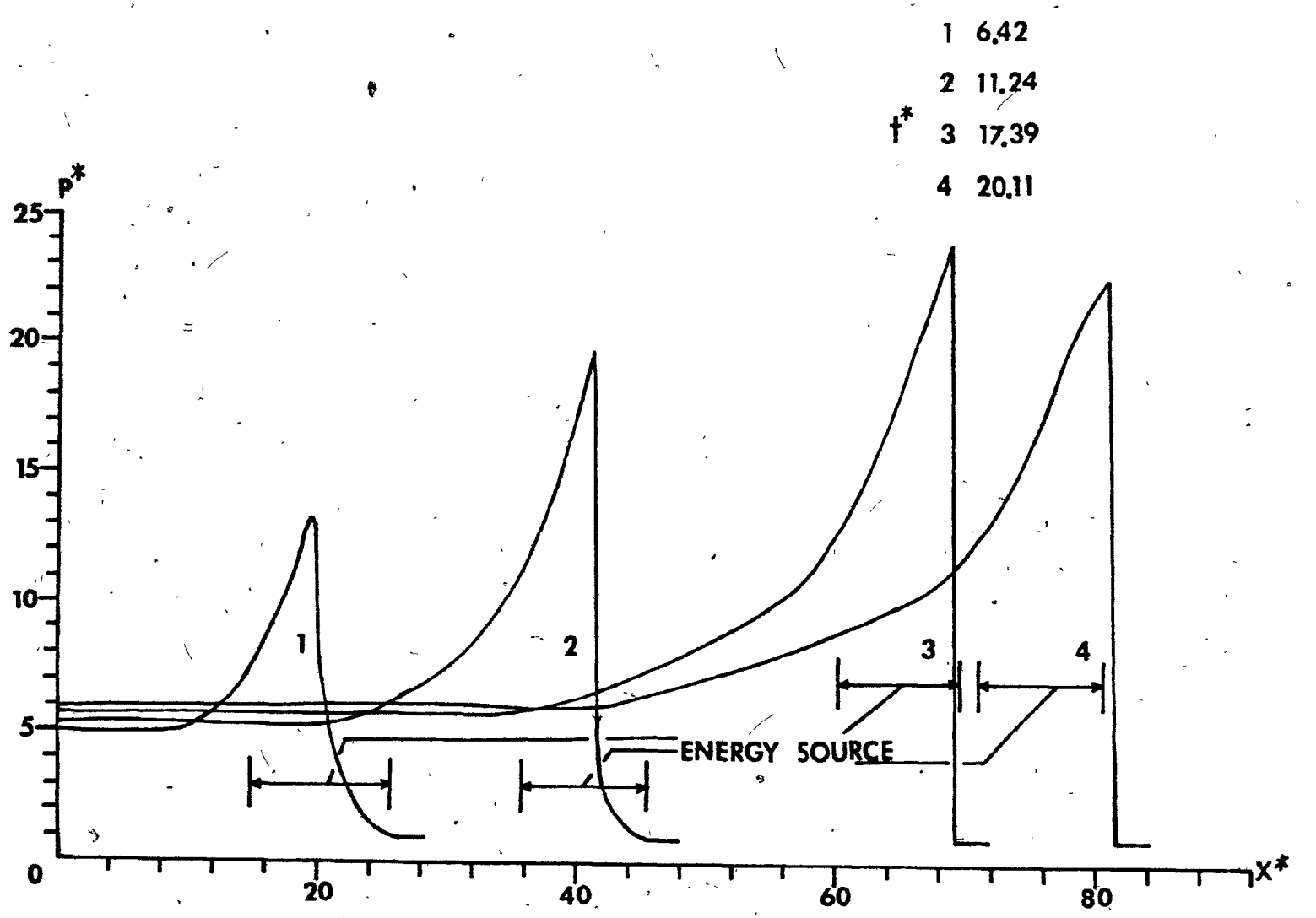

FIG. 23 PRESSURE PROFILE FOR $\gamma = 1.4$, $Q^* = 10$ and $A = 4.0$

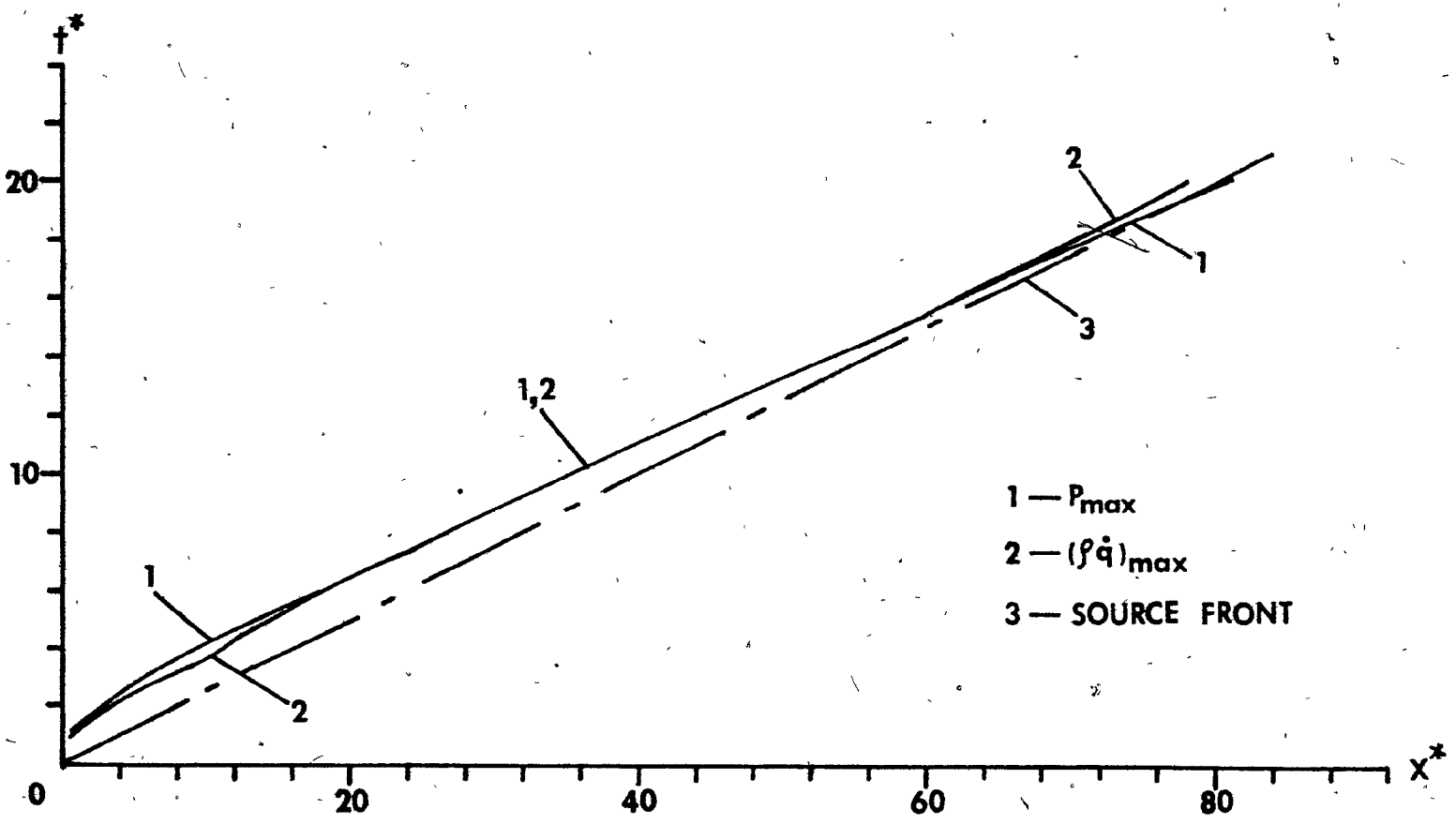

FIG. 24 X-t DIAGRAM FOR $\gamma = 1.4, Q^* = 10$ and $A = 4.0$

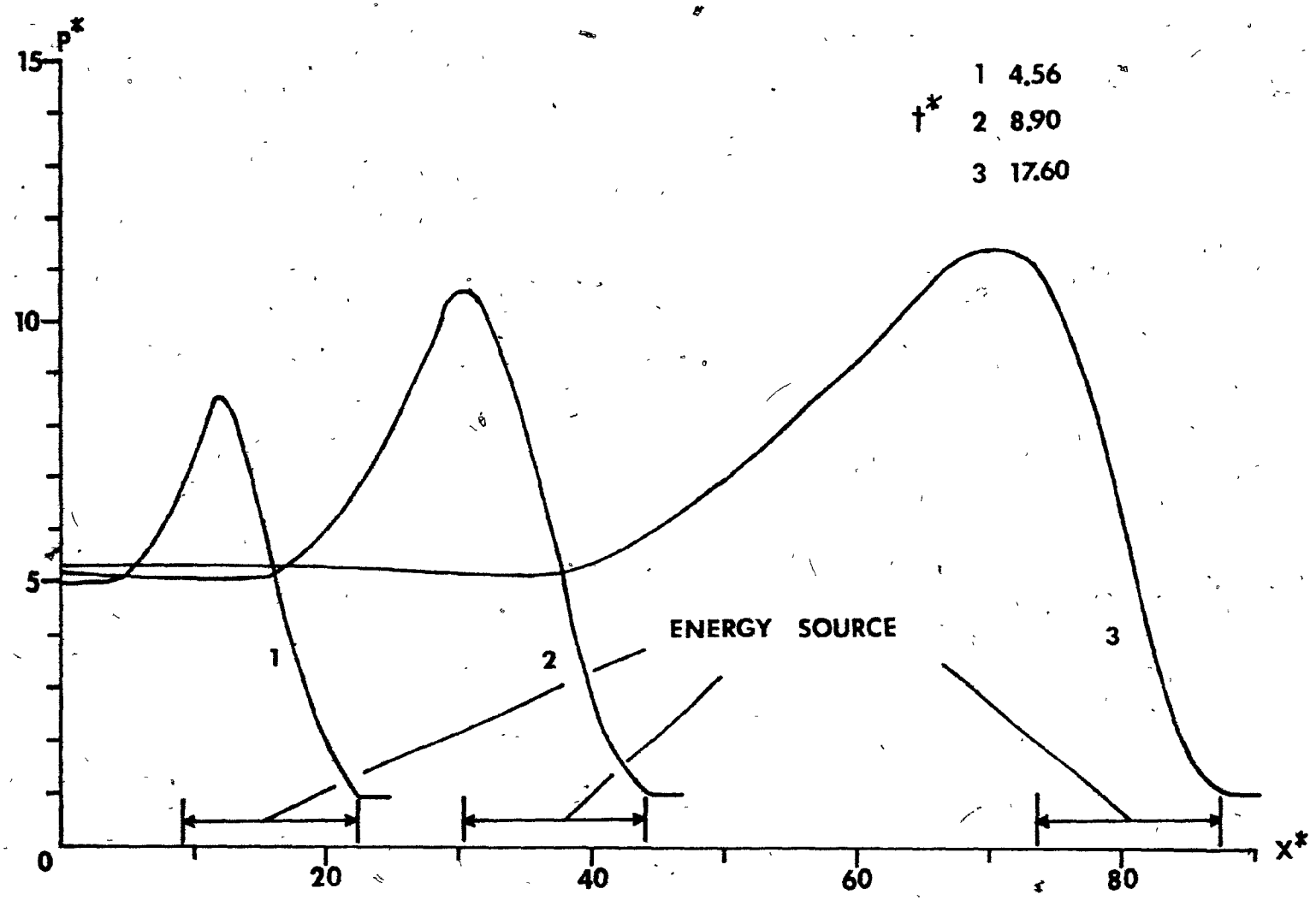

FIG. 25 PRESSURE PROFILE FOR $\gamma=1.4, Q^*=10$ and $A=5.0$

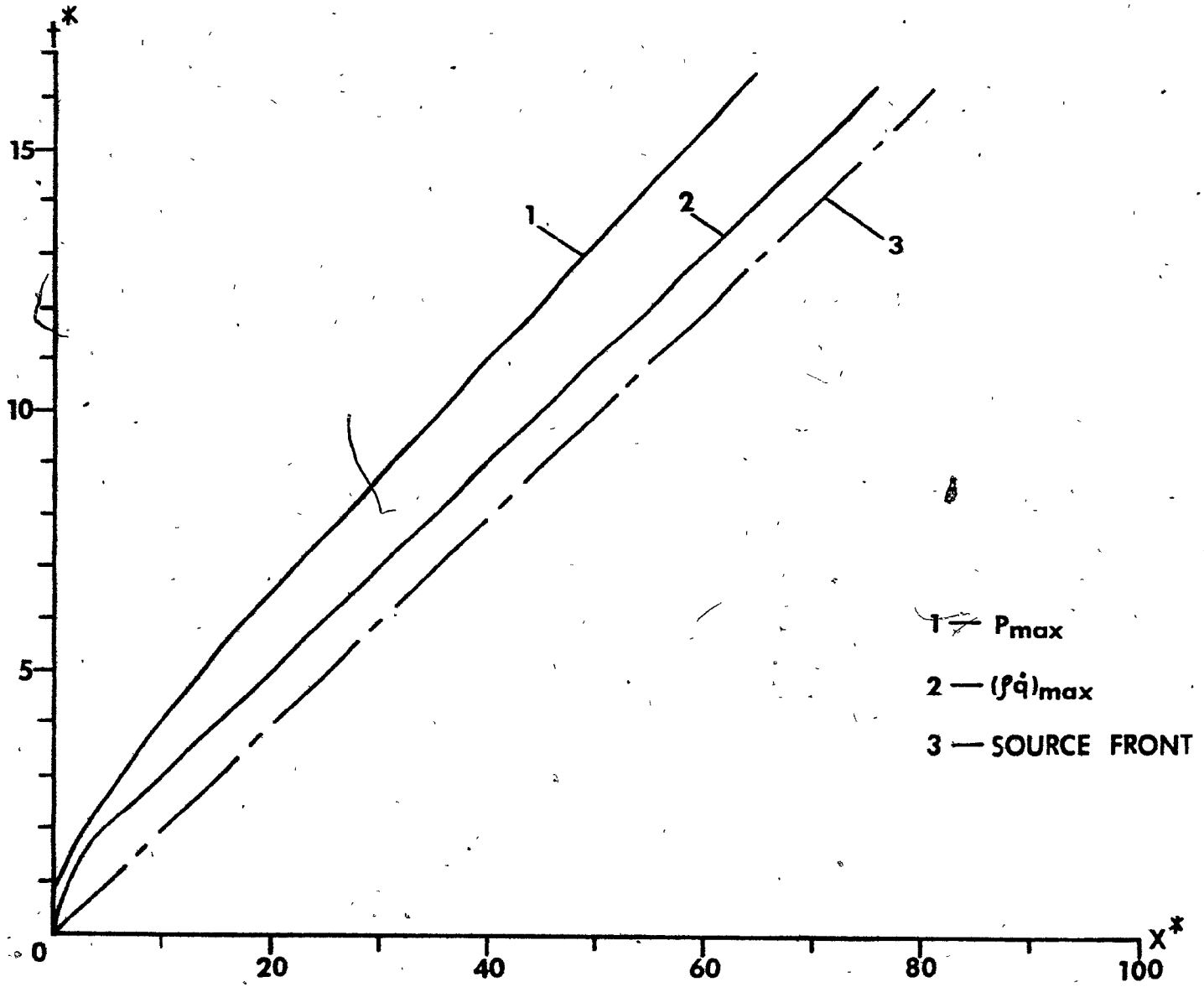

FIG. 26 X-t DIAGRAM FOR $\gamma = 1.4$, $Q^* = 10$ and $A = 5.0$

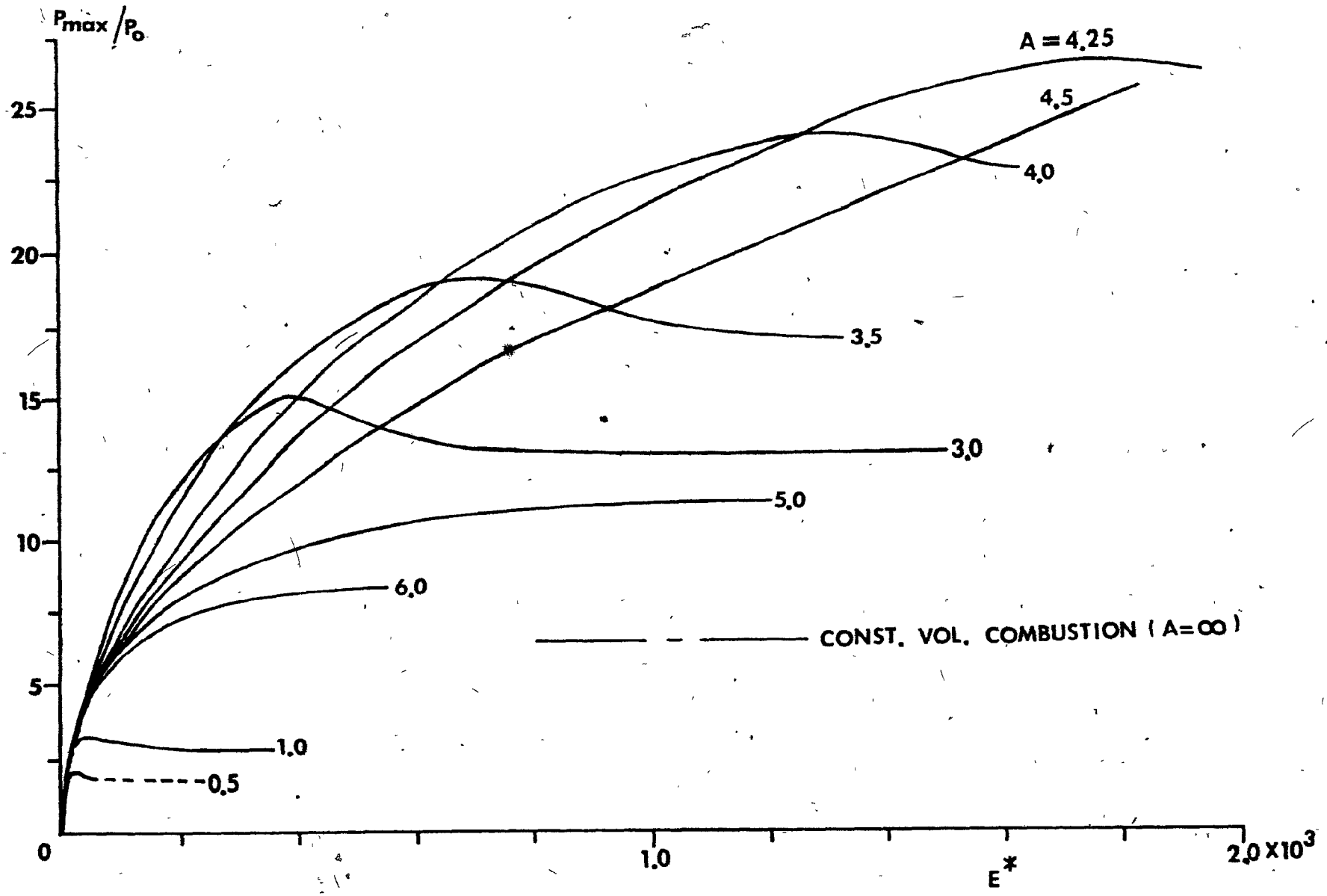

FIG. 27 PEAK PRESSURE vs. TOTAL ENERGY RELEASED FOR VARIOUS ENERGY SOURCE MACH NUMBER

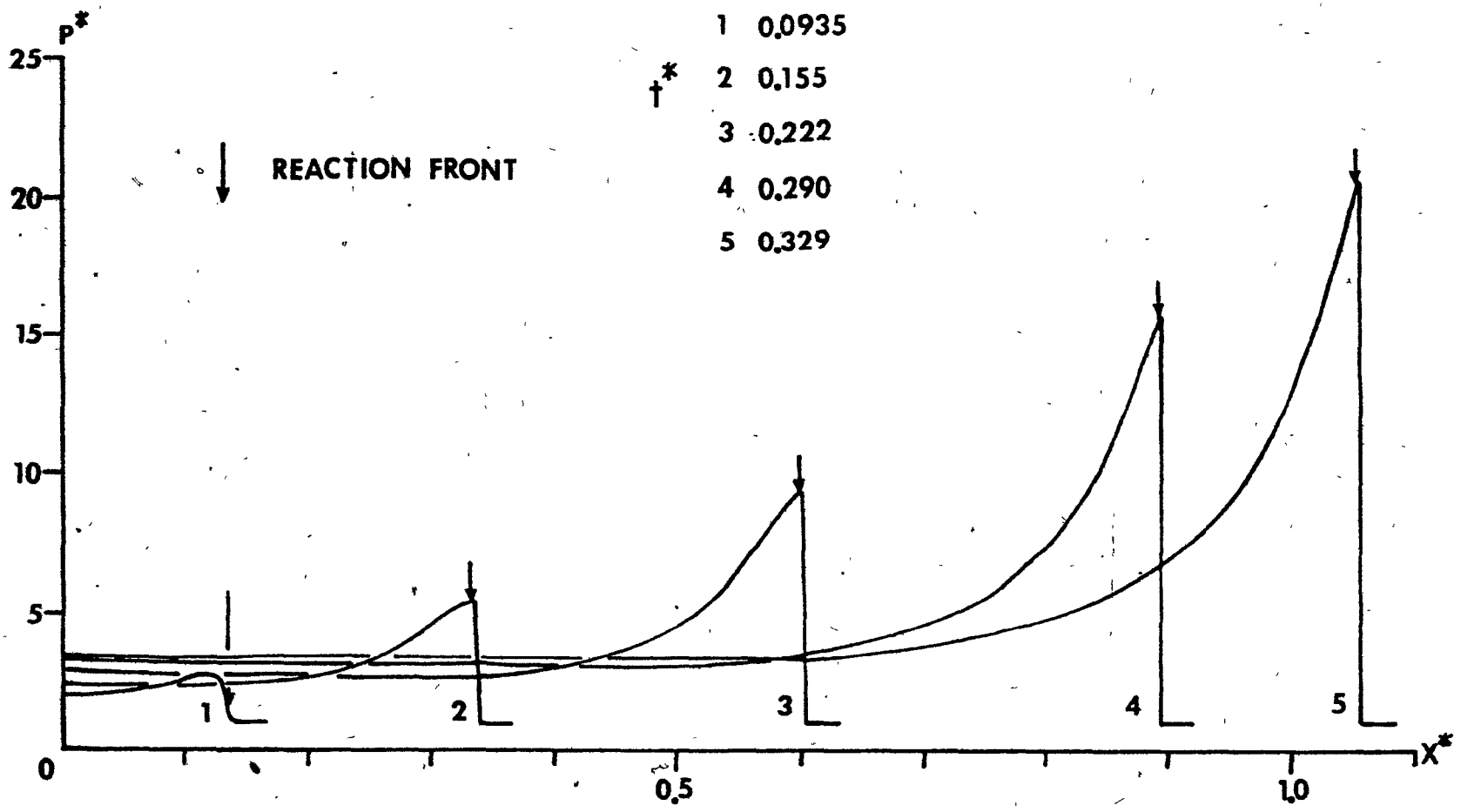

FIG. 28 PRESSURE PROFILE FOR $\alpha = 45.45$ and $\beta = 27.58$ (RUN NO. 18)

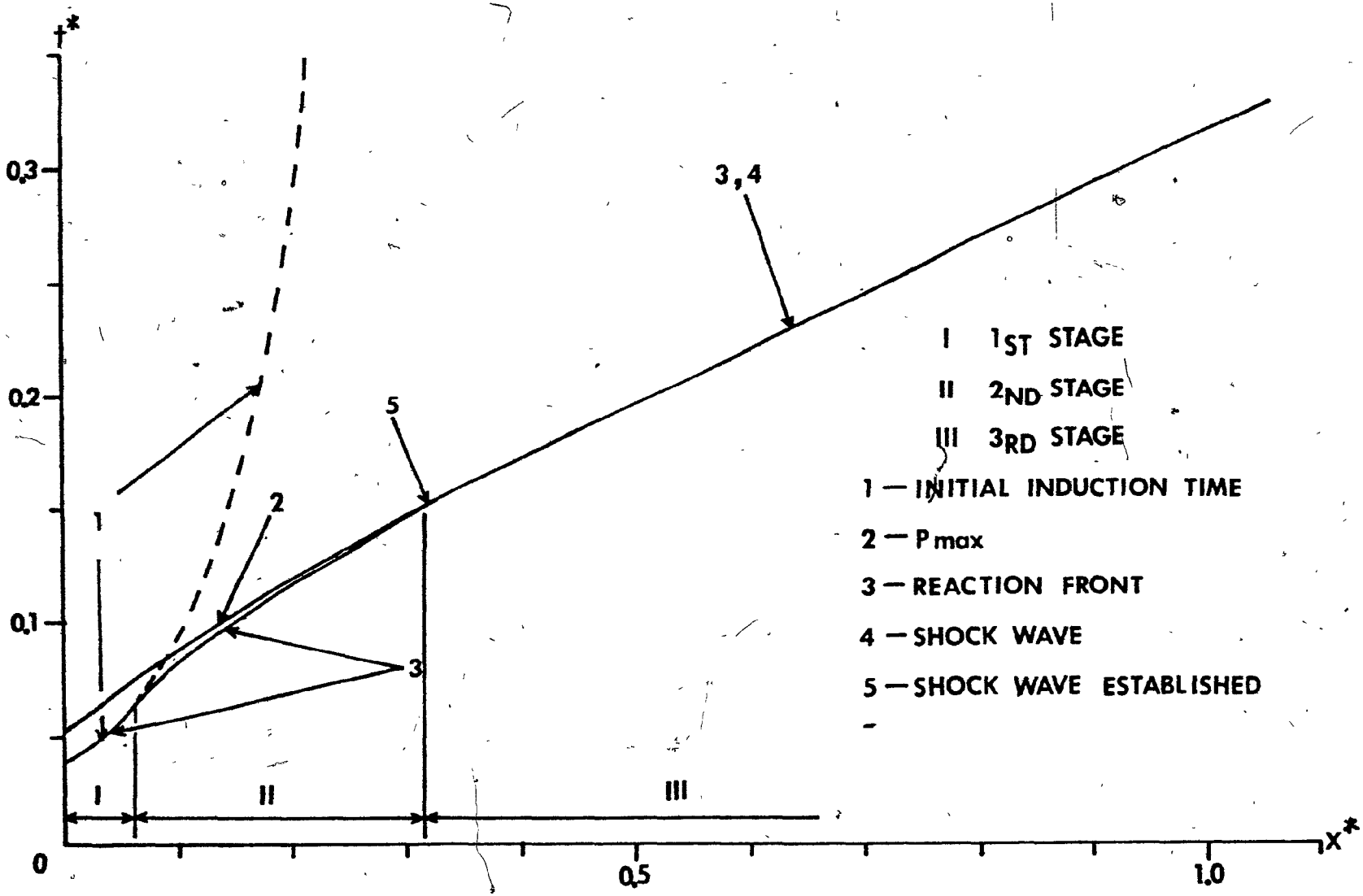

FIG. 29 X - t DIAGRAM FOR $\alpha = 45{,}45$ and $\beta = 27{,}58$ (RUN NO. 18)

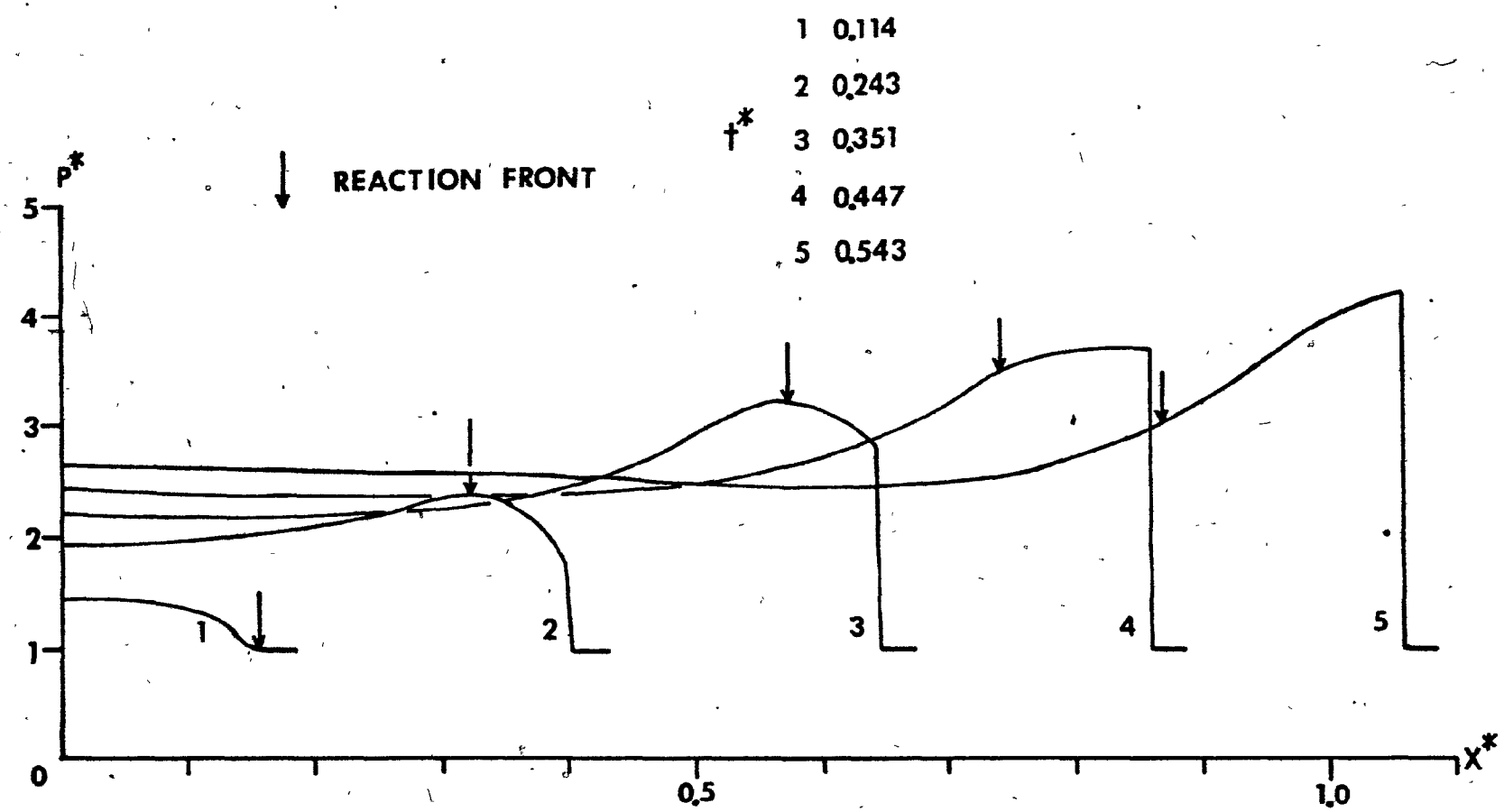

FIG. 30 PRESSURE PROFILE FOR α=11.36 and β=27.58 (RUN NO. 2)

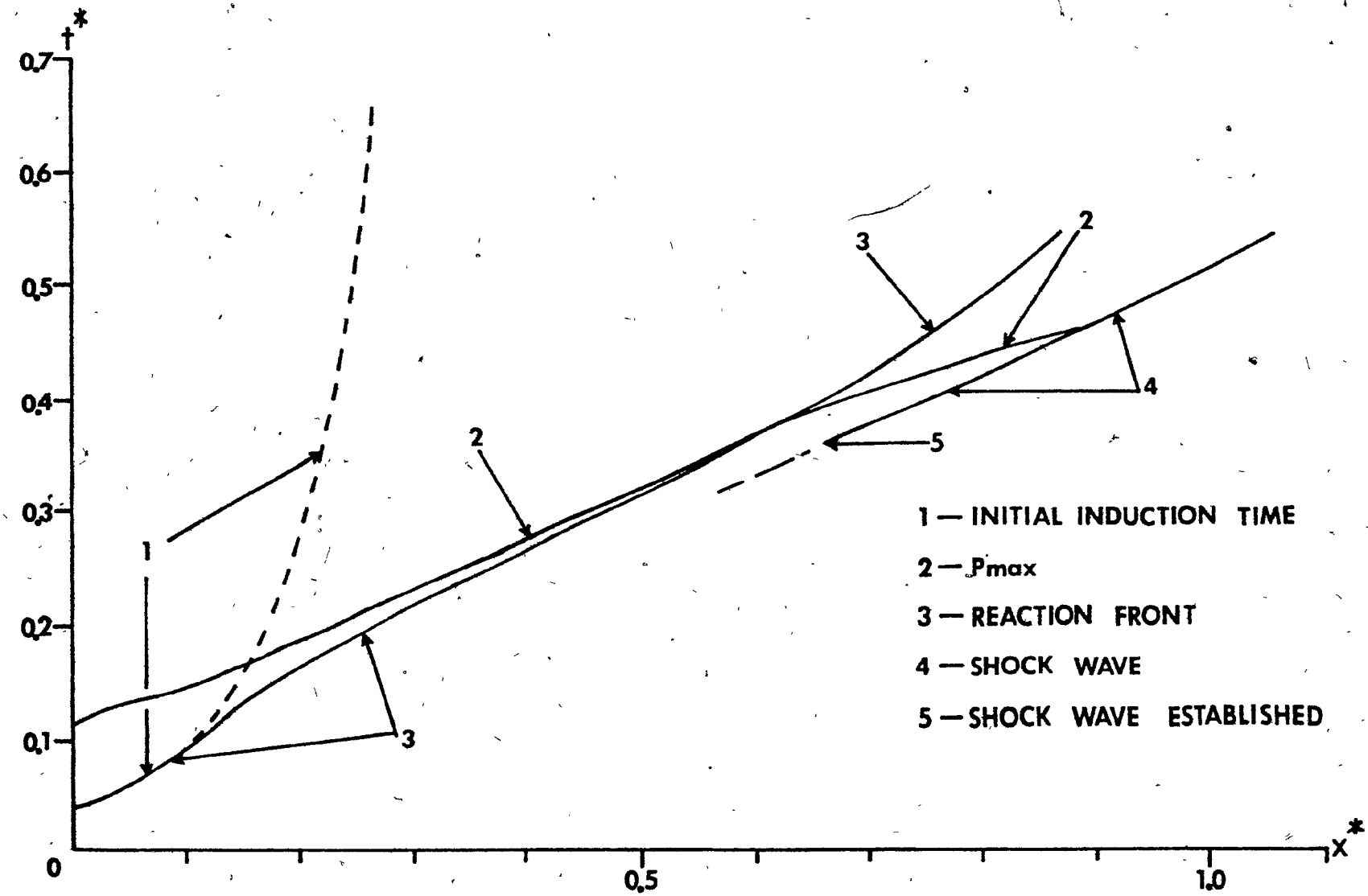

FIG. 31 X-t DIAGRAM FOR α=11.36 and β=27.58 (RUN NO. 2)

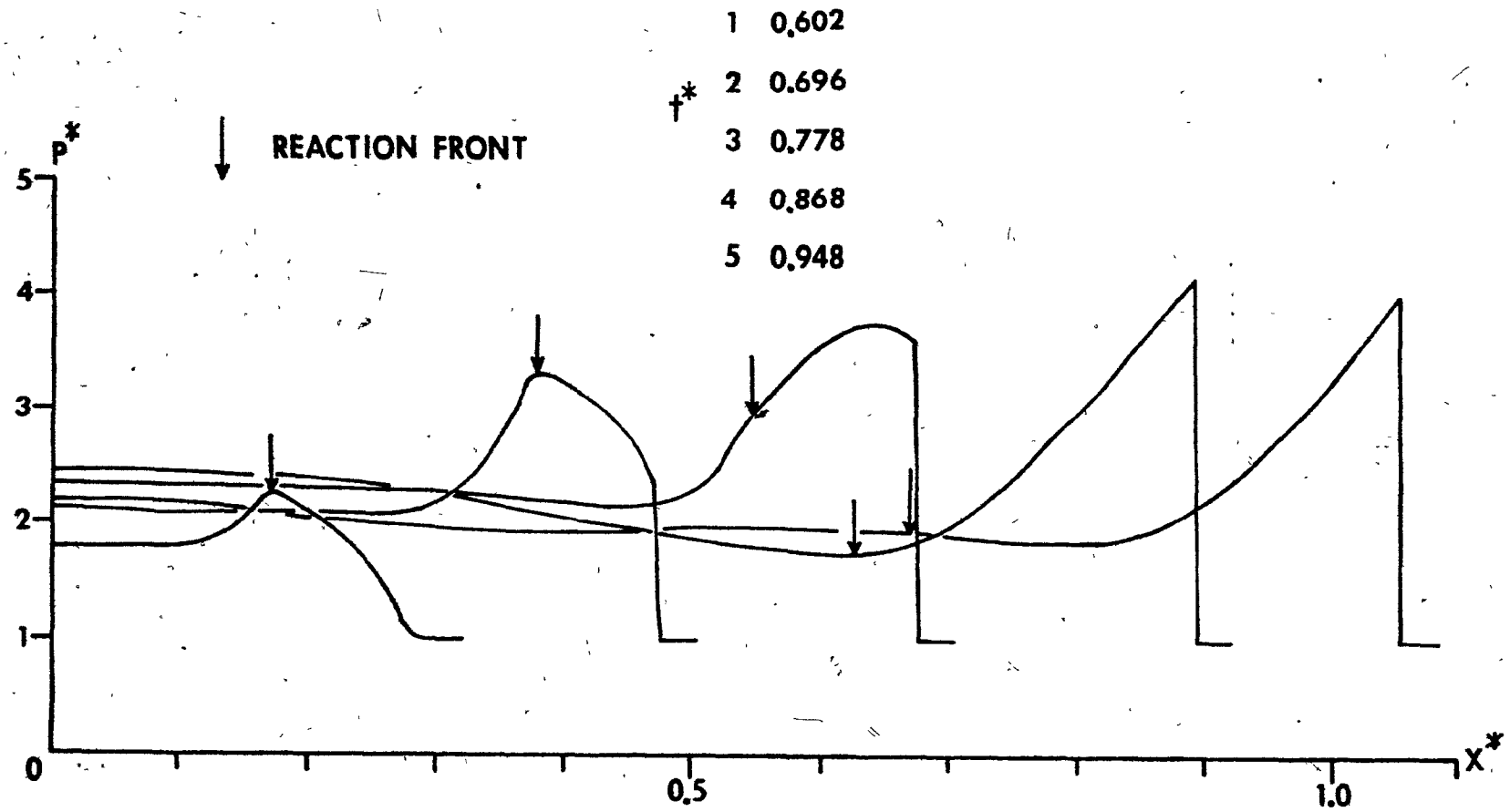

FIG. 32 PRESSURE PROFILE FOR $\alpha = 45.45$ and $\beta = 2.207$ (RUN NO. 16)

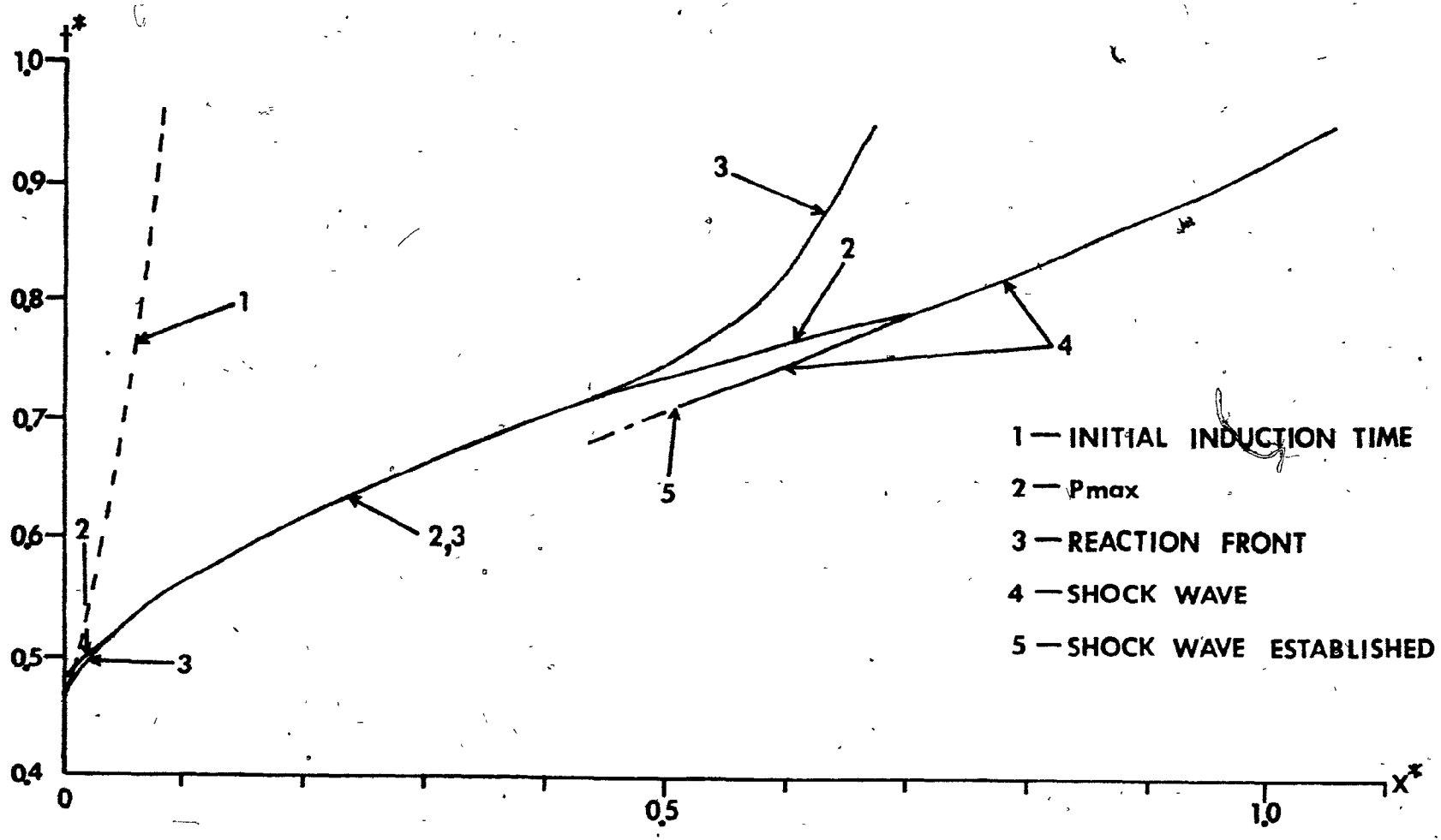

FIG. 33 X — t DIAGRAM FOR $\alpha = 45{,}45$ and $\beta = 2{,}207$ (RUN NO. 16)

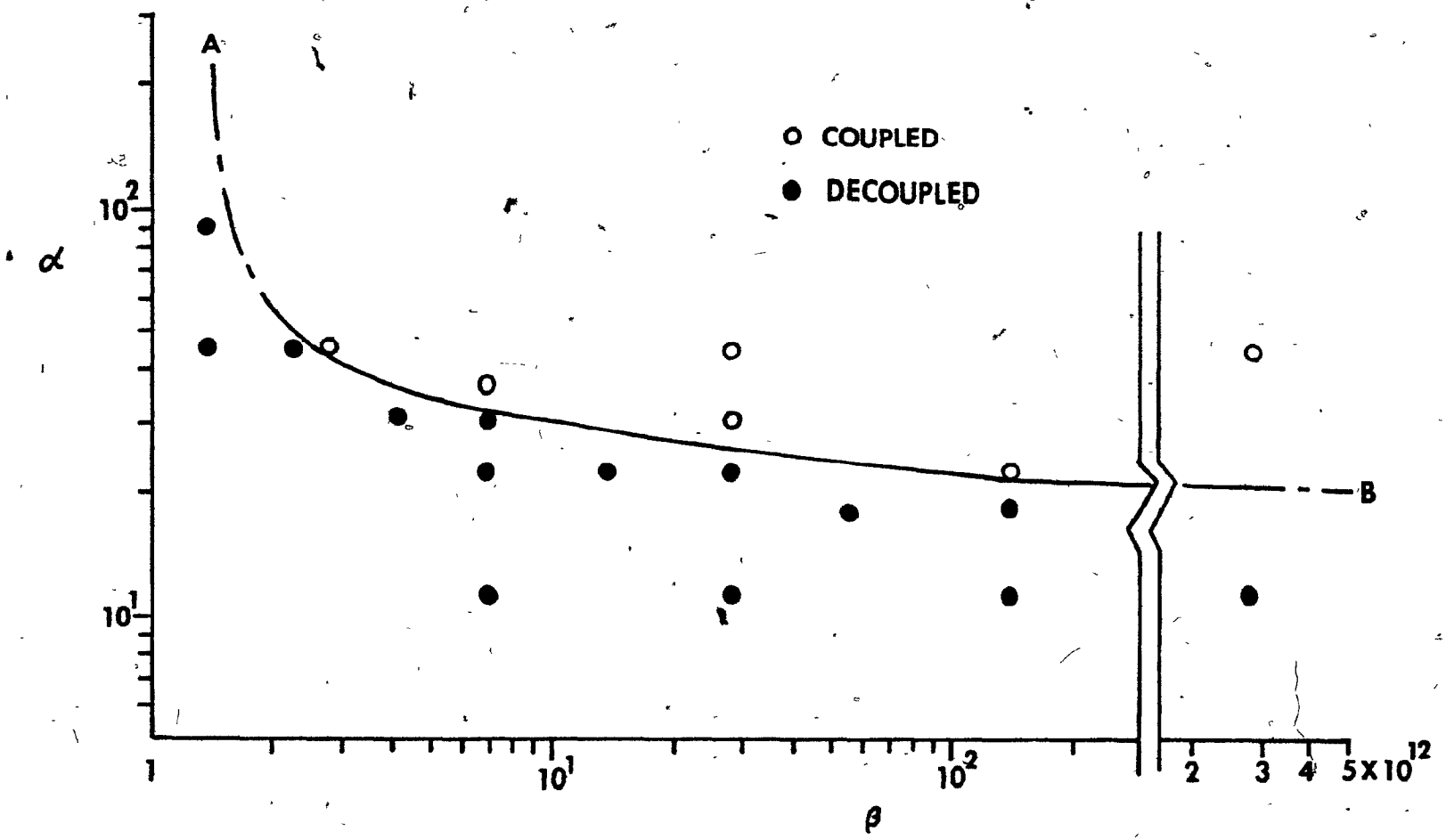

FIG. 34 LIMIT OF SWACER IN TERMS OF α & β

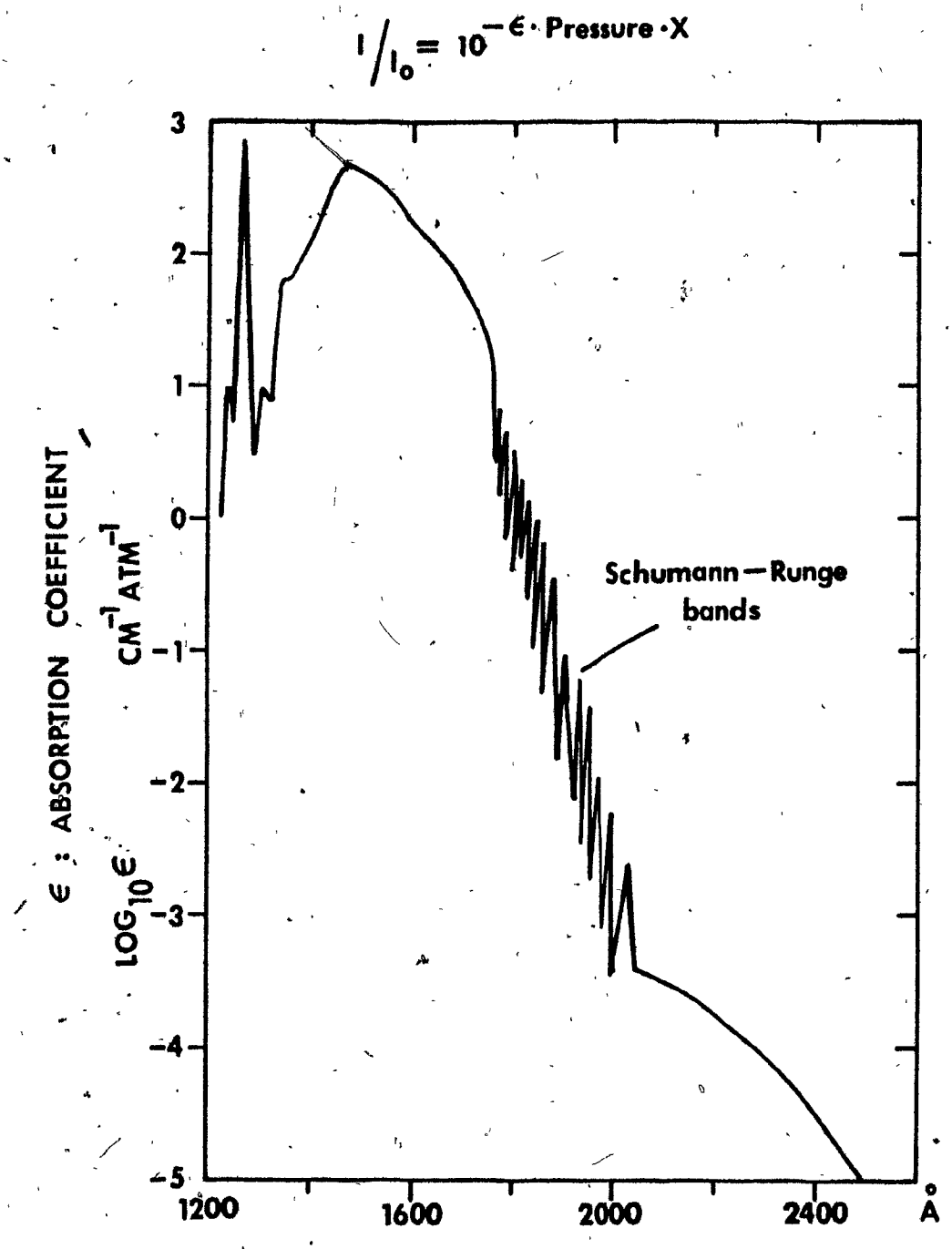

FIG. 35 ABSORPTION SPECTRUM OF O_2 AT 273°K (REF. 35)

$$I/I_0 = \text{EXP}(-\epsilon [NO_2] X)$$

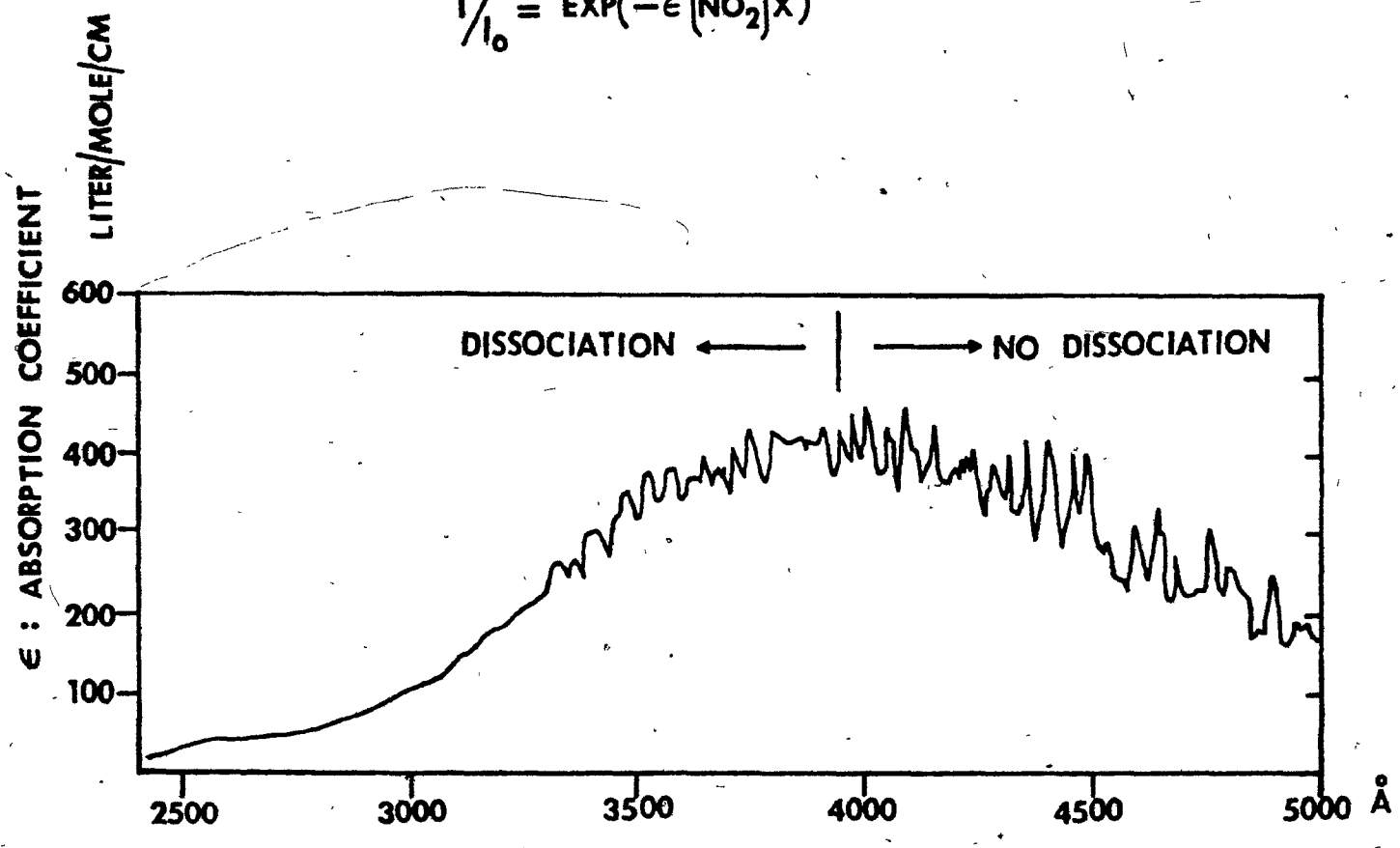

FIG. 36 ABSORPTION SPECTRUM OF NO_2 AT 298°K (REF. 35)

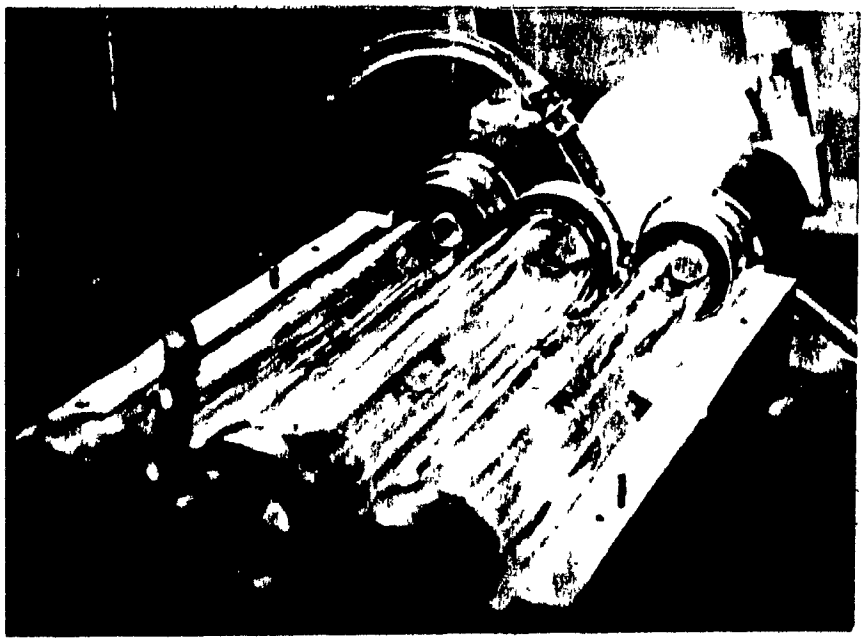

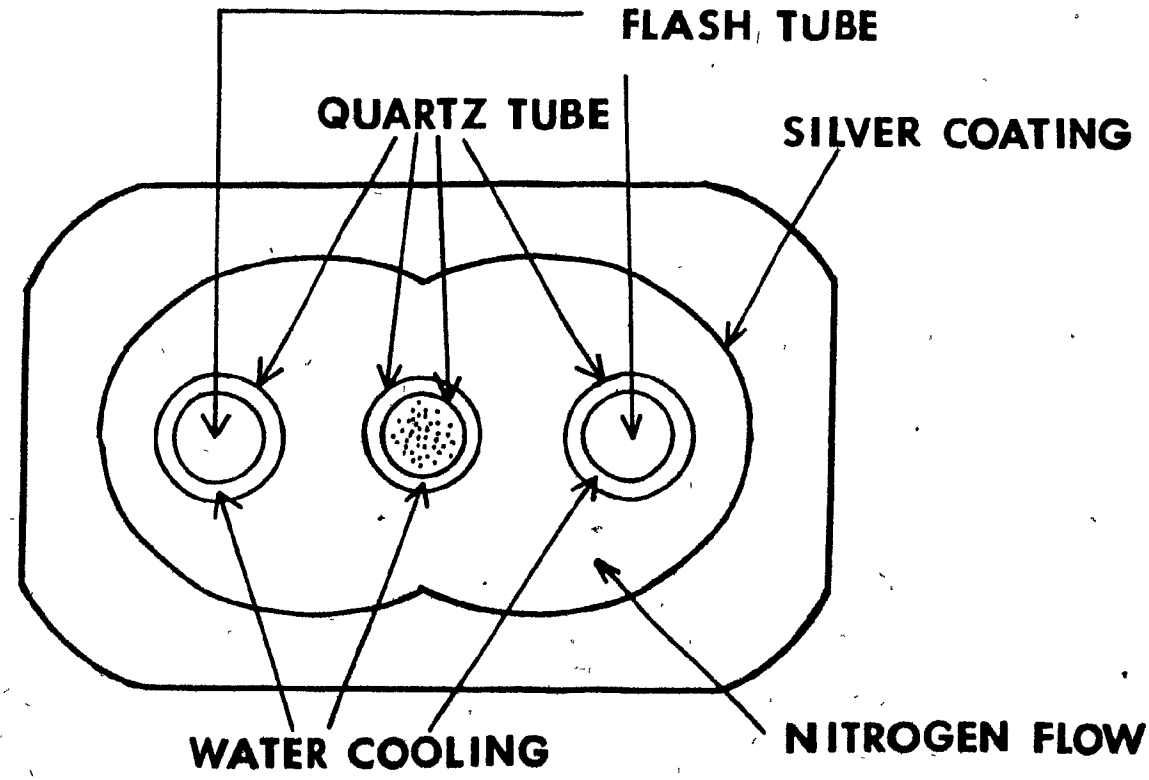

FIG. 37 CLOSEUP VIEW OF FLASH CAVITY AND SCHEMATIC DIAGRAM OF CROSS-SECTION OF FLASH CAVITY

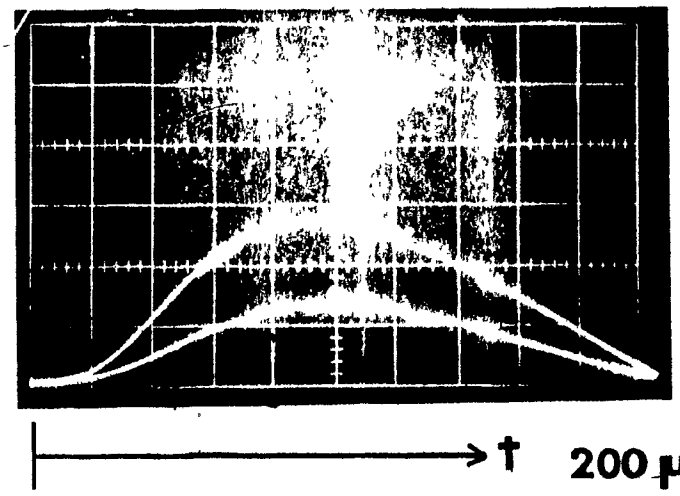

FIG.38 RADIATION OUTPUT OF FLASH TUBES (EG&G FX47C)

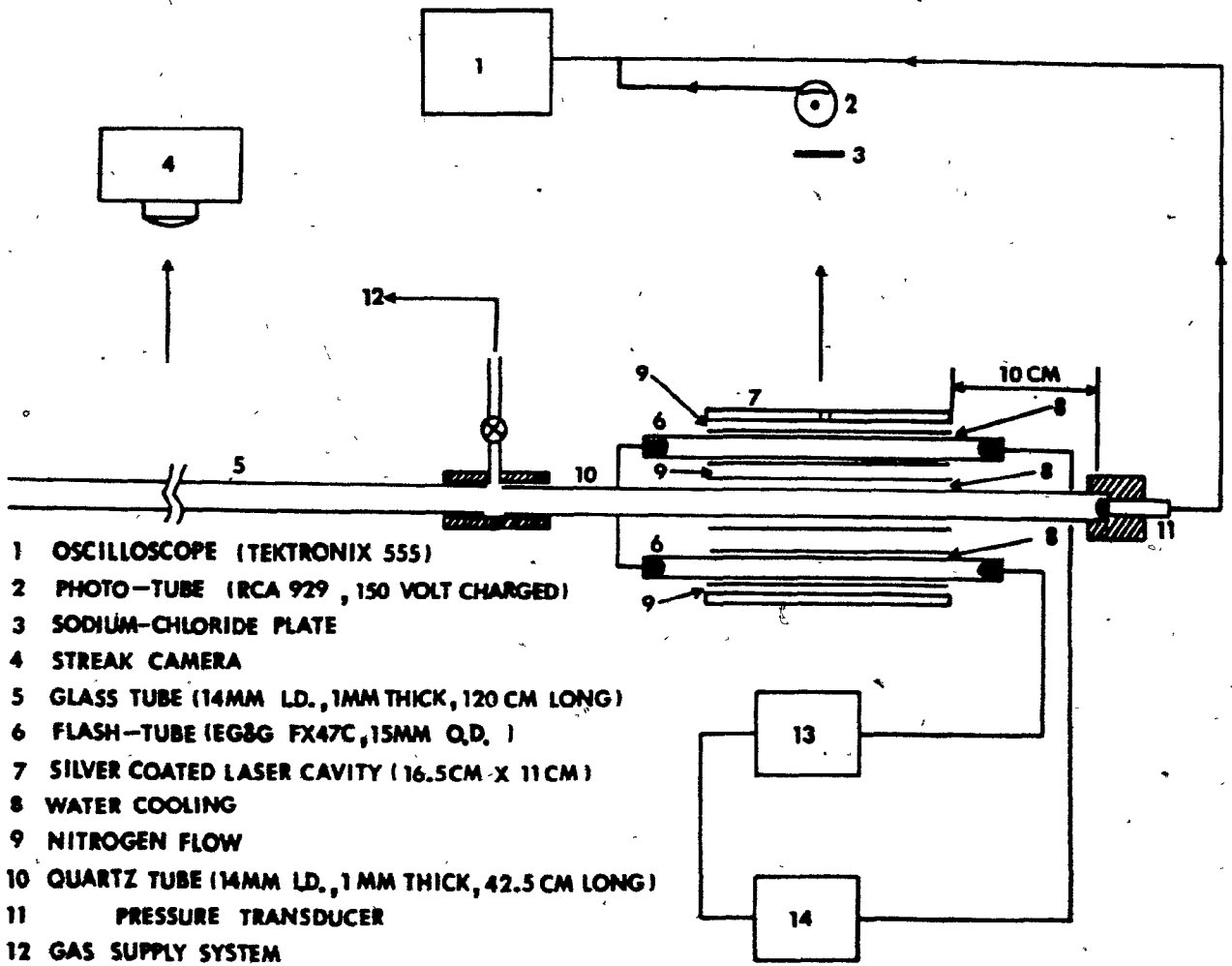

1 OSCILLOSCOPE (TEKTRONIX 555)
2 PHOTO-TUBE (RCA 929, 150 VOLT CHARGED)
3 SODIUM-CHLORIDE PLATE
4 STREAK CAMERA
5 GLASS TUBE (14MM I.D., 1MM THICK, 120 CM LONG)
6 FLASH-TUBE (EG&G FX47C, 15MM O.D.)
7 SILVER COATED LASER CAVITY (16.5CM X 11CM)
8 WATER COOLING
9 NITROGEN FLOW
10 QUARTZ TUBE (14MM I.D., 1 MM THICK, 42.5 CM LONG)
11 PRESSURE TRANSDUCER
12 GAS SUPPLY SYSTEM
13 CAPACITOR BANK (2250 μF)
14 POWER SUPPLY & TRIGGER UNIT (TRIGGER VOLTAGE 3 KV)

FIG. 39 SCHEMATIC DIAGRAM OF ENTIRE EXPERIMENTAL SYSTEM

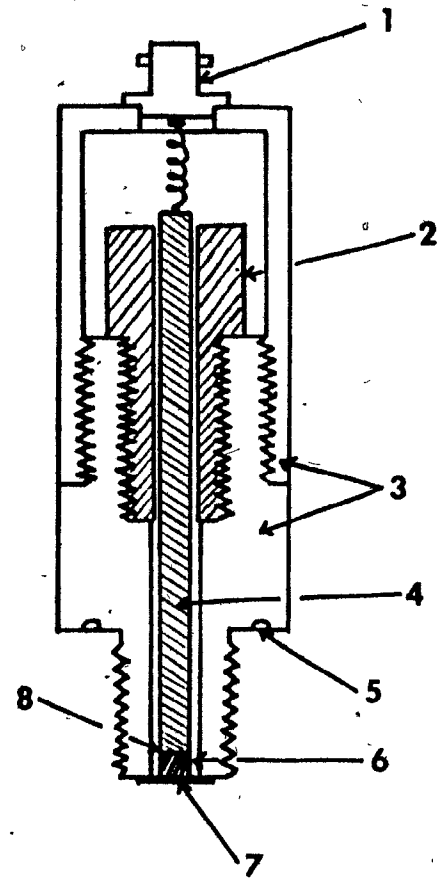

1 BNC ADAPTER
2 PLEXIGLASS ADAPTER
3 BRASS HOUSING
4 ZINC ROD
5 "O" RING GROOVE
6 BARIUM TITANATE CRYSTAL
7 SILVER EPOXY BOND
8 COPPER WIRE

FIG. 40 SKETCH OF HOME-MADE PRESSURE TRANSDUCER

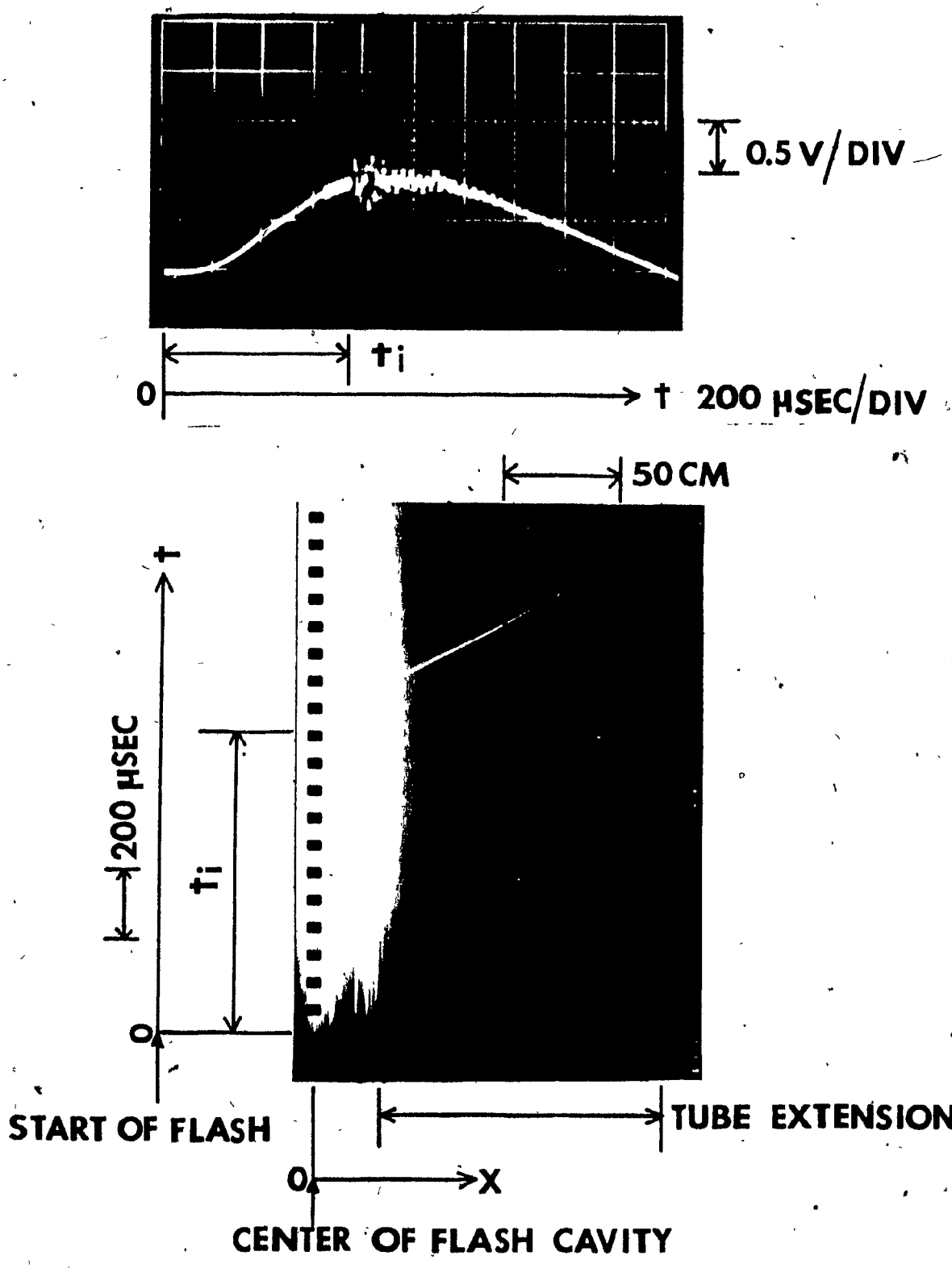

FIG.41 SIMULTANEOUS RECORD OF FLASH INTENSITY AND PRESSURE RISE (UPPER) AND STREAK RECORD OF DETONATION INITIATION

(C_2H_2 47.5 % – O_2 47.5% – NO_2 5% AT 100 TORR , FLASH ENERGY 6 KJ)

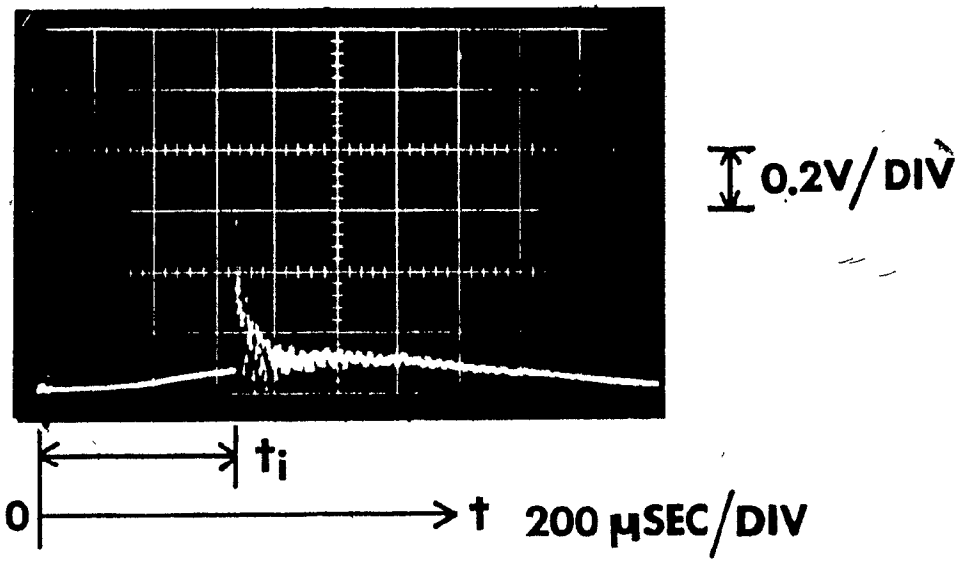

FIG. 42 SIMULTANEOUS RECORD OF FLASH INTENSITY AND PRESSURE RISE IN EQUI-MOLAR H_2-Cl_2 AT 180 TORR (FLASH ENERGY 1 KJ)

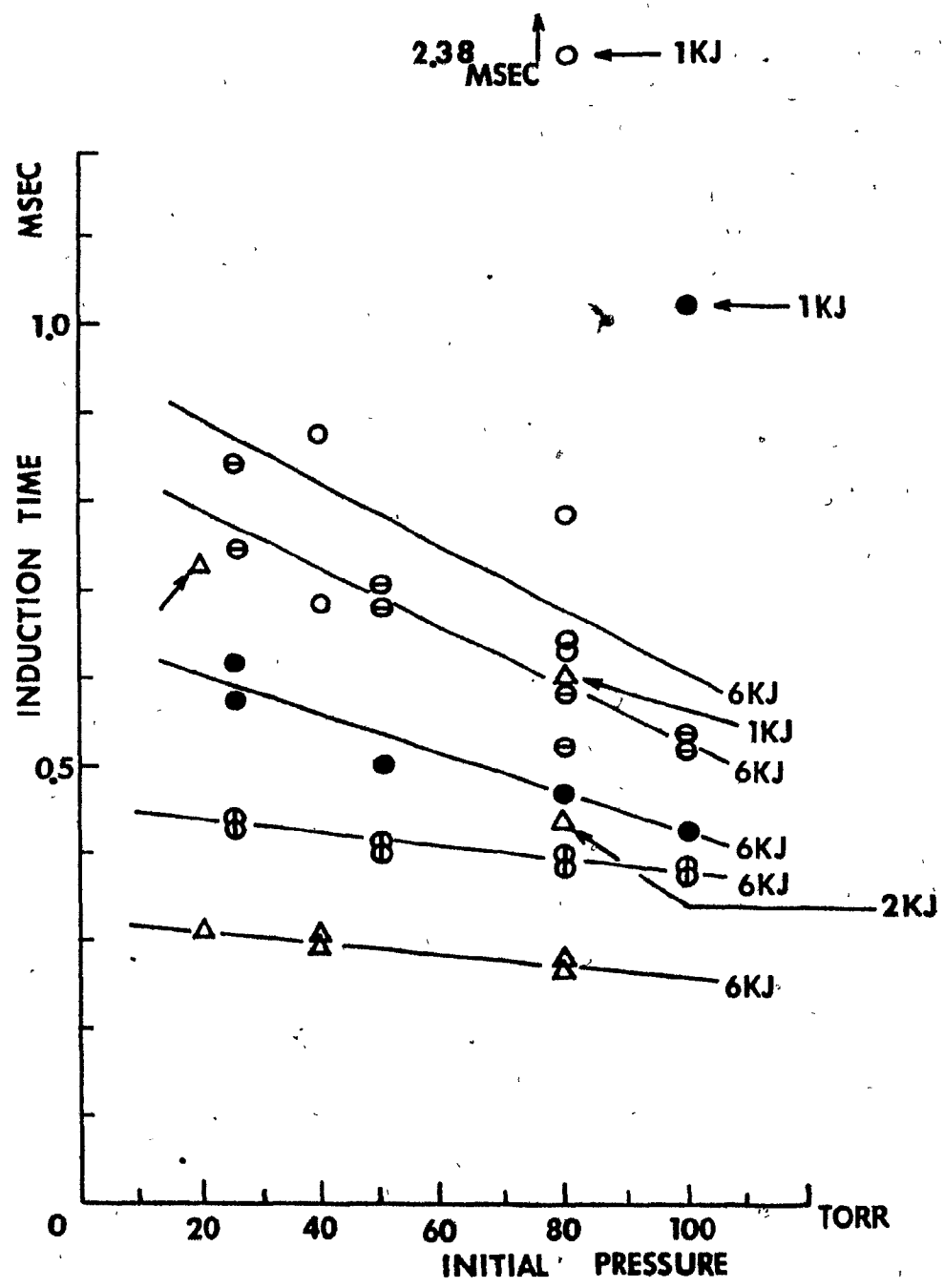

FIG. 43 VARIATION OF INDUCTION TIME FOR DETONATION INITIATION

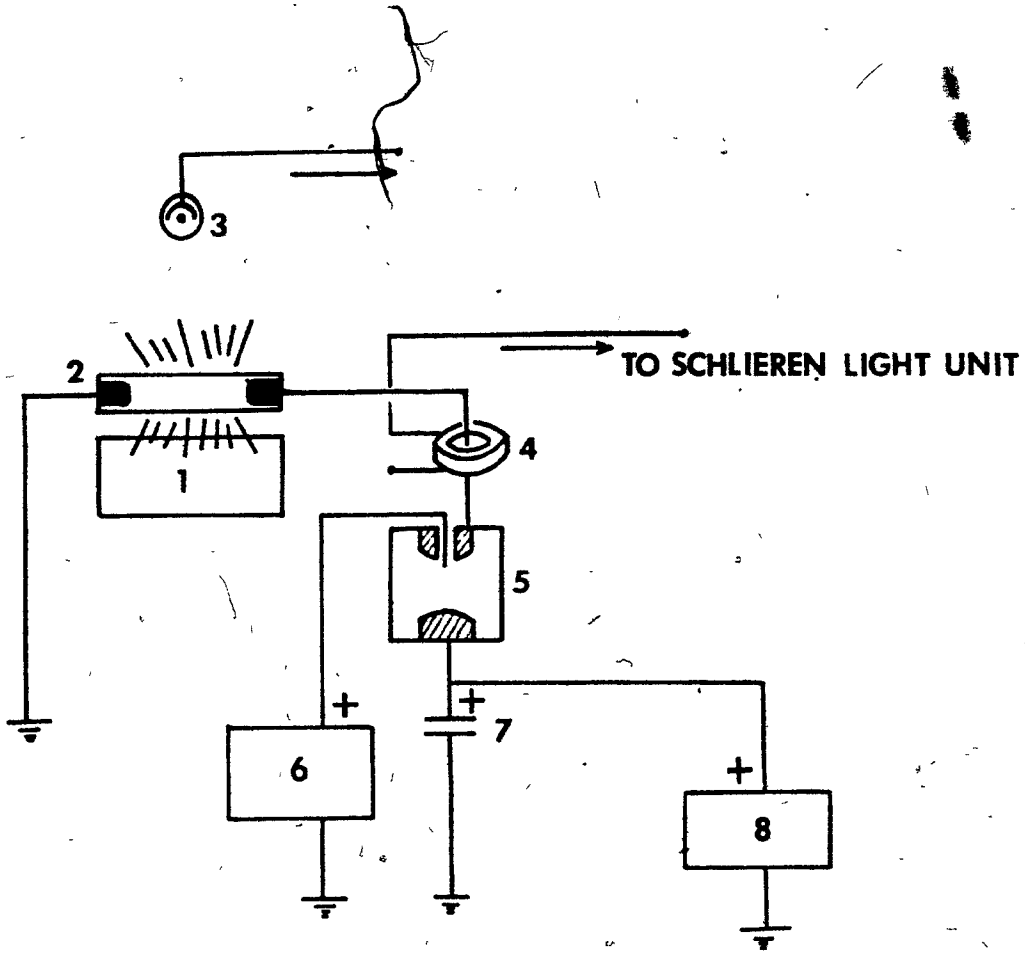

1 EXPLOSION CHAMBER
2 FLASH TUBE
3 PHOTO-TUBE
4 CURRENT TRANSFORMER
5 SWITCH
6 TRIGGER MODULE
7 CAPACITOR
8 DC POWER SUPPLY

FIG.44 SCHEMATIC DIAGRAM OF RADIATION SOURCE SYSTEM

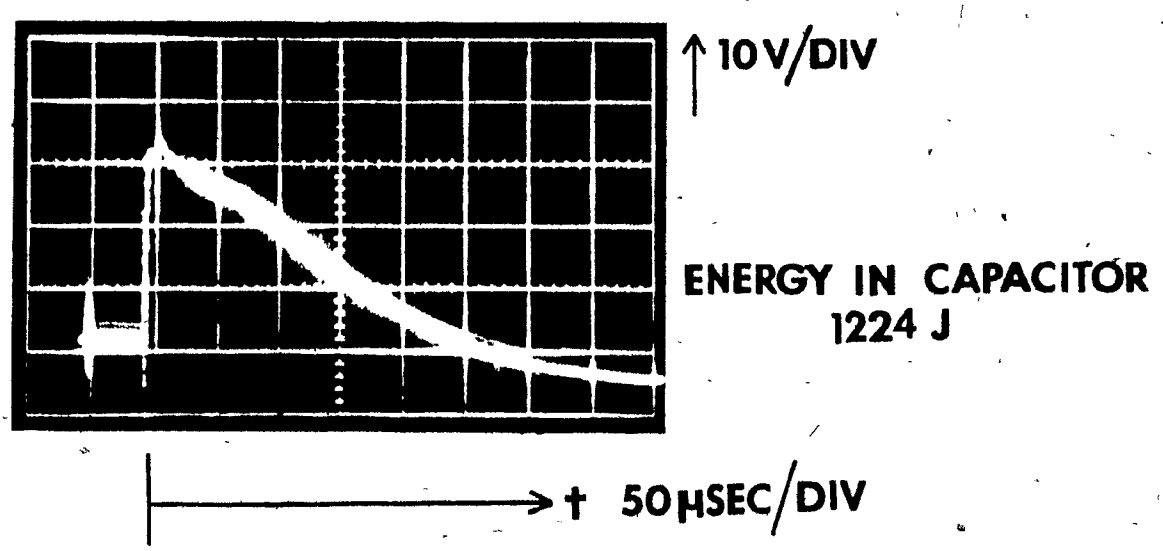

FIG. 45 RADIATION OUTPUT OF FLASH TUBE (XENON CORP. FPA-8-100C)

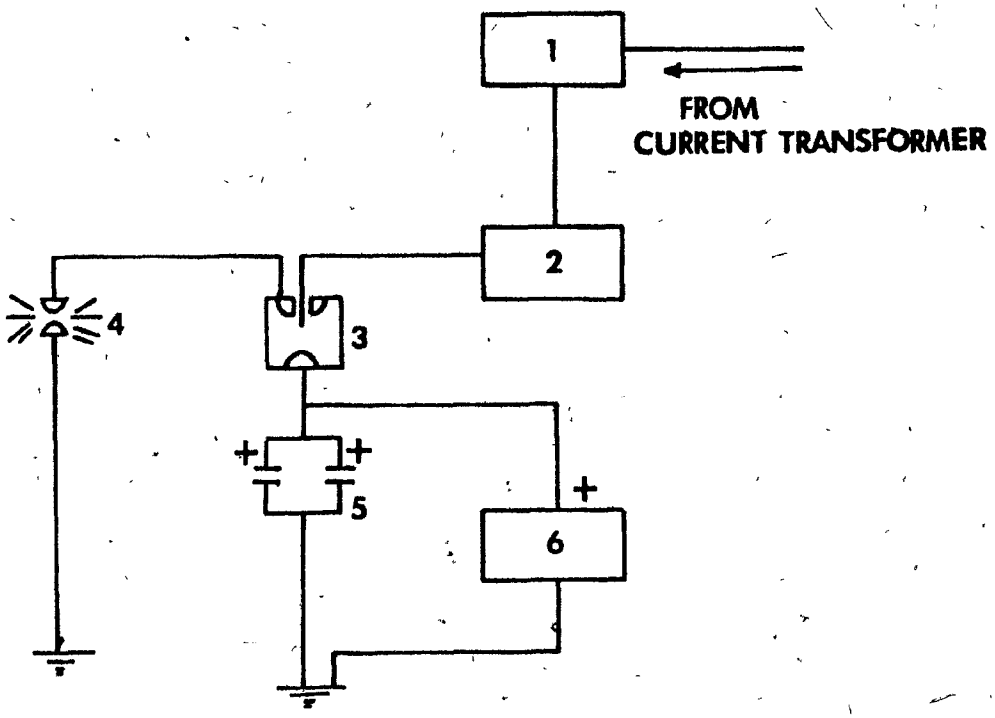

1 DELAY PULSE GENERATOR

2 TRIGGER MODULE

3 SWITCH

4 SPARK LIGHT ELECTRODES

5 CAPACITORS

6 DC POWER SUPPLY

FIG. 46 SCHEMATIC DIAGRAM OF SCHLIEREN LIGHT SYSTEM

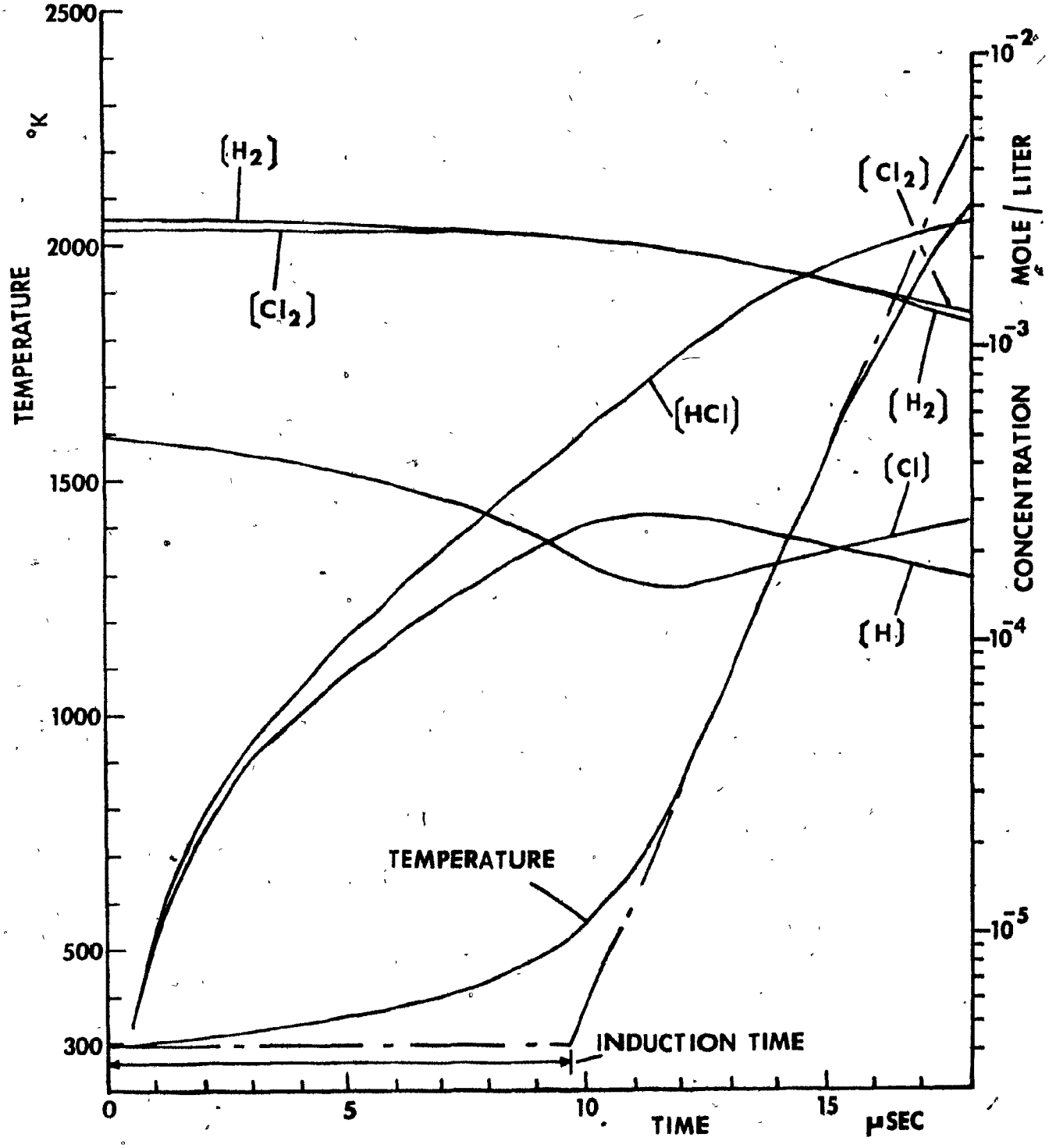

FIG. 47 CONSTANT VOLUME EXPLOSION BY IDEAL PHOTOCHEMICAL IGNITION (EQUI-MOLAR H_2-Cl_2 AT 100 TORR AND 298°K, INITIAL Cl CONCENTRATION 5×10^{-4} MOLE/LITER)

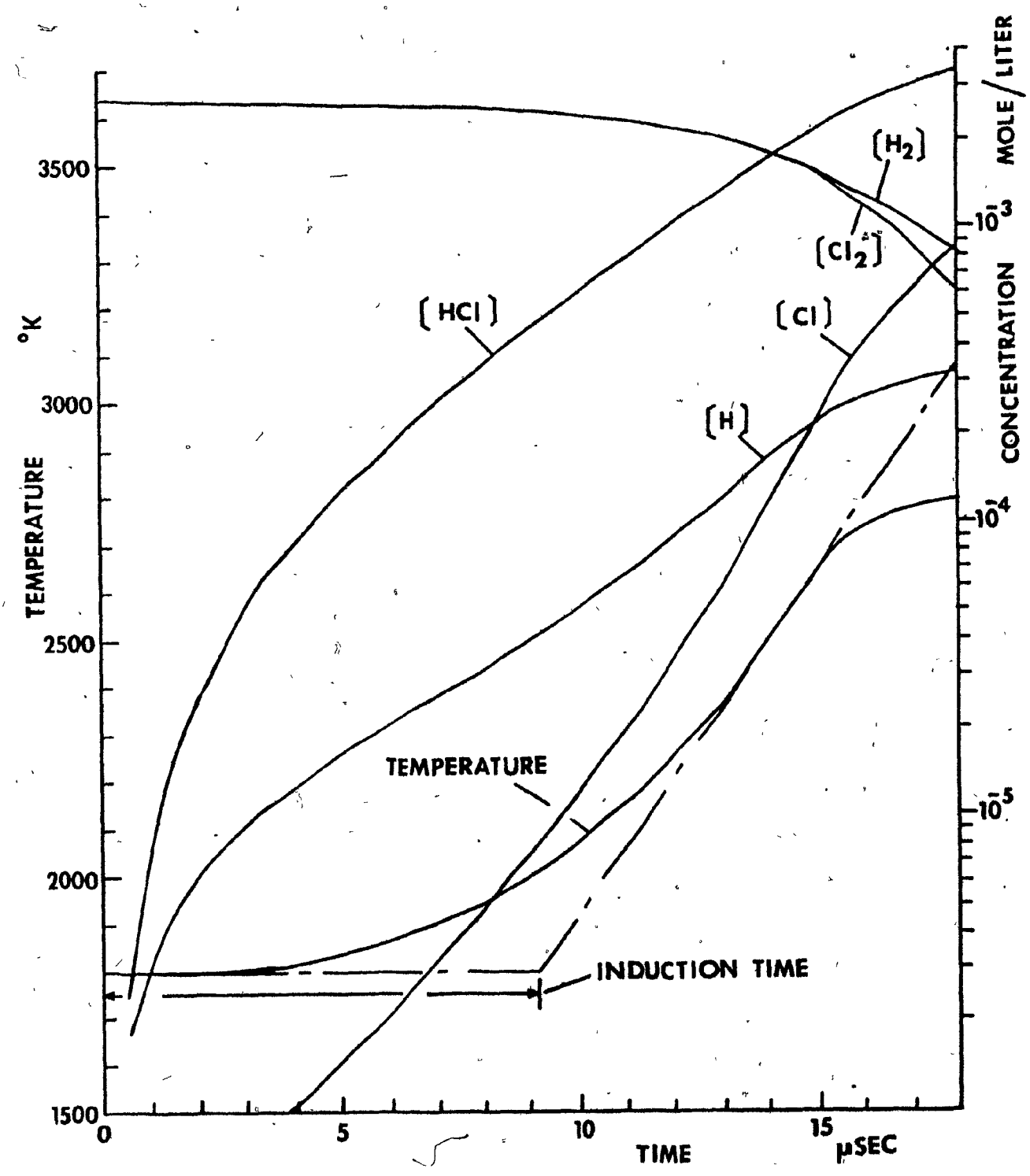

FIG. 48 THERMAL CONSTANT VOLUME EXPLOSION (EQUI-MOLAR H_2-Cl_2 AT 100 TORR AND 298°K, HEATED UP TO 1800°K)

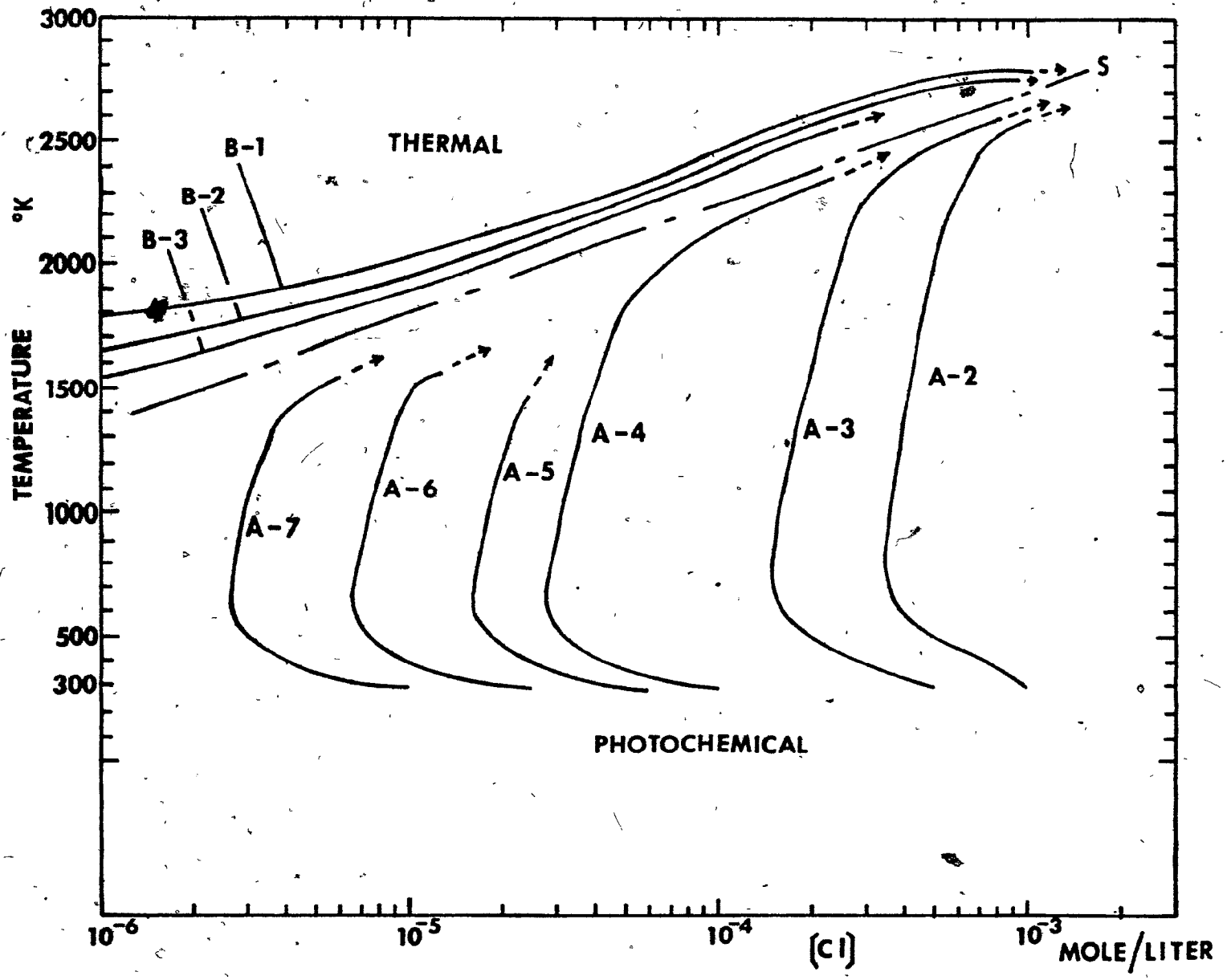

FIG. 49 PHASE DIAGRAM DISTINGUISHING BETWEEN PHOTOCHEMICAL AND THERMAL IGNITIONS

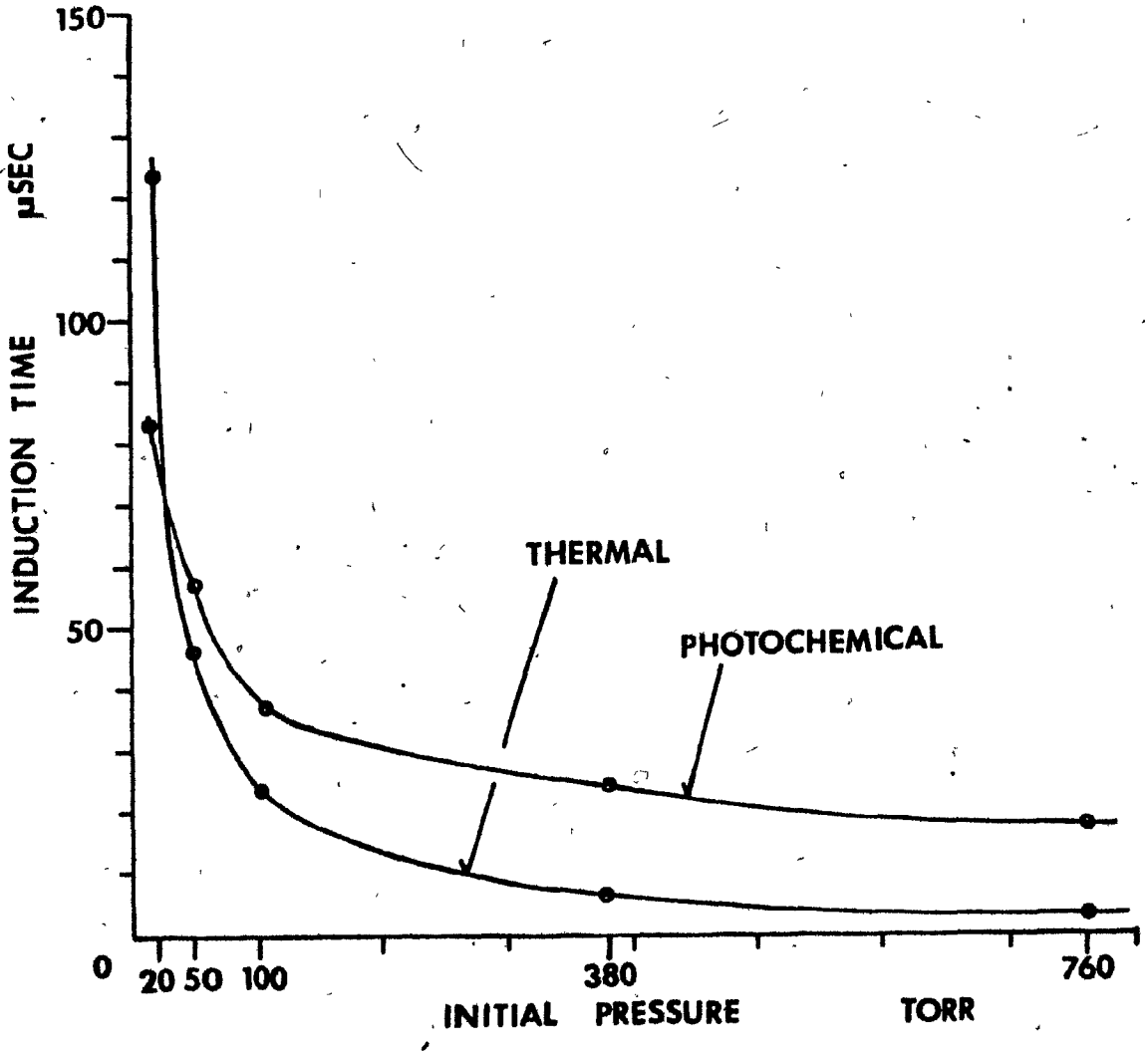

FIG. 50 EFFECT OF INITIAL PRESSURE ON INDUCTION TIME IN PHOTOCHEMICAL AND THERMAL IGNITIONS

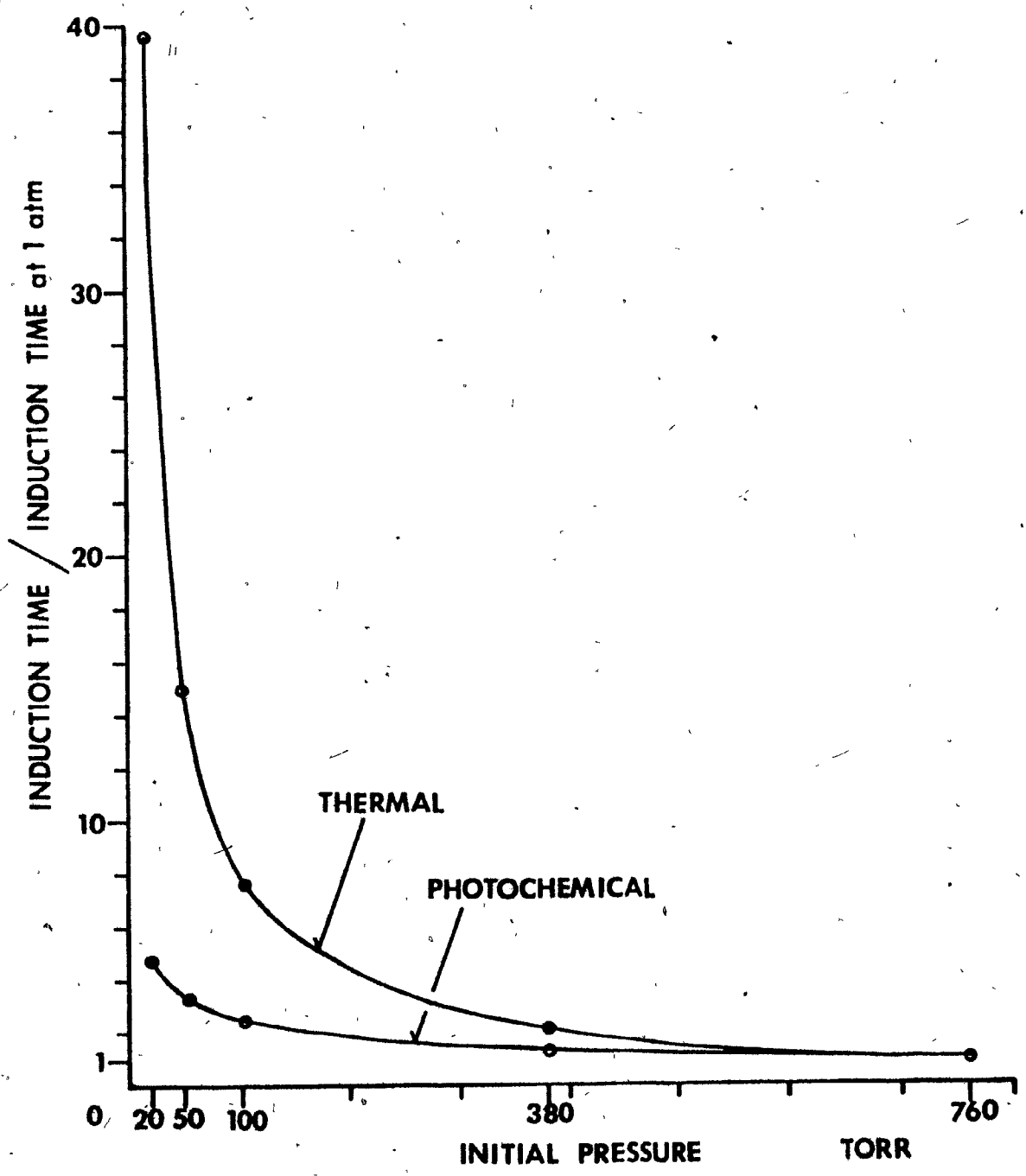

FIG. 51 RELATIVE EFFECIENCY OF PHOTOCHEMICAL vs. THERMAL IGNITION